# SEISMIC DESIGN COEFFICIENTS FOR COMPOSITE PLATE SHEAR WALLS - CONCRETE FILLED (C-PSW/CF)

by

Shubham Agrawal

A Thesis

Submitted to the Faculty of Purdue University

In Partial Fulfillment of the Requirements for the degree of

Master of Science in Civil Engineering

Lyles School of Civil Engineering

West Lafayette, Indiana

May 2020

THE PURDUE UNIVERSITY GRADUATE SCHOOL
STATEMENT OF COMMITTEE APPROVAL

Dr. Amit H. Varma, Chair

School of Civil Engineering

Dr. Mark D. Bowman

School of Civil Engineering

Dr. Christopher Williams

School of Civil Engineering

Approved by:

Dr. Dulcy M. Abraham

School of Civil Engineering

Dedicated to my family and friends for all their support.

ACKNOWLEDGEMENTS

TABLE OF CONTENTS

LIST OF FIGURES

LIST OF TABLES

ABSTRACT

This study aims to recommend seismic design coefficients for Composite Plate Shear Walls – Concrete Filled (C-PSW/CF). These design coefficients include the seismic response modification factor, *R factor*, deflection amplification factor, C_d, and overstrength factor, Ω_o. C-PSW/CFs are an efficient seismic force-resisting system, and seismic design coefficients for the system are already listed in ASCE 7-16. ASCE 7-16 prescribes a response modification factor of 6.5, a deflection amplification factor of 5.5, and an overstrength factor of 2.5 for C-PSW/CF. These values were selected based on the performance of similar systems and engineering judgment of the committee. This study seeks to validate these seismic design coefficients and factors and propose any changes required based on the results.

The procedure to quantify these design coefficients is detailed in FEMA P695. These guidelines are designed to either establish seismic performance parameters of a new seismic resisting system or to check the reliability of the existing system.

The C-PSW/CF system is typically provided in the building's elevator core with coupled walls in one direction and uncoupled walls in the perpendicular direction. A previous study on coupled C-PSW/CF system found that a higher *R* factor of 8 better captures coupled C-PSW/CF behavior. As the uncoupled C-PSW/CF system is not expected to provide a similar level of ductility, the original response modification factor of 6.5 is expected to be sufficient. This difference in ductility is expected because coupled wall systems can rely on coupling beams to provide additional energy dissipation.

This study evaluated the behavior and performance of four planar (3-story, 6-story, 9-story, and 12-story) and three C-shaped (15-story, 18-story, and 22-story) C-PSW/CF walls. The FEMA P695 procedure included the development of representative planar and C-shaped C-PSW/CF archetypes, developing and calibrating numerical models for these archetypes, and subjecting these models to nonlinear static (pushover) analysis and incremental dynamic (time history) analysis. OpenSees, an open-source structural analysis software, was used to develop the nonlinear FEA model and conduct the nonlinear analyses. The behavior of walls without closure plates was also analyzed and compared to the performance of walls with closure plates/boundary elements.

The results of this study indicate that seismic design coefficients of an R factor of 6.5, C_d factor of 5.5, and Ω_o factor of 2.5 for the C-PSW/CF system appropriately quantify the seismic performance and should be specified in ASCE7. Although no formal study was performed on walls with half-circular or full-circular boundary elements, the findings in the study can be reasonably extended to these walls as the ductility in these walls is greater due to limited stress concentrations at the corners. Walls without closure plates were also analyzed and determined to have insufficient ductility to meet the performance objectives when designed using an R factor of 6.5, C_d factor of 5.5, and Ω_o factor of 2.5. Therefore, the table should be updated to differentiate the performance of C-PSW/CFs based on the inclusion of boundary plates.

1   INTRODUCTION

Composite Plate Shear Walls – Concrete Filled (C-PSW/CF) are a highly efficient and effective seismic force resisting system. C-PSW/CFs are comprised of two steel faceplates with concrete infill in between. The steel faceplates are connected using tie bars which are embedded in the infill concrete. Shear headed stud anchors also can be provided, in combination with tie bars, to achieve composite action with the concrete. Closure plates or boundary elements can be provided at the ends of steel faceplates. Here, the steel faceplate acts as the primary shear reinforcement, and replaces the normal formwork required in reinforced concrete wall construction. The steel plates also provide confinement to the infill concrete. The tie-bars and infill concrete help to prevent buckling of the steel faceplates.

Figure 1.1 shows the typical components present in a C-PSW/CF system. Some of the benefits of using C-PSW/CFs includes (a.) similar or better strength and stiffness compared to reinforced concrete wall, (b.) does not require any complex formwork as faceplates and closure plates acts as formwork, (c.) does not suffer from rebar congestion, (d.) empty steel module can be designed as falsework for construction activities instead of waiting for concrete to gain strength usually required in reinforced concrete walls (Varma et al. 2017, Shafaei et al. 2019). Overall C-PSW/CFs significantly improve construction speed and efficiency (Varma et al. 2019).
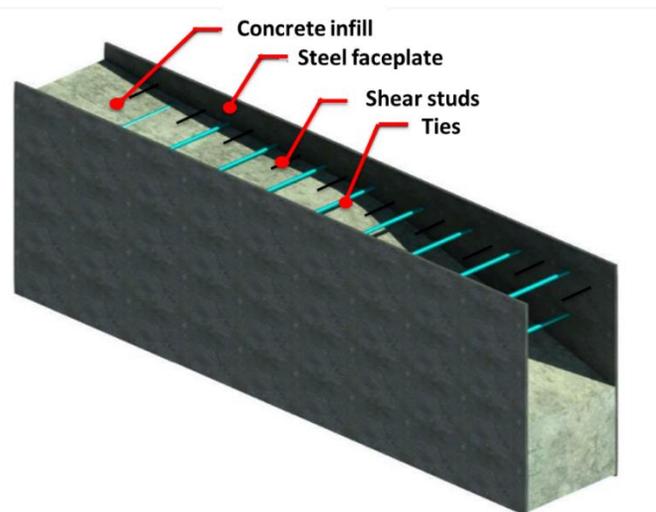
Figure 1.1. Typical components in C-PSW/CF (Shafaei et al. 2019, Broberg et al. 2019)

The C-PSW/CF system consists generally of planar, C-shaped or I-shaped walls. In this study, the seismic design criteria for uncoupled C-PSW/CF wall is based on AISC 341-16, Section H7, with some minor modifications. Section H7 of AISC 341-16 permits the use of walls with or without any boundary elements, where the boundary elements are permitted to be half-circular as shown in Figure 1.2b or full-circular concrete filled tubes (CFTs) as shown in Figure 1.2c. Rectangular planar walls with flange plates (closure plates) as the boundary elements, as shown in Figure 1.2a, are also permitted, based on the research of Wang et al. 2018.

C-shaped or - shaped walls, as shown in Figure 1.2d is generally used for mid-rise or high-rise structures. Wall without any boundary elements (Figure 1.3) have different behavior compared to walls with boundary elements (Figure 1.2), which is discussed in Chapter 11 and in Kurt et al. 2017. Walls with half-circular and full-circular boundary elements are not common and are not included in this study because of the perceived constructability issues and architectural considerations. It is important to note that the cyclic behavior of walls with half-circular or full-circular boundary elements is typically better than that of rectangular walls with flange plates. Therefore, the findings from this study can be extended to those walls with half-circular or full-circular boundary elements.
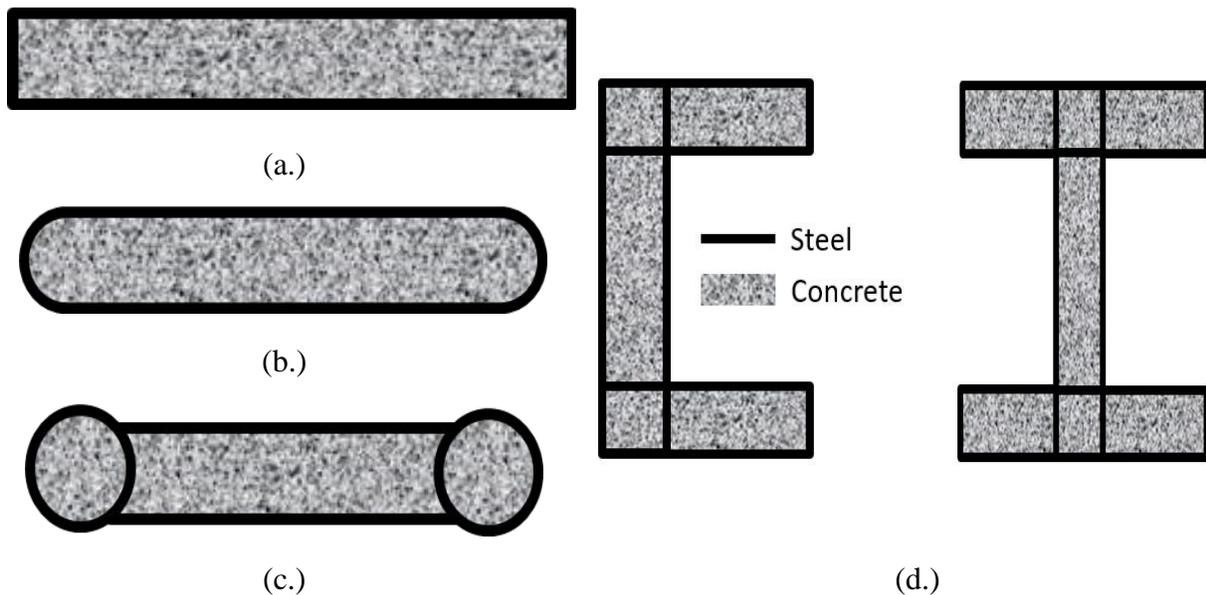
Figure 1.2. Walls with boundary elements (a.) Planar walls with closure plate; (b.) Planar walls with half-circular boundary elements; (c.) Planar walls with full-circular concrete filled tubes; (d.) C-shaped or I-shaped walls
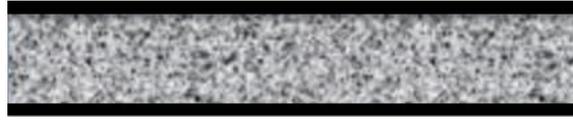
Figure 1.3 Wall without boundary element

1.1 Objective and Scope

Quantifying the seismic response of a structure is a necessary part of many structural designs. The seismic response of structures is often estimated using the Equivalent Lateral Force (ELF) analysis method, as presented in ASCE 7-16. This method relies on three factors: (1) response modification factor, R, (2) deflection amplification factor, C_d, and (3) system overstrength factor, Ω_0. These factors are used with the ELF approach to approximate the nonlinear forces and deflections from the linear analysis.

This study seeks to confirm the seismic response factors (R, C_d, and Ω_0) for composite plate shear walls concrete-filled (C-PSW/CFs). ASCE 7-16 assigns a response modification factor of 6.5, a deflection amplification factor of 5.5, and an overstrength factor of 2.5 to C-PSW/CFs. These values were selected based on the engineering judgment of the committee and on previously known response capabilities of similar systems. This study seeks to apply *FEMA P695 Quantification of Building Seismic Performance Factors* analysis methods to rigorously investigate the appropriateness of the current values and make recommendations for the future iteration of the code.

A companion FEMA P695 study was recently completed for the coupled composite walls system (Broberg et al. 2019, Kizilarslan et al. 2019). This study found a higher R factor of 8 was appropriate for coupled C-PSW/CF systems as the coupling beams contributed to the system's energy dissipation, improving the seismic performance of the system. The model benchmarking, material models, and structure models developed herein follow the approaches recommended in this study.

1.2 C-PSW/CF and Coupled C-PSW/CF Seismic System

The C-PSW/CF seismic force-resisting system can be designed as (1) uncoupled Composite Plate Shear Walls – Concrete Filled (also called as C-PSW/CF) and (2) Coupled Composite Plate Shear Walls – Concrete Filled (also called as CC-PSW/CF). The uncoupled system (C-PSW/CF) consists of independent walls. The coupled system (CC-PSW/CF) consists of walls and composite coupling beams at most of the floors along the height of the structure.

Figure 1.4 shows the typical configuration of the planar C-PSW/CF and CC-PSW/CF for a 5-story structure. The uncoupled system is typically provided as independent shear walls, and the coupled system is generally provided around the elevator cores. Figure 1.5 shows the typical configuration of the C-shaped and I-shaped composite walls around the elevator core. Here, two C-shaped composite walls are connected to a I-shaped composite wall using composite coupling beams on each floor. As a result, coupled configuration is provided in one direction to create an opening for the elevator system and uncoupled configuration is provided in the perpendicular direction.

(a.) (b.)
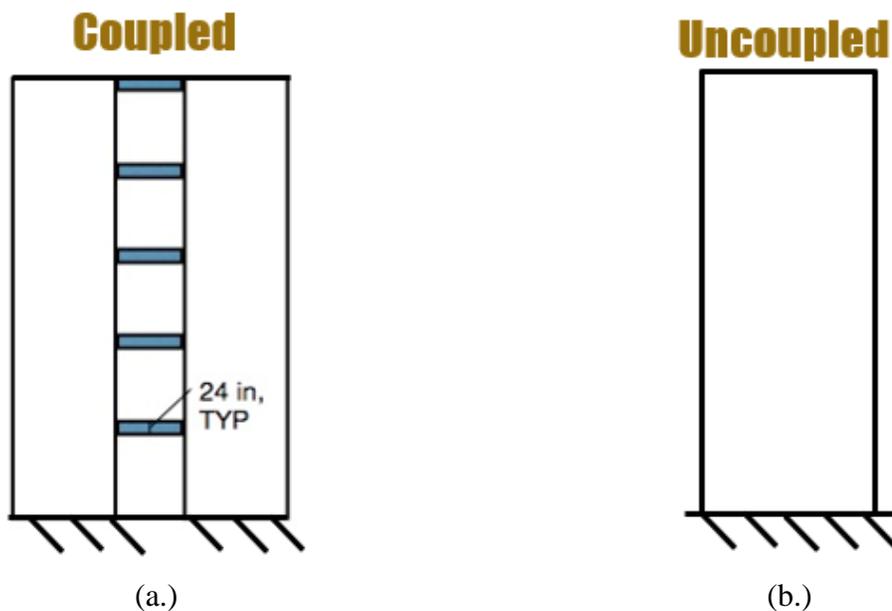
Figure 1.4. Planar Walls seismic force-resisting system for 5-story structure (a.) CC-PSW/CF; (b.) C-PSW/CF

20
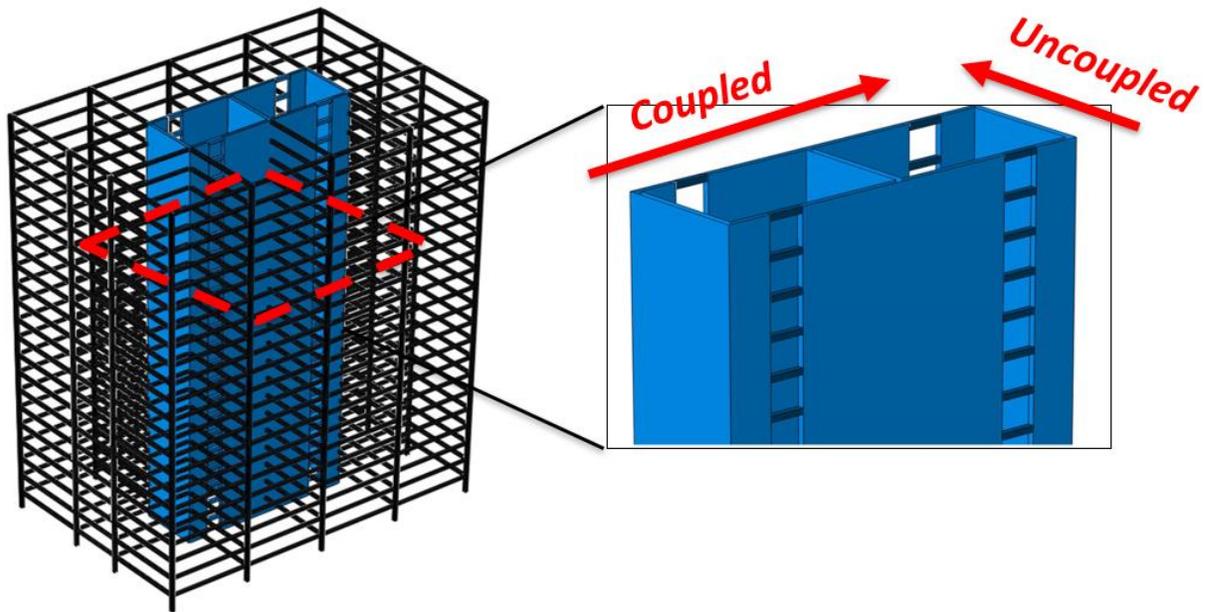
Figure 1.5. C -shaped and I-shaped composite walls around elevator cores (Shafaei et al. 2019)

The behavior and the seismic performance of the coupled system (CC-PSW/CF) differs from that of uncoupled system (C-PSW/CF system). The CC-PSW/CF system has better ductility and energy dissipation compared to the uncoupled C-PSW/CF system. In the coupled CC-PSW/CF system both composite walls and coupling beams are designed to have ductile behavior and develop inelastic flexural capacity during severe ground motion. The design criteria for the CC-PSW/CF system is based on strong-wall and weak-beam design philosophy.

Figure 1.6 shows the typical nonlinear static pushover behavior and assumed mechanism of the plastic hinge formation in the CC-PSW/CF system. At first, composite coupling beam near the mid-height undergoes flexural yielding, as shown in point A. As the lateral forces are increased, rest of the composite coupling beams undergoes plastic hinging. At point B, all the composite coupling beams develops flexural hinges at both ends. At point C, the base of the composite walls yields and forms plastic hinges. Finally, fracture failure of the CC-PSW/CF is represented by point D.

In comparison to the CC-PSW/CF system, the C-PSW/CF undergoes plastic hinging just at the base of the wall. The plastic hinging and energy dissipation in the composite coupling beams along the height of the structure results in greater R factor of 8 for CC-PSW/CF system compared to R factor of 6.5 for the C-PSW/CF system.
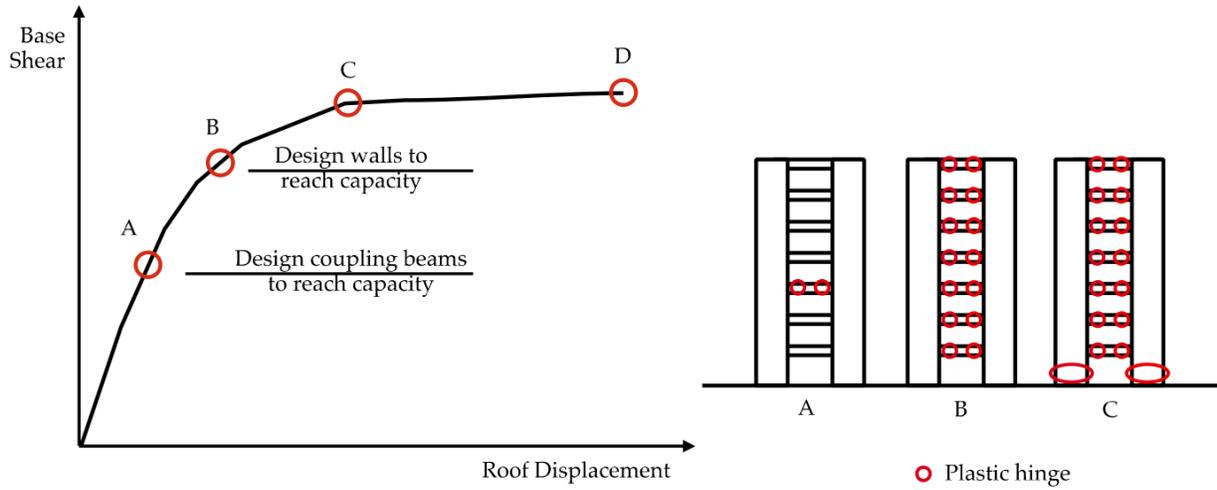
Figure 1.6. Nonlinear static pushover behavior and plastic hinge formation sequence in CC-PSW/CF system (Broberg et al. 2019)

Table 1-1 summarizes the seismic performance factors for both coupled (CC-PSW/CF) and uncoupled (C-PSW/CF) systems. The R factor of 8 for the CC-PSW/CF was validated using FEMA P695 study completed by Broberg et al. (2019) and Kizilarslan et al. (2019). This thesis will mainly focus on the FEMA P695 based study for the C-PSW/CF to verify an R factor of 6.5.

Table 1-1. Seismic design coefficients (a.) CC-PSW/CF; (b.) C-PSW/CF

Parameter	CC-PSW/CF	C-PSW/CF
Response Modification Factor	8	6.5
Seismic Ductility Factor, C_d	5.5	5.5
Overstrength Factor, Ω	2.5	2.5

1.3   Report Outline

This section outlines the general layout of this report. Chapter 2 outlines the FEMA P695 procedure used to quantify C-PSW/CF performance. This chapter serves as an outline of the steps required to determine the R, C_d and Ω_0 factors. Chapter 3 details the design requirements for C-PSW/CF walls. These requirements are implemented in the detailed design procedure presented in Chapter 4. Chapter 5 presents the structural designs following the requirements and recommendations of Chapter 3 and 4. Material models and model benchmarking are performed in Chapter 6 and 7, respectively.

The structural model combines these elements into one model in Chapter 8. The analysis results are presented in Chapter 9, 10 and 11 for planar walls, C-shape walls, and walls without closure plates, respectively. The seismic performance factors are detailed in Chapter 12. The model results are further post-processed in Chapter 13.

Summary and conclusions are presented in Chapter 14. The steps for plastic moment calculation and stiffness calculation are detailed in Appendix A. An example of the equivalent lateral force calculation is presented in Appendix B. An example of a planar and C-shaped archetype design procedure is summarized in Appendix C.

2   FEMA P695 PROCEDURE

This chapter details the FEMA P695 methodology used for quantifying the performance of building systems and to define initial parameters used for seismic design. FEMA P695 presents a standard procedure to quantify the inelastic response characteristics and the ability of the seismic system to meet desired performance objectives. The methodology is used to establish seismic response parameters of a new seismic resisting system and check the reliability of the existing system. The seismic performance factors quantified in this procedure include the response modification factor (R factor), deflection amplification factor (C_d), and the system overstrength factor (Ω_0). These factors are then used to estimate the strength and deformation demand of a nonlinear response using only a linear analysis method (Equivalent lateral force method). Figure 2.1 lists the various steps required to conduct FEMA P695 based study on C-PSW/CF. The FEMA P695 procedure for evaluating seismic design factors consists of: (1.) developing system concepts like selecting the seismic force-resisting system and system components, (2.) obtaining required system information like design criteria, seismic design coefficients, and nonlinear response for the system, (3.) designing several archetypes in accordance with the design requirements to represent the design space, (4.) developing and benchmarking a numerical modeling approach, (5.) conducting incremental dynamic analyses for 22 sets of appropriately scaled ground motions, and (6.) analyzing results (collapse margin ratio, CMR and adjusted collapse margin ratio, $ACMR$) to evaluate the performance and adequacy of seismic design factors for the system. These details are further outlined in this chapter.
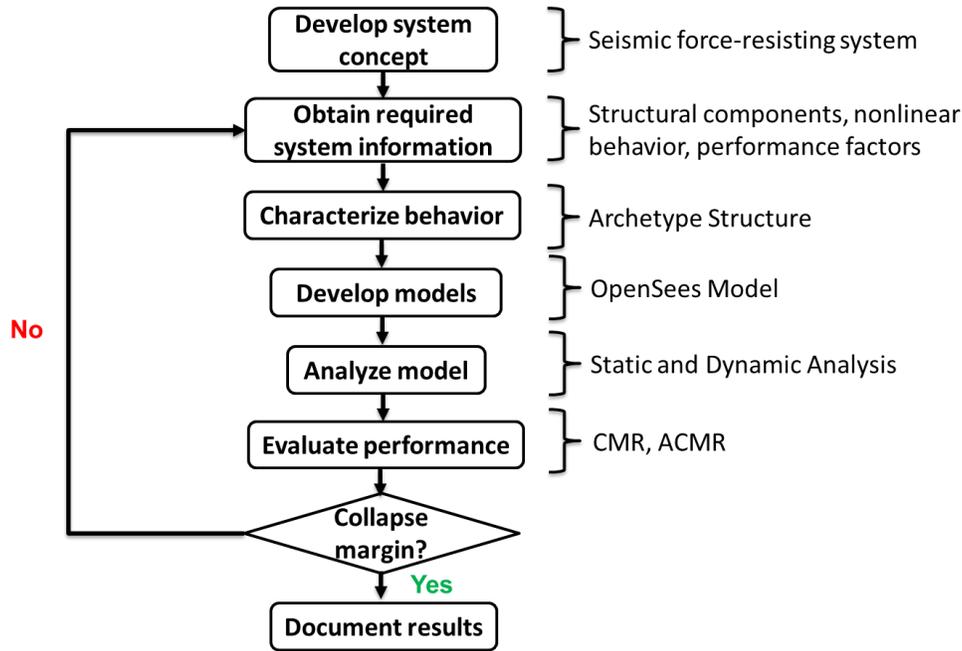
Figure 2.1. Flow chart FEMA P695 procedure

2.1 System Information

This section presents the steps FEMA P695 process to obtain the required system information for the composite walls. The required information includes a comprehensive description, construction methods, design requirements, test data, and other supporting information for the proposed system. Chapter 3 of FEMA P695 documents describe the detailed procedure for obtaining the required information and assessing the quality of design requirements. This information and requirements are then used for the development of the archetype models for the proposed system. The details and requirements for the C-PSW/CFs system were discussed in Chapters 3 and 4.

2.2 Archetype Development

An archetype configuration of the seismic resisting system that incorporates the behavior and features related to seismic performance is developed. The archetype structure design uses trial values of seismic performance factors R, C_d, and Ω_0, selected for performance evaluation. The developed archetype structures must provide a reasonable representation of the design space and help to quantify the performance of the entire class of structures and not only a single specific structure. The archetype structure should represent the range of feasible design space and situations permitted by the design guidelines. The details of the steps and procedures used to develop the

25

archetype structure are provided in chapter 4 of FEMA P695 guidelines. The planar and C-shaped archetype structures developed for the seismic performance evaluation are presented in Chapter 5. Figure 2.2 lists the steps required to design the seismic force-resisting member for the given archetype. These steps are elaborated in Chapter 3, Chapter 4 and Chapter 5.
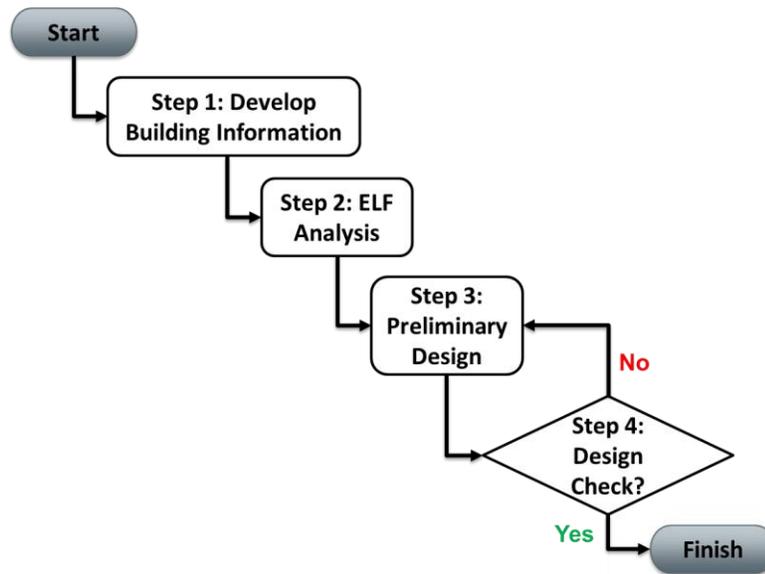
Figure 2.2. Flow chart for the archetype design procedure

2.3 Nonlinear Model Development

After developing the archetype structures, an analytical model of the seismic force-resisting system is developed for seismic performance evaluation and collapse assessment. The nonlinear model is able to capture key design features and behavioral modes of the proposed seismic resisting system. The model can capture nonlinear effects, strength, stiffness degradation, inelastic deformation, cyclic deterioration, and collapse behavior. The details of steel and concrete material models and nonlinear OpenSees FEA model developed for performance evaluation are presented in Chapter 8.

2.4 Nonlinear Analysis and Performance Evaluation

The nonlinear model developed in the previous step is analyzed for collapse assessment in this step. Nonlinear pushover analysis and response history analyses is performed on all the archetype models developed using the methods described in Chapter 3. The nonlinear static analyses are

performed to obtain the system's overstrength, Ω, and period-based ductility, μ_t. The nonlinear dynamic analysis shall be performed to assess the median spectral acceleration collapse intensity, S_{CT}, and collapse margin ratio, *CMR*. Then the acceptability of the trial seismic performance factor value is assessed based on the results of pushover and response history analyses. The nonlinear analyses and performance evaluation conducted on planar and C-shaped archetype structure are detailed in Chapter 9 and Chapter 10, respectively. The nonlinear analyses and evaluation of walls without boundary elements or closure plates are detailed in Chapter 11.

2.4.1   Nonlinear Static (Pushover) Analyses

The nonlinear pushover analysis is performed based on the nonlinear static procedure provided in ASCE41. The nonlinear pushover analysis shall be conducted for the factored gravity load combination and static lateral forces. As mentioned previously this analysis is performed to estimate the overstrength, Ω, and period-based ductility, μ_t. The lateral forces, F_i, at each story level, i, is proportional to the fundamental mode shape of the archetype as shown by Equation 2.1.

$$F_i = m_i \Phi_{1,i} \tag{2.1}$$

where m_i is the mass of structure at level i and $\Phi_{1,i}$ is the ordinate of the fundamental mode at level i.

The overstrength factor, Ω, of a given archetype is defined as the ratio of the maximum base shear resistance capacity, V_{max}, to the design base shear, V, per Equation 2.2.

$$\Omega = \frac{V_{max}}{V} \tag{2.2}$$

The period-based ductility, μ_t, is determined by dividing the ultimate roof displacement, δ_u, at 20% loss of strength ($0.8V_{max}$) by the effective yield roof displacement, $\delta_{y,eff}$, per Equation 2.3. Here, δ_u is the roof displacement obtained at 80% V_{max} limit on the descending branch. The effective yield roof displacement depends on the coefficient C_0, fundamental period, T (C_uT_a, Equation 4.1), fundamental period using eigenvalue analysis, T_1, and normalized maximum base shear, V_{max}/W.

The coefficient C_0 is calculated based on Equation 2.5, where $\Phi_{1,r}$ is the ordinate of the fundamental mode at the roof and N is the total number of levels.

$$\mu_t = \frac{\delta_u}{\delta_{y,eff}}$$ (2.3)

$$\delta_{y,eff} = C_0 \frac{V_{max}}{W} \left[\frac{g}{4\pi^2}\right] (\max(T, T_1))^2$$ (2.4)

$$C_0 = \phi_{1,r} \frac{\sum_1^N m_i \phi_{1,i}}{\sum_1^N m_i \phi_{1,i}^2}$$ (2.5)

Figure 2.3 shows the idealized pushover behavior of a typical seismic force-resisting system. It defines maximum base shear capacity, V_{max}, and the ultimate roof displacement at 80% reduction in shear carrying capacity, δ_u discussed previously.
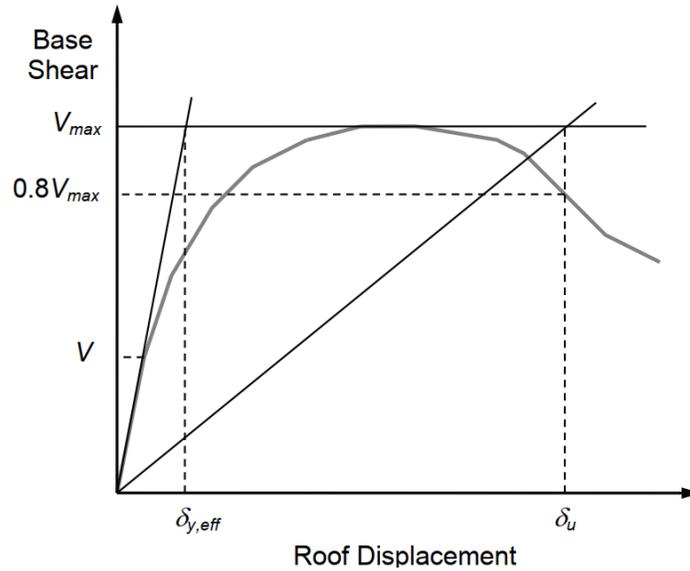
Figure 2.3. Idealized nonlinear static (pushover) curve (FEMA P695)

2.4.2 Nonlinear Dynamic Analyses

Nonlinear dynamic analysis is performed to establish the collapse margin ratio, *CMR*, which is then used to evaluate performance and probability of collapse. Incremental dynamic analysis (IDA) is performed for a given archetype using a series of successive time history analyses. The intensity of ground motions is scaled up gradually until the collapse of the given archetype is

28

reached. For the purpose of this study, 44 far-field ground motion as specified in FEMA P695 were considered. These ground motions are gradually scaled up from low intensity to the intensity that causes structural collapse. The individual ground motion records are first normalized by their peak ground velocities to remove any unwarranted variability in between different records. After normalizing the ground motions, the records are collectively scaled for anchoring the far-field recordset to Maximum Considered Earthquake (MCE) spectral demand. The details of normalization and scaling of ground motion are discussed in Appendix A of FEMA P695. The increment step size for each analysis was limited to maintain enough accuracy. Further reducing step size would have been computationally intensive for a small gain in accuracy. The calculation of the collapse margin ratio was performed for different collapse criteria with different inter-story drift limits ranging from three percent to five percent. Based on the experimental results and recommendation from industry experts and review panel the lesser but more conservative inter-story drift limit (i.e. three percent) was used for the collapse margin ratio calculation.

The collapse margin ratio is determined as the ratio of median collapse intensity, $\hat{S}_{CT}$, and the MCE ground motion spectral acceleration, S_{MT}, per Equation 2.6. Here, the median collapse intensity, $\hat{S}_{CT}$, is taken as the spectral acceleration which results in the collapse of the structure for half of the 44 ground records.

$$\text{CMR} = \frac{\hat{S}_{CT}}{S_{MT}} \qquad (2.6)$$

2.4.3   Collapse Performance Evaluation

After establishing the collapse margin ratio for archetype structures, the performance of the proposed lateral-force resisting system is assessed. In this step, the acceptability of the seismic performance factor selected is determined. This evaluation utilizes the results of the nonlinear static analyses and incremental dynamic analyses performed on the archetype structures. The collapse margin ratio obtained from IDA analyses is adjusted for the effects of the fundamental period, T, and period-based ductility, μ_t, system uncertainty, β, and established collapse probability

limits. The adjusted collapse margin ratio, *ACMR*, is determined for different levels of collapse probability, i %, and depends on spectral shape factor, *SSF*, and collapse margin ratio, *CMR,* per Equation 2.7.

$$\text{ACMR}_i = SSF_i \times CMR_i$$

<div align="right">(2.7)</div>

The values of spectral shape factor, *SSF,* are provided in Table 7-1 from FEMA P965 guidelines.

The calculated adjusted collapse margin ratio for a given archetype structure is then compared to the acceptance value of $\text{ACMR}_{10\%}$ provided in Table 7-3 of FEMA P695. The $\text{ACMR}_{10\%}$ value corresponds to the 10% acceptable collapse probability. FEMA P695 requires less than 20% probability of collapse for MCE ground intensity for each individual archetype and less than 10% probability of collapse across the performance group. Since only one structure was analyzed in each performance group, the more stringent requirement of a 10% failure probability was used. Table 2-1 lists the value of ACMR required for 20% and 10% probability of collapse for different levels of uncertainty.

This entire procedure including archetype design, nonlinear modeling and analyses, and performance evaluation are critically evaluated by a group of experts as an independent peer review panel. The peer review panel provided their review and comments on design requirements, archetype development, nonlinear analysis, and final selection of the systems proposed seismic performance factors. The detailed analysis procedure, performance evaluation, and seismic performance factor validation for C-PSW/CFs are provided in later sections of this report.

Table 2-1. Required adjusted collapse margin ratio

β_{TOTAL}	ACMR$_{20\%}$	ACMR$_{10\%}$
	Worst Structure	Group Average
Superior	1.46	1.78
Good	1.56	1.96
Fair	1.84	2.53
Poor	2.22	3.38

The detailed flow chart representing FEMA P695 procedure is described in Figure 2.4 below.
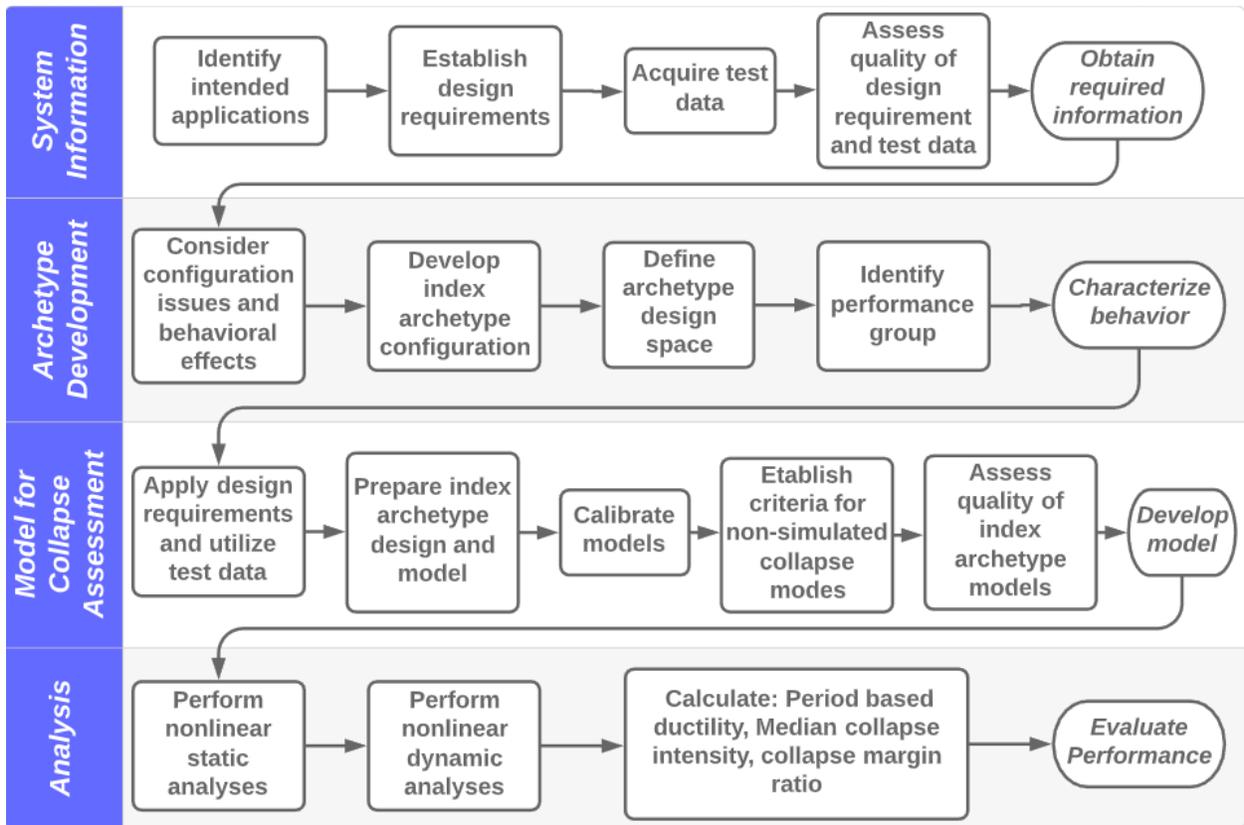
Figure 2.4. Detailed flow chart for FEMA P695 procedure

3 DESIGN REQUIREMENTS FOR COMPOSITE PLATE SHEAR WALLS/CONCRETE FILLED (C-PSW/CF)

3.1 General

Composite plate shear walls shall be designed in conformance with this section.

3.1.1 Scope

Composite walls shall be rectangular, C-shaped or I-shaped walls. Rectangular walls consist of two steel faceplates, steel closure plates (flange plates) and concrete infill in between. Parallel steel plates shall have equal nominal thickness. Closure plates shall have a thickness greater than or equal to the thickness of faceplates. Future provisions may allow a W-section as a closure element. C-shaped and I-shaped walls shall consist of steel plates covering the section parameter with concrete infill. The C-shaped and I-shaped walls were analyzed in the uncoupled direction (ground motion parallel to the web of the walls). Interior steel plates can be provided to achieve further confinement in the concrete infill. Tie bars connecting faceplates shall be provided to achieve composite action between the steel faceplates and concrete infill. Steel headed stud anchors in combination with tie bars can be used to reduce the number of tie bars required and to achieve the desired composite action. Steel plate thickness and concrete infill may be reduced at higher stories based on drift and strength requirements.

3.1.2 Notations

The symbols listed below are to be used in addition to or as replacements for those in AISC 360 and AISC 341.

A_c Area of concrete in the composite cross-section, in.^{2} (mm^2)

E_c Modulus of elasticity of concrete

E_s Modulus of elasticity of steel = 29,000 ksi (200,000 MPa)

F_y Specified minimum yield stress, ksi (MPa). As used in the Specification, AISC 360, "yield stress" denotes either the minimum specified yield point (for steels that have a yield point) or the specified yield strength (for steels that do not have a yield point).

R_c Factor to account for expected strength of concrete = 1.5

R_y Ratio of the expected yield stress to the specified minimum yield stress, F_y

f_c' Specified compressive strength of concrete, ksi (MPa)

3.1.3   Glossary

The terms listed below are to be used in addition to those in AISC 360 and AISC 341. Some commonly used terms are repeated here for convenience.

Applicable building code. Building code under which the structure is designed. [AISC 360-16]

Available strength. Design strength or allowable strength, as applicable. [AISC 341-16]

Composite. Condition in which steel and concrete elements and members work as a unit in the distribution of internal forces. [AISC 360-16]

Flexural buckling. Buckling mode in which a compression member deflects laterally without twist or change in cross-sectional shape. [AISC 360-16]

Load effect. Forces, stresses, and deformations produced in a structural component by the applied loads. [AISC 360-16]

Nominal strength. Strength of a structure or component (without the resistance factor or safety factor applied) to resist load effects, as determined in accordance with the Specification, AISC 360. [AISC 341-16]

Required strength. Forces, stresses, and deformations acting on a structural component, determined by either structural analysis, for the LRFD or ASD load combinations, as applicable, or as specified by this Specification or Standard. [AISC 360-16]

Resistance factor, ϕ. The factor that accounts for unavoidable deviations of the nominal strength from the actual strength and for the manner and consequences of failure. [AISC 341-16]

Steel anchor. Headed stud or hot rolled channel welded to a steel member and embodied in the concrete of a composite member to transmit shear, tension, or a combination of shear and tension at the interface of the two materials. [AISC 360-16]

Stiffness. Resistance to deformation of a member or structure, measured by the ratio of the applied force (or moment) to the corresponding displacement (or rotation). [AISC 360-16]

3.2   Basis of Design

Composite walls designed in accordance with these provisions are expected to provide inelastic deformation capacity through yielding at the base of composite wall elements.

3.3   Analysis

C-PSW/CF walls shall be analyzed in accordance with this section.

3.3.1   Required Flexural Strength

The required flexural strength for the composite walls shall be calculated in accordance with applicable seismic design guidelines.

3.3.2   Required Shear Strength

The required shear strength of the composite walls shall be determined as the shear force obtained from the seismic analysis amplified by a factor of four.

3.3.3   Stiffness

Effective flexural and axial stiffnesses of planar, C-shaped, and I-shaped composite walls shall be calculated using cracked transformed section properties corresponding to 60% of the nominal flexural capacity. Alternatively, the effective flexural stiffness for walls is permitted to be calculated per Equation 3.1 (AISC 360-16 Equation I2-12) with C_3 taken as 0.35. The effective shear stiffness shall be calculated using uncracked properties of the composite walls.

$$EI_{eff} = E_s I_s + E_s I_{sr} + C_3 E_c I_c \tag{3.1}$$

3.3.4 Composite Walls Requirements

The design of composite walls shall be in accordance with the following requirements.

3.3.5 Minimum Thickness of Plate

The steel faceplates and closure plates shall have a minimum thickness of three sixteenth of an inch.

3.3.6 Minimum Area of the Steel

The steel plates provided shall be at least 1% of the total cross-section area.

3.3.7 Tie Spacing Requirement for Composite Walls

The tie spacing to plate thickness ratio, S/t_p, shall be limited as follows:

$$\frac{S}{t_p} \leq 1.00 \sqrt{\frac{E_s}{2\alpha + 1}} \tag{3.2}$$

$$\alpha = 1.7 \left[\frac{t_{sc}}{t_p} - 2\right] \left[\frac{t_p}{d_{tie}}\right]^4 \tag{3.3}$$

where,

S = largest clear spacing of the ties

t_p = thickness of the steel plate

t_{sc} = thickness of the composite wall

d_{tie} = effective diameter of the tie

3.3.8 Tie-to-Plate Connection

The tie bar to steel plate connection shall develop the full yield strength of the tie bar.

3.4 Composite Wall Strength

The nominal strength of the composite walls shall be calculated in accordance with this section. A resistance factor (ϕ) equal to 0.90 shall be used to calculate the available strength of the composite walls.

3.4.1 *Flexural Strength*

The nominal flexural strength shall be computed based on plastic limit analysis of the cross-section using the plastic stress distribution method according to Specification I1.2b. The steel plates shall be assumed to reach the yield stress of F_y in either tension or compression. The concrete infill shall be assumed to have reached compressive stress equal to $0.85f'_c$, ksi. Concrete in tension shall be assumed to have zero stress capacity.
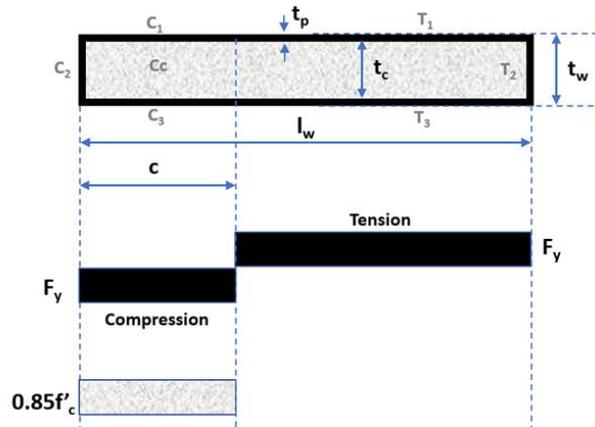
Figure 3.1. Plastic stress distribution for C-PSW/CF with boundary elements

3.4.2 *Compressive Strength*

The nominal compressive strength shall be determined in accordance with AISC360, Section I2.1b for the limit state of flexural buckling. The effective flexural stiffness used to calculate the elastic critical buckling load shall be based on Section 3.3.3. The axial load capacity of the composite section shall be determined using Equation 3.4. Resistance factor (ϕ) equal to 0.75 shall be used to calculate the available compressive strength.

$$P_{no} = A_s F_y + 0.85 f'_c A_c \tag{3.4}$$

3.4.3 Tensile Strength

The nominal tensile strength, P_n, shall be determined for the limit state of yielding as:

$$P_n = A_s F_y \tag{3.5}$$

where, A_s = area of steel plates in the wall cross-section

3.4.4 Shear Strength

The nominal in-plane shear strength, V_n, shall be determined as follows:

$$V_n = \frac{K_s + K_{sc}}{\sqrt{3K_s^2 + K_{sc}^2}} \times F_y \times A_{sw} \tag{3.6}$$

where,

$$K_s = G_s A_{sw} \tag{3.7}$$

$$K_{sc} = \frac{0.7(E_c A_c)(E_s A_{sw})}{4E_s A_{sw} + E_c A_c} \tag{3.8}$$

where,

A_{sw} = Area of the steel plates in the direction of in-plane shear

A_c = Area of the concrete infill

G_s = Shear modulus of steel, ksi (MPa)

3.5 Composite Wall-to-Foundation Connections

Where the composite walls are connected directly to the foundation at a point of the maximum moment in the walls, the composite wall-to-foundation connections shall be designed in accordance with the requirements of this section.

3.5.1 Required Strengths

The required strengths for the composite wall-to-foundation connections shall be determined using the capacity-limited seismic load effect. The composite walls shall also be assumed to have developed plastic hinges at the base with an expected flexural capacity of $1.2M_{p,exp}$ while accounting for the effects of simultaneous axial force. The required shear strength for the composite wall-to-foundation connections shall be equal to the required shear strength for the composite walls calculated in accordance with Section 3.3.2.

3.6 Protected Zones

The requirements for protected zones shall be in accordance with AISC 341 Section D1.3 and Section I2.1. The regions at the base of the composite walls subject to inelastic straining shall be designated as protected zones.

3.7 Demand Critical Welds in Connections

The requirements for demand critical welds shall be in accordance with AISC 341 Section A3.4b and Section I2.3.

The following welds shall be demand critical and shall satisfy the applicable requirements:

(a) Welds connecting the composite wall closure plates to the faceplates

(b) Welds in the composite wall steel plate splices

(c) Welds at composite wall steel plate-to-base plate connections

3.8 Wall Foundation

The wall-to-basemat connections shall be designed for the expected flexural capacity of the composite wall accounting axial effects and the amplified shear force demand (amplification of 4). The C-shaped and I-shaped walls shall also be designed for the expected axial forces due to capacity-limited shear forces in coupling beams. The examples of typical wall foundation and connection details are shown in Figure 3.2.
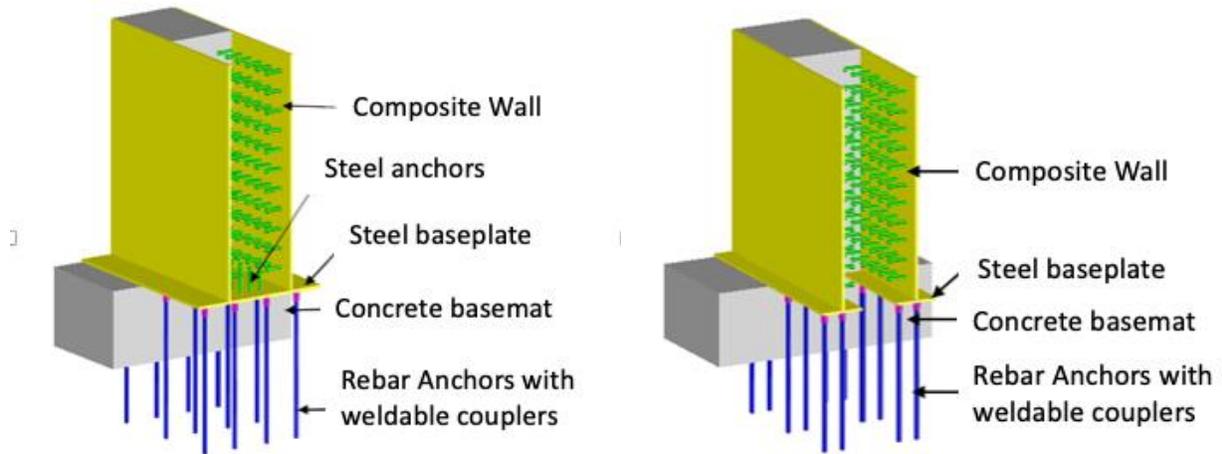
(a)
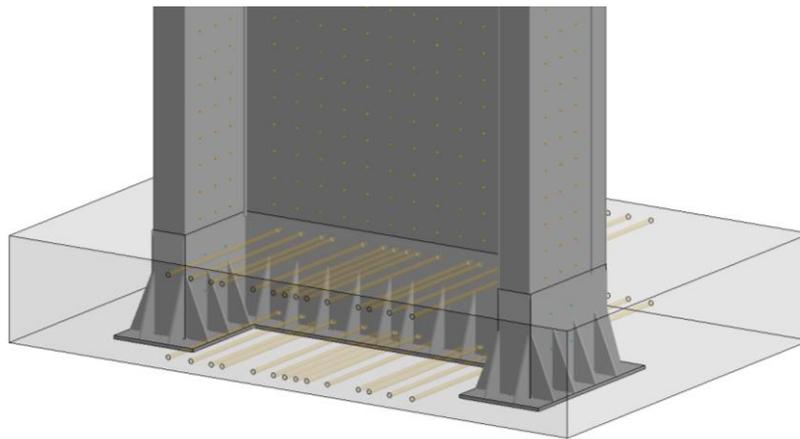
(b)

Figure 3.2. Composite wall to basement connections (a) with welded base plate and rebar couplers (Bhardwaj and Varma, 2016); (b) wall embedded into the concrete foundation (Bruneau et al., 2019)

4   DETAILED DESIGN PROCEDURE FOR ARCHETYPE STRUCTURES

This chapter describes the detailed design approach used to design the low to mid-rise (3-22 stories) office buildings archetype structures with C-PSW/CF walls. The low-rise structures (3-12 stories) used planar composite walls, and the mid-rise structures (15-22 stories) used C-shaped composite walls as the seismic force-resisting system. The walls were designed following the provisions of applicable building code, seismic design code, and FEMA P695. The design procedure involved selecting initial parameters including building floor plan, load requirements, and seismic parameters. These parameters were selected after several iterations based on feedback from industry professionals and the FEMA review panel. The archetype structures were designed to represent low-rise and mid-rise office buildings with dimensions following architectural considerations. One such architectural limitation was the length of composite walls which was limited to typical bay lengths and was varied in multiples of 5ft. The parameters used for this study will be discussed further in this chapter.

Two composite walls were provided in the direction of consideration for both planar and C-shapes composite walls systems. The planar composite walls were designed to resist lateral forces along the length of the wall. C-shaped walls were designed as uncoupled walls in the direction of consideration of seismic ground motion (parallel to the web). These walls would be coupled in the perpendicular direction with the coupling action achieved using composite coupling beams connecting both the walls at each floor. Figure 4.1 shows the typical cross-section of the planar composite wall and C-shaped composite walls.
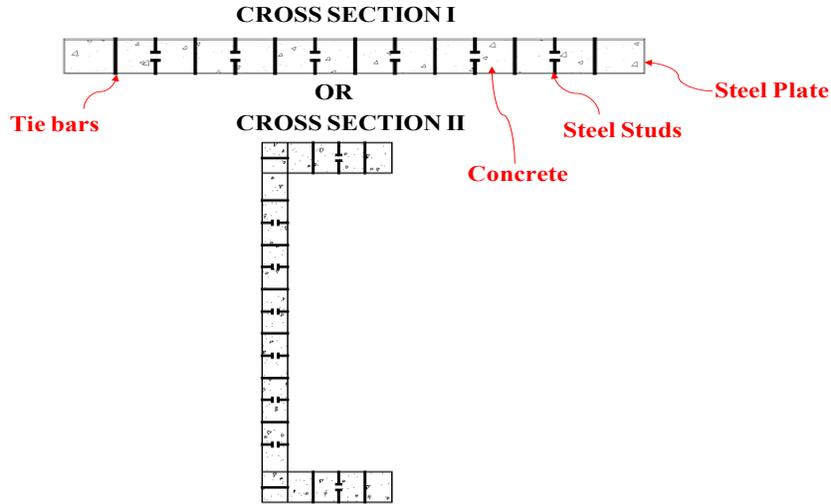
Figure 4.1. C-PSW/CF typical cross-section: I) Planar C-PSW/CF; II) C-shaped C-PSW/CF

4.1 Archetype Structure Initial Parameters

Archetype structure parameters were based on the review panel recommendations and general industry practices. Considering the complexity and rigorous analysis requirements, the archetype design was limited to four structures with planar composite walls (3,6,9 and 12 stories) and three structures with C-shaped composite walls (15, 18 and 22 stories). The floor plan (Figure 4.2) varied based on the length of the composite walls. Seven bays were used in the east-west direction and three bays in the north-south direction. Two walls in both directions were used as lateral load carrying members for the archetype structure. Figure 4.3 shows the basic configuration of planar C-PSW/CF and C-shaped C-PSW/CF. The initial archetype parameters are listed in Table 4-1 below.

The seismic design parameters listed below in Table 4-2 were based on ACSE 7-16 guidelines and peer review committee recommendations. A response modification factor, R, of 6.5 was chosen for validation in line with current ASCE 7-16 recommendations. A seismic ductility factor, C_d, of 5.5 was used. An importance factor, I_e, of 1.0 was used for risk category II.
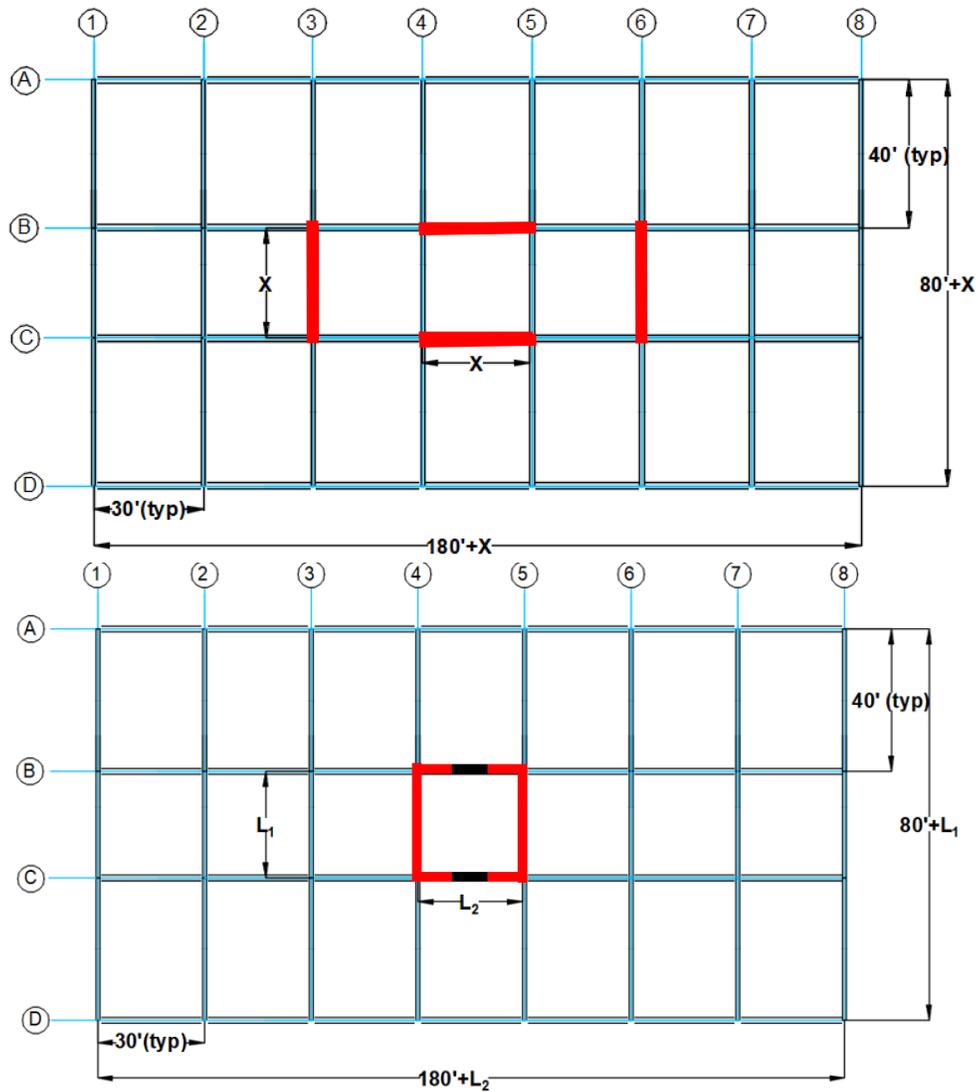
Figure 4.2. Floor plan a) planar walls b) C-shaped walls

Planar walls   **C-shaped walls**
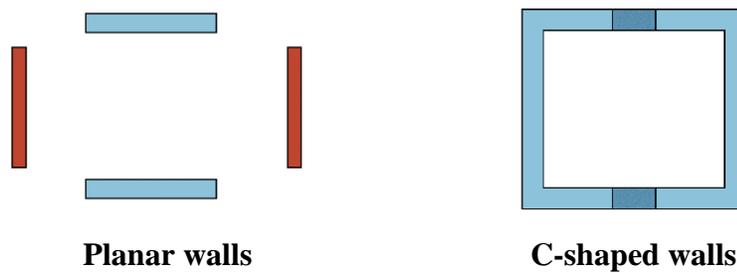
Figure 4.3. Basic configuration of walls

42

Table 4-1. Archetype building parameters

Parameter	Value	Reasoning
Floor Dimensions	(80+X) ft x (180+X) ft where X is the length of the center bay.	Review panel recommendation for typical buildings
Story Height	First story: 17ft Typical story: 14ft	Review panel recommendation for typical story heights
Number of Stories	3 to 22 Stories	Panel recommendation to represent low- and mid-rise office buildings
Seismic Weight	Floor load of 120psf	Estimated from components: Steel framing (12 psf) 2.5" Normal Weight Concrete on 3" Steel Deck (50 psf) Curtain Wall (15 psf on facade area) Superimposed Dead Load (15 psf) Partitions (15 psf)
Risk Category	II	Office Building

Table 4-2. Seismic design parameters

Parameter	Value
Response Modification Factor	6.5
Seismic Ductility Factor, C_d	5.5
Overstrength Factor, Ω	2.5

4.2 Equivalent Lateral Force Analysis

The seismic forces on the composite walls were calculated using the Equivalent Lateral Force (ELF) analysis following ASCE 7-16 guidelines. The steps used are summarized below.

4.2.1 Response Spectra

The design response spectrum was built based on guidelines provided in Chapter 11 of ASCE7. The spectral response acceleration curve is plotted based on the design earthquake spectral acceleration parameters S_{DS} and S_{D1}. The spectral acceleration parameters are dependent on the site class, soil condition, mapped ground motion values and importance factor. S_{DS} and S_{D1} values of 1.0g and 0.6g, respectively, as specified in the FEMA P695, were used for the analysis.

4.2.2 Approximate Fundamental Period

The approximate fundamental period, T_a, was calculated based on guidelines provided in Chapter 12 of ASCE7. The approximate fundamental period is calculated using Equation 4.1 considering approximate period coefficient C_t as 0.02 and x as 0.75 per section 12.8-2 of ASCE7. The coefficient of the upper limit period, C_u, is taken as 1.4 based on a seismic acceleration parameter S_{D1} of 0.6. The upper limit of the fundamental period can be calculated using Equation 4.2. Once the initial guess of section size is developed, the fundamental period based on modal analysis is determined. The fundamental period is adjusted to the minimum of the fundamental period from modal analysis and upper limit fundamental period.

$$T_a = C_t h_n{}^x \tag{4.1}$$

$$T_{upper} = C_u T_a \tag{4.2}$$

4.2.3 Seismic Response Coefficient, C_s

The seismic response coefficient, C_s, is calculated according to section 12.8.1 of ASCE7 guidelines. The guidelines and equations used for the calculation are summarized here. The seismic response coefficient, C_s shall be calculated in accordance with Equation 4.3. The seismic response coefficient shall be adjusted according to the minimum and maximum allowable value based on Equation 4.4 – 4.7. A response modification factor, R, of 6.5, importance factor, I_e, of 1.0 and long period, T_L of 8s were used for the C_s calculations.

$$C_s = \frac{S_{DS}}{\left(\dfrac{R}{I_e}\right)} \tag{4.3}$$

$$C_{s,max} = \frac{S_{D1}}{T\left(\dfrac{R}{I_e}\right)} \text{ for } T \leq T_L \tag{4.4}$$

$$C_{s,max} = \frac{S_{D1}T_L}{T^2\left(\dfrac{R}{I_e}\right)} \text{ for } T > T_L \tag{4.5}$$

$$C_{s,min} = 0.044S_{DS}I_e \text{ for } \geq 0.01 \tag{4.6}$$

$$\text{If } S_1 \geq 0.6g \;\; C_{s,min} = \frac{0.5S_1}{\left(\dfrac{R}{I_e}\right)} \tag{4.7}$$

4.2.4 Base Shear Calculations

The base shear, V, is calculated per Eq. 12.8-1 of ASCE7 as shown in Equation 4.8 below. The seismic weight, W, is taken from Table 4-1 and coefficient, C_s, is determined in Step 4.2.3.

$$V = C_s W \tag{4.8}$$

4.2.5 Vertical Distribution of Seismic Forces

The lateral seismic force distributed at any level of the building is determined by following Section 12.8.3 of ASCE7. The vertical distribution factor, C_{vx}, is determined according to Equation 4.9 using story level weight, w_i and w_x, assigned to level i or x, and height, h_i and h_x, from the base to level i or x. The story level shear is then calculated using Equation 4.10.

$$C_{vx} = \frac{w_x h_x^k}{\sum_{i=1}^{n} w_i h_i^k} \tag{4.9}$$

$$F_x = C_{vx} V \tag{4.10}$$

4.2.6 Composite Walls Required Shear Strength and Amplification Factor

The required wall base shear strength is adjusted. A base shear amplification factor of four is used to account for amplification found in higher modes of tall structures. This amplification factor is used only to calculate shear demand and is not used for overturning moment calculation. Figure 4.4 shows the typical vertical distribution of seismic forces along the height of the C-PSW/CF.
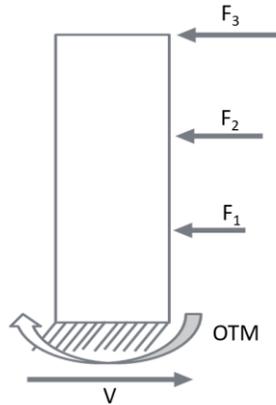
Figure 4.4. Distribution of vertical forces

4.2.7 Overturning Moment at the Base

The overturning moment at the base, OTM, of the wall is calculated based on the vertical distribution of seismic forces per section 4.2.5 (see Figure 4.4). The amplification factor of four is not applied during the calculation of the overturning moment.

4.3 Preliminary Design

The preliminary design of composite walls consists of selecting wall length, total wall thickness, and steel plate thickness. The preliminary design was selected to withstand design forces and to satisfy drift requirements. The length of the walls is selected such that the height to length ratio is greater than 3 to maintain a flexural controlled design.

4.4 Structural Analysis

After selecting a preliminary design, structural analysis is performed. The composite walls are modeled in accordance with Chapter 3. The required strength in shear and flexure are accurately

computed based on equivalent lateral force analysis presented in section 4.2. The story defections due to lateral loads are also calculated in this step.

4.5   Design Checks

The composite wall design check includes steel plate slenderness requirements, tie reinforcement requirements, empty module requirements, shear and flexural strength check, and inter-story drift check. The required design checks are summarized in this section.

4.5.1   Wall Steel Plate Slenderness Requirement

The composite wall steel plate slenderness requirement shall satisfy tie spacing, s, requirement before and after placement of concrete using the guidelines provided in Section 3.3.7.

4.5.2   Corner Box Steel Pate Slenderness

The corner box steel plate slenderness requirement is in accordance with Table I1.1a of AISC360-16. The spacing limit is applied to corner box sections which are found in composite walls with C-shaped or I-shaped configuration. The limit is also checked for rectangular walls which has the box section formed by more than two closer plates at each end. The required limit on tie spacing is reproduced in Equation 4.11 below.

$$\frac{b}{t_p} \text{ or } \frac{s}{t_p} \leq 2.37 \sqrt{\frac{E_s}{R_y F_y}} \tag{4.11}$$

4.5.3   Wall Shear Strength

The in-plane shear strength required for the composite walls is calculated based on the amplified base shear computed in Section 4.2.6. The total base shear is then divided by the number of walls to distribute the forces to all walls equally to calculate the required shear strength on each wall. The available design shear strength is calculated according to Section 3.4.4.

4.5.4   Wall Flexural Strength

The required flexural strength of the composite walls is calculated as the overturning moment (OTM) computed from Section 4.2.7 divided by the number of walls. The available design flexural strength of composite walls is calculated according to Section 3.4.1.

4.5.5   Inter-Story Drift Ratio

The inter-story drift ratio (IDR) is calculated from the story displacement found from the structural analysis performed in Section 4.4. The IDR for each level is calculated as the ratio of the difference in the story displacement of two adjacent levels to the story height. The maximum IDR shall be checked against a 2% limit per Table 12.12-1 of ASCE7-16.

4.6   Final Check and Redesign

The design checks as mentioned in Section 4.5 shall be performed. Redesign of composite walls may be necessary, and the design of the walls is adjusted until the system meets all design requirements. Parameters like wall length, wall thickness, plate thickness, and the number of composite walls, can be adjusted to obtain the desired performance.

5   DESIGNED ARCHETYPES

Archetype structures were divided into two performance groups, low-rise structures, and mid-rise structures. Planar/rectangular composite walls were used as the lateral system for the low-rise archetype structures and C-shaped composite walls were used for the mid-rise archetype structures. Figure 5.1, Figure 5.2 and Figure 5.3 represent the configuration and nomenclature of the lateral system used for the planar and C-shaped archetypes. The bay length of the center bay was varied for each archetype based on the length of the composite walls. The details of archetypes structures used for the FEMA P695 procedure are presented in this chapter.
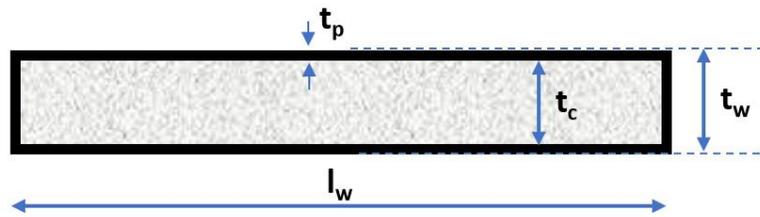
Figure 5.1. Planar C-PSW/CF
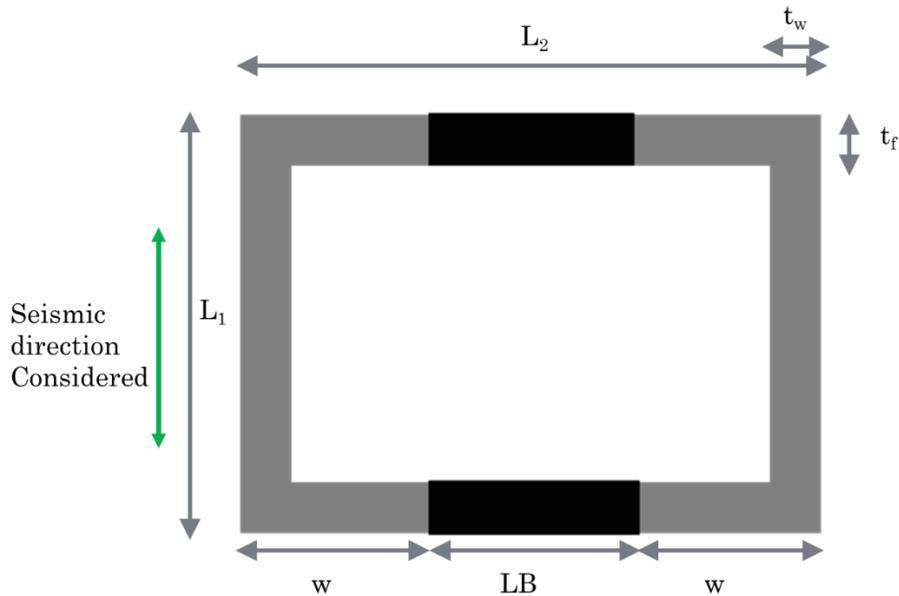
Figure 5.2. C-shaped composite plate shear wall archetype configuration
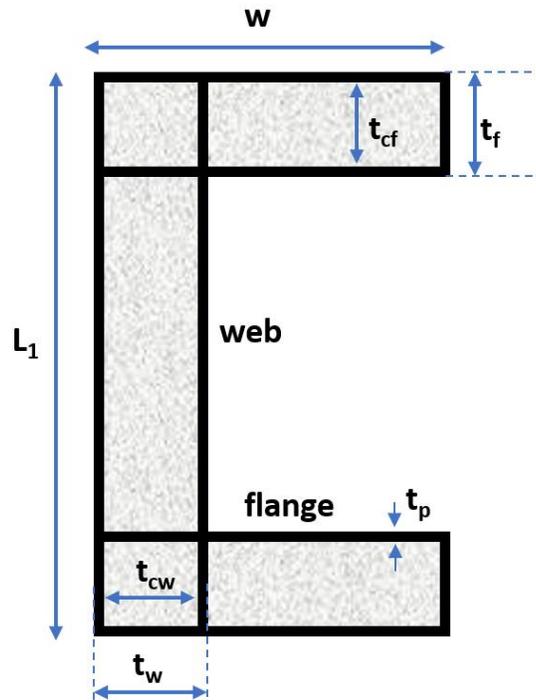
Figure 5.3. C-shaped composite plate shear wall cross-section

5.1 Planar Archetype

Four archetypes (3, 6, 9 and 12 story) were designed using planar composite walls as the lateral resisting system. The configuration of planar composite walls used for the archetype structure is presented in Figure 5.1. Two walls in each direction were used. The flange plate thickness was kept the same as the thickness of the web plates. Table 5-1 presents the floor plan used for the planar archetypes.

Table 5-2 summarizes the dimensions of the wall used for each of the archetypes. Table 5-3 presents additional information on the designed lateral system including the wall aspect ratio and design strength compared to the required strength. This table also summarizes the maximum inter-story drift ratio estimated using the nonlinear finite element models.

Table 5-1. Floor plans for planar archetype structures

Case	No. of Stories	Center Bay Length, ft	Center Bay Width, ft	Length, ft	Width, ft	Story Weight, kip
1	3	20	20	200	100	2400
2	6	25	25	205	105	2583
3	9	30	30	210	110	2772
4	12	35	35	215	115	2967

Table 5-2. Planar composite wall archetypes

Case	No. of Stories	Wall Thickness, in	Wall Length, ft	Plate thickness, in	Height, ft
1	3	12	15	4/16	45
2	6	16	25	5/16	87
3	9	24	30	7/16	129
4	12	32	35	8/16	171

Table 5-3. Planar archetype structures – aspect ratio, strength, and inter-story drift ratio

Case	No. of Story	H_T/L	H_{1st}/T_{sc}	Wall Strength Margin		Max. Inter-story Drift Ratio, FE Model (%)
				$\phi M_{n,wall}/M_{u,elf}$	$\phi V_{n,wall}/4V_{u,elf}$	
1	3	3	17	1.30	1.83	2.0
2	6	3.5	12.8	1.42	2.19	2.0
3	9	4.3	8.5	1.78	3.30	2.0
4	12	4.9	6.8	1.97	4.07	2.0

5.2 C-shaped Archetype

Three archetypes (15, 18, and 22 story) were designed using the C-shaped composite walls lateral resisting system. The floor plan used for each of the archetypes is presented in Table 5-4. Two C-shaped walls as shown in Figure 5.3 were used for lateral resistance. For the three archetype structures, C-shaped walls were designed as the uncoupled system in the north-south direction and coupled system in the east-west direction. The analysis was only conducted in the uncoupled direction. The coupled direction involves the use of different seismic performance factors compared to the uncoupled direction. A separate lateral analysis shall be performed for these walls

51

in the coupled direction. The design iteration of these walls involves the variation of flange thickness, t_f, flange width, w, web length, L_1, web thickness, t_w, and steel plate thickness, t_p. The design was selected to satisfy architectural constraints and accommodate the elevator core in between two C-shaped walls. Thicker flanges compared to web thickness were used in 22 story which helped to increase the overall stiffness and hence reduce the inter-story drift ratio of the structure while maintaining the architectural constraints. The thickness of steel plates was kept the same for web and flange plates.

Table 5-5 summarizes the dimensions of C-shaped archetype structures. Table 5-6 presents the additional information for the C-shaped composite walls including the ratio of design strength compared to the required strength and the maximum inter-story drift ratio for the equivalent lateral forces.

Table 5-4. Floor plans for C-shaped archetype structures

Case	No. of Stories	Center Bay Length, ft	Center Bay Width, ft	Length, ft	Width, ft	Story Weight, kip
5	15	30	30	210	110	2772
6	18	30	40	210	120	3024
7	22	30	40	210	120	3024

Table 5-5. C-shaped composite wall archetype structures

Case	No. of Stories	Web Depth, ft	Flange Length, ft	Web Thickness, in	Flange Thickness, in	Plate Thickness, in	Coupling Beam Length, ft
5	15	30	11	22	22	8/16	8
6	18	40	10	18	18	8/16	10
7	22	40	11	28	32	9/16	8

Table 5-6. Archetype structures - strength and inter-story drift ratio

Case	No. of Story	Height, ft	Wall Strength Margin		I_{eff}, in^4	Max. Inter-story Drift Ratio, %
			$\phi M_{n,wall}/M_{u,elf}$	$\phi V_{n,wall}/4V_{u,elf}$		
5	15	213	2.1	3.3	2.3E7	1.9
6	18	255	2.2	3.7	4.1E7	1.9
7	22	311	2.1	4.1	5.7E7	2.0

Appendix B and Appendix C in this report provide a detailed design for the 6-story planar C-PSW/CF archetype and 18-story C-shaped C-PSW/CF archetype.

6   MATERIAL MODELS FOR NONLINEAR ANALYSES

This section presents the details of steel and concrete materials nonlinear models used for the finite element model and incremental dynamic analysis.

6.1   General

OpenSees, an open-source earthquake simulation software, was used to conduct the FEMA P695 analyses. The material models present in the OpenSees element library (McKenna et al. 2016) were used to model the steel and concrete components of the composite walls. As described in Section 2.4, the FEMA P695 procedure involves a large number of analyses/simulations and needs to be repeated several times for different earthquakes records. Such a large number of analyses results in intense computation. OpenSees uses a macro fiber to model nonlinear behavior allowing rapid execution compared to other finite element software packages available. OpenSees have been utilized by several other researchers for FEMA P695 based IDA studies, e.g., (Kanvinde 2003; Rodgers et. al 2006; Lignos et. al 2008; Broberg et al. 2019).

The material models were taken from the previous research conducted on coupled composite walls (Broberg et al. 2019). The details of the material models developed for the purpose of IDA analysis are described in this section. The steel material model used for the IDA study is described in Section 6.2. The steel effective stress-strain curve was developed to account for buckling of the steel plates, low-cycle fatigue, and isotropic strain hardening. Section 6.3 presents the details of the concrete material model used for this study. The material model for concrete was developed to account for the confinement provided by steel faceplates and closure plates (Broberg et al. 2019). The behavior of the model was then verified using the existing tests on the planar composite plate shear wall conducted by Purdue University (Wang et al. 2018). These material models were derived and verified using 3D FEA in ABAQUS (Shafaei et al. 2019).

The performance of walls without the closure flange plates was also compared with walls with closure plates. A previous study (Kurt et. al 2008) showed that concrete and steel behave differently in walls with and without closure plates. Boundary elements like closure plate or a W section provide high confinement to the concrete compared to walls without any boundary

elements. Hence, a different set of steel and concrete material models were used for walls without closer plates. These parameters are presented in Chapter 11 of this report.

6.2 Steel Model

The *ReinforcingSteel* material model from OpenSees material library was used to model steel fibers in the composite wall. The model was developed based on the work of Chang and Mander (1994) and Kunnath et al. (2009). It simulates compression buckling, low-cycle fatigue, and fracture. *ReinforcingSteel* is the only material in the OpenSees library capable of accounting the steel fracture. Past experiments conducted showed that fracture rather than local buckling leads to strength degradation in the composite walls. To define the true tensile and compressive stress curve, *ReinforcingSteel* uses an effective stress-strain tensile backbone curve. Figure 6.1 represents the backbone curve compared to the engineering stress-strain curve. The parameters required to create the curve are yield stress, f_y, ultimate stress, f_u, initial Young's modulus, E_s, Modulus at strain hardening, E_{sh}, strain corresponding to initial strain hardening, ε_{sh}, and ultimate strain at peak stress, ε_u.
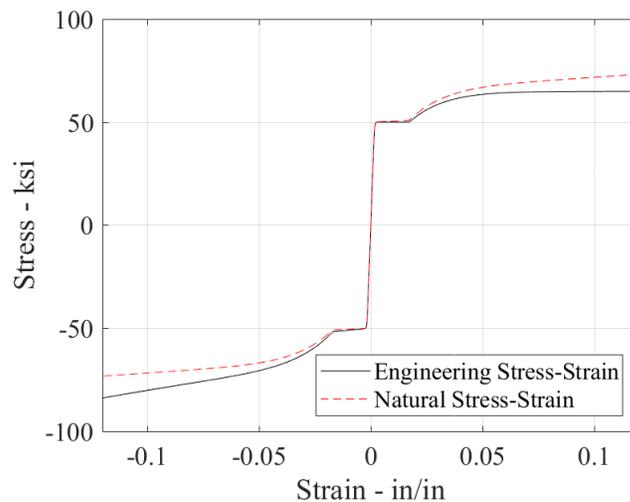
Figure 6.1. Steel backbone curve

6.2.1 Compression Buckling

The buckling model of *ReinforcingSteel* material was based on Gomes and Appleton (1997). This model considers four parameters to model the buckling behavior in steel. These parameters are slenderness ratio, l_{SR}, amplification factor, β, buckling reduction factor, **r**, and a buckling constant,

γ. The slenderness ratio, l_{SR}, for buckling of steel fibers is defined as the ratio of unsupported length, L_u, and diameter of re-bars, d_b, as shown in Equation 5.1.

$$l_{SR} = \frac{L_u}{d_b}$$ (6.1)

The unsupported length, L_u, of steel modules in the composite walls was taken as the spacing between the tie bars. The re-bar diameter, d_b, was taken to be the effective bar diameter, $d_{b,eff}$, determined by equating radius of gyration of the steel plate of the walls to the radius of gyration of a re-bar having $d_{b,eff}$. The effective re-bar diameter can be determined using Equation 6.2a and 6.2b as shown below.

$$I_{plate} = \frac{bt_p^3}{12(1 - v^2)}$$ (6.2a)

$$I_{rebar} = \frac{\pi d_b^4}{64}$$ (6.2b)

Figure 6.2 describes the use of the amplification factor, β, buckling reduction factor, r, and the buckling constant, γ. The amplification factor, β, scales the buckling curve and adjusts the location of the bifurcation point. The buckling reduction factor, r, helps to adjust the shape of the post-buckling curve. The value of r ranges between 0 to 1, with 1.0 representing unbuckled shape. The buckling constant, γ, helps in the imitation of buckling by reducing the stresses after γf_{su}. Figure 6.3 shows the effect of the variation of sample parameters on the buckling model. The values of buckling parameters used for the nonlinear model are defined in Chapter 8.

$$\Omega_b = \beta \frac{\sqrt{32}}{3\pi l_{SR}\sqrt{\varepsilon_s - \varepsilon_o}}$$

$$\sigma_b = \gamma f_u - \frac{\Omega_b + \gamma}{1+\gamma}(\gamma f_u - \sigma)$$

$r = 0.0$

$r = 0.5$

$r = 1.0$ Unbuckled σ vs. ε
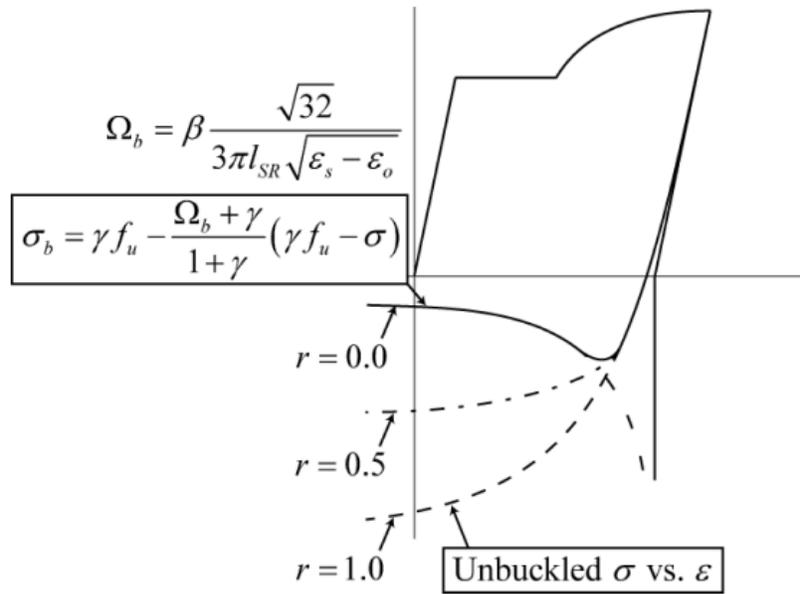
Figure 6.2. Buckled stress-strain curve (McKenna et al. 2016)
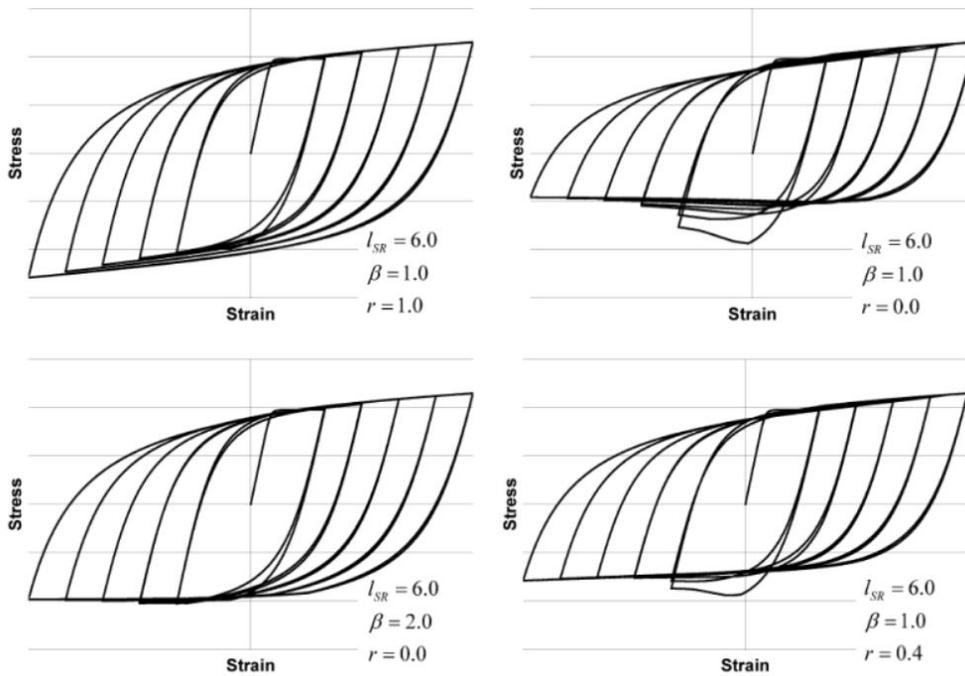
Figure 6.3. Effect of change in sample parameters on buckling model (McKenna et al. 2016).

6.2.2 Low-Cycle Fatigue

The strength degradation in composite walls is caused mainly due to the progress of fracture across the wall cross-section. The *ReinforcingSteel* model uses the Coffin-Mansion fatigue life equations (Coffin 1954; Manson 1965; Coffin 1971) to model low-cycle fatigue, shown in Equation 6.3. Here $\Delta\varepsilon_P$ represents the plastic strain amplitude; $2N_f$ (Equation 6.4) represents the number of half-cycles to failure; ε_f' represents the fatigue ductility coefficient; α represents the fatigue ductility exponent.

$$C_f = \Delta\varepsilon_P = \varepsilon_f' * (2N_f)^\alpha \tag{6.3}$$

$$2N_f = N_{HalfCycles} \tag{6.4}$$

The amplitude of the plastic strain half cycle, ε_p, in tension and compression is measured by Equation (6.5). The total number of half-cycles to failure is calculated in Equation 6.4. The cumulative damage factor, D_f, at various stages of half-cycles is determined using Equation 6.8. The cumulative damage factor, D_0, of zero is applied to the fiber prior to the start of the application of strains. The final cumulative damage factor is 1.0 at fracture and once the steel fracture the stress carrying capacity rapidly degrades to zero.

$$\Delta\varepsilon_P = \varepsilon_t - \frac{\sigma_t}{E_S} \tag{6.5}$$

$$N_{HalfCycles} = \left(\frac{\Delta\varepsilon_P}{\varepsilon_f'}\right)^{-\frac{1}{\alpha}} \tag{6.6}$$

$$D_i = \left(\frac{1}{N_{HalfCycles}}\right) \tag{6.7}$$

$$D_f = \Sigma D_i \tag{6.8}$$

where $\Delta\varepsilon_p$ is the plastic strain amplitude, ε_t is the total strain, σ_t is the stress amplitudes per cycle, C_f and α are material constants, D_i is the fatigue damage per cycle, and D_f is the cumulative fatigue damage.

The *ReinforcingSteel* model also implements strength degradation linked to damage caused by fatigue. The cumulative strength degradation is proportional to the cumulative fatigue damage. The strength degradation is measured in terms of the per cycle loss of strength, f_{SR}, per Equation 6.9 (Kunnath et al. 2009).

$$\sum_{i=1}^{n}(f_{SR})_i = Z_d * D_f \tag{6.9}$$

6.2.3   Isotropic Strain Hardening

The *ReinforcingSteel* material also accounts for isotropic hardening and diminishing yield plateau. Hardening constant, a1, and hardening limit, *HL*, are used to define the hardening and yield plateau and to calculate the hardening factor, *HF* (Equation 6.10a). The stress-strain relationship in the region after the initiation of strain hardening is calculated based on Equation 6.11a and 6.12.

$$HF = 1.0 - a1 * \Delta\varepsilon_p \tag{6.10a}$$

$$if \ HF < HL \ then \ HF = HL \tag{6.10b}$$

$$if \ HF > 1.0 \ then \ HF = 1.0 \tag{6.10c}$$

$$\varepsilon_{sh\_location} = \varepsilon_y + HF * (\varepsilon_{sh} + \varepsilon_y) \tag{6.11a}$$

$$\varepsilon_{sh} = log(1.0 + \varepsilon_{sh\_location}) \tag{6.11b}$$

$$f_{shp} = f_y * (1.0 + \varepsilon_{sh\_location}) \tag{6.12}$$

6.3   Concrete Model

The *Concrete02* material model from the OpenSees material library was used for the composite walls. This model is based on the work of Hisham and Yassin (1994). It accounts for the effect of confinement provided by steel module, tension stiffening, degradation of stiffness in unloading and reloading curves, cyclic lading hysteretic response, and concrete crushing. The material model is computationally efficient and requires less memory compared to other materials like ConcreteCM present in OpenSees material library. Figure 6.4 shows the stress-strain curve definition and parameters required for the Concrete02 model definition. The parameters required

are concrete compressive strength, f_{pc}; strain at compressive strength, ε_0; crushing strength, f_{pcU}; strain at crushing strength, ε_U; the ratio between unloading slope at ε_U and initial slope $(2*f_{pc}/\varepsilon_0)$, lambda; tensile strength, f_t; and tension softening stiffness, E_{ts}. The values used for the concrete model were taken from the works of Broberg and Soheil (2018).
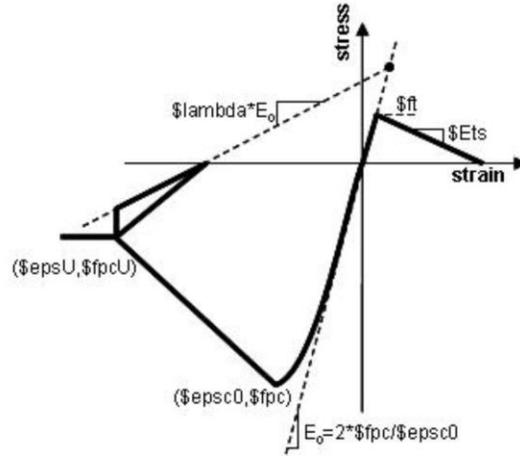
Figure 6.4. *Concrete02* model in OpenSees (McKenna et al. 2016)

The steel faceplates and closure plates help to provide confinement to the infill concrete. The confined concrete model was developed based on the work of Susantha et al. (2001) on confined concrete uniaxial stress-strain for concrete-filled steel tubes. Susantha et al. model provided an empirical formula as shown in Equation 6.13 to calculate the strength of the confined concrete, f'_{cc}. Here f'_c is the strength of the unconfined concrete, f_{rp} is the maximum radial pressure on infill concrete, and m is an empirical coefficient taken as 4.0. A reduction factor of 0.85 is applied on the strength of unconfined concrete, f'_c.

$$f'_{cc} = f'_c + m * f_{rp}$$

(6.13)

7 MODEL BENCHMARKING AND CALIBRATION

This section presents the details of the numerical calibration of the planar and C-PSW/CF.

7.1 General

The OpenSees steel and concrete materials used for the nonlinear model and Incremental Dynamic Analysis are described in Chapter 6. The model calibration and verification were done using existing experimental results for the planar walls performed by Wang et. al (2018). Five planar composite walls (SP1 to SP5) were tested, and the results of the test specimens and the final calibrated parameters are summarized in this section. The test walls were subjected to axial (compression) and lateral (monotonic and cyclic) load. These walls had a length of 36 in. and a height of 108 in. resulting in an h/L ratio of 3. The steel faceplate and closure plates were 3/16 in. thick and the infill concrete had a thickness of 9 in. The details on axial compression and steel and concrete material are presented in Table 7-1. Two different material models were developed. The assumed stress-strain curves, presented in Figure 7.1, for the steel and concrete were built to match the effective stress-strain curves form the 3D ABAQUS model. These assumed curves follow the material behavior but are slightly more conservative than the effective stress-strain curve. Although the effective stress-strain curve provides a better representation of the behavior, the assumed stress-strain curve is conservative, and it saves a significant amount of computation time. The assumed material effective stress-strain curve for steel and concrete is discussed further in this section.

Table 7-1. C-PSW/CF Test Walls SP1 to SP5

#	Name	P applied, kip	Day of Testing Concrete Strength, ksi	3/16" Plate Fy, ksi	3/16" Plate Fu, ksi
SP1	CW-42-55-10-T	210.0	6.5	61.2	71.0
SP2	CW-42-55-20-T	505.0	7.8	61.2	71.0
SP3	CW-42-14-20-T	560.0	8.7	61.2	71.0
SP4	CW-42-14-20-TS	540.0	8.4	61.2	71.0
SP5	CW-42-55-30-T	710.0	7.4	61.2	71.0

7.2   Proposed Material Models

The *ReinforcingSteel* material as described in Section 6.2 was used to model steel faceplates and closure plates. The steel model was developed to include Coffin-Manson fatigue degradation and fracture, Gomes-Appleton buckling, and isometric hardening. The steel in tension was considered as elastic-plastic with strain hardening and the steel in compression was considered as elastic-plastic response. The infill concrete was modeled using *Concrete02* material from OpenSees library as described in Section 6.3. The concrete compression uniaxial effective stress-strain is developed based upon confined concrete ascending and descending branches by Tao et al. (2013). In the descending branch, the concrete strength reduces to 60% of capacity f_c' and becomes constant to account for the effect of confinement provided by steel modules. Figure 7.1 shows the proposed effective stress-strain for steel in compression and tension and concrete in compression.

(a)   (b)
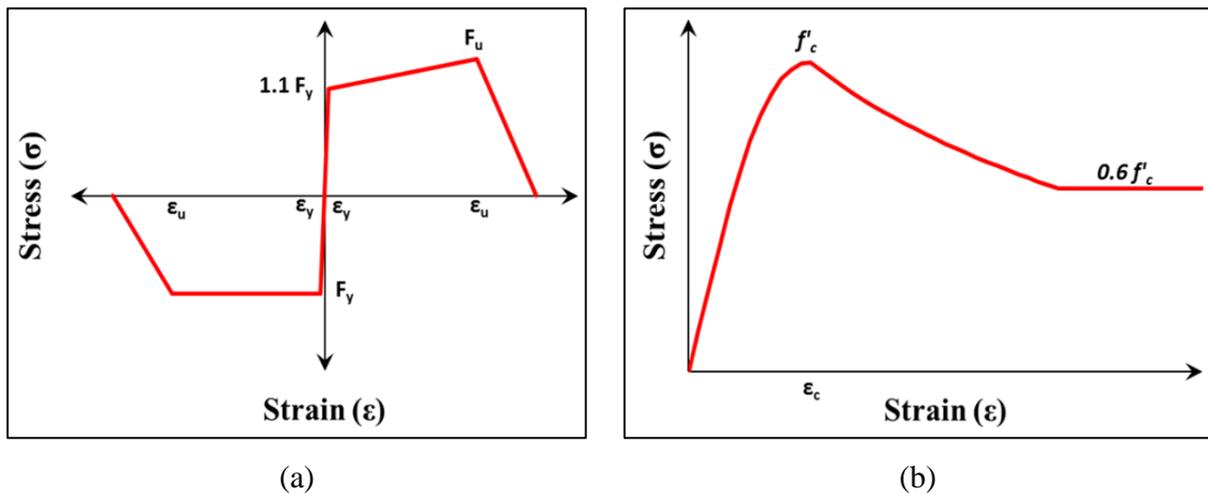
Figure 7.1. Proposed effective steel stress-strain curve for (a) steel and (b) concrete (Soheil et al. 2019, Broberg et al. 2019)

7.3   OpenSees Material Model and Parameters

The OpenSees proposed material models as presented in Figure 7.1 were used to model this behavior. Table 7-2 and Table 7-3 present the OpenSees material parameters used to develop the assumed stress-strain relationships for steel and concrete, respectively. Figure 7.2 and Figure 7.3 show the comparison of the assumed stress-strain curve (OpenSees material behavior) developed using the above material parameters and ABAQUS FEA model for steel and concrete, respectively.

This material behavior was then used to create OpenSees fiber models and benchmark its behavior with the experimental results conducted on planar walls.

Table 7-2. Steel material parameters for assumed stress-strain curves

Parameter	Value	Parameter	Value
E (ksi)	29000	L_{sr}	20.8
b	0.025	beta	1
E_{sh} (ksi)	725.0	r	0.8
F_y (ksi)	60.0	gamma	0.5
F_u (ksi)	71.0	C_f	0.3
e_{sh}	0.003	alpha	0.52
e_{ult}	0.153	C_d	0.32
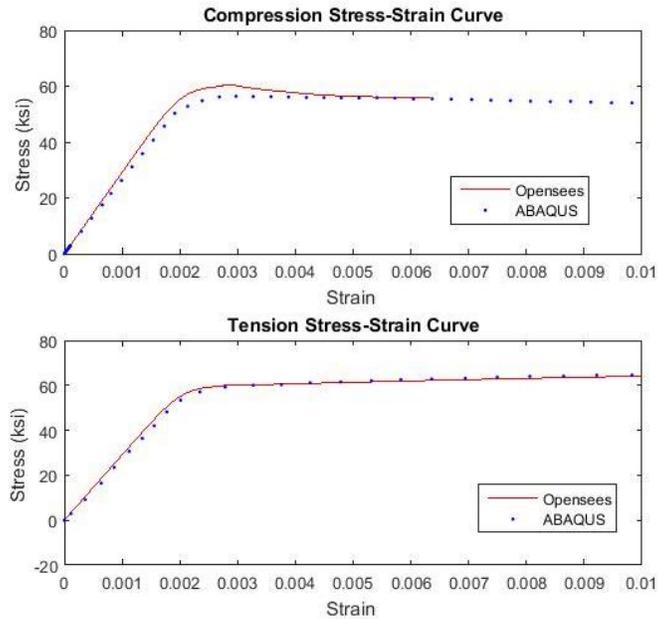
Figure 7.2. Comparison between steel effective steel stress-strain curve in OpenSees to the model developed in Abaqus (Broberg et al., Soheil et al. 2019)
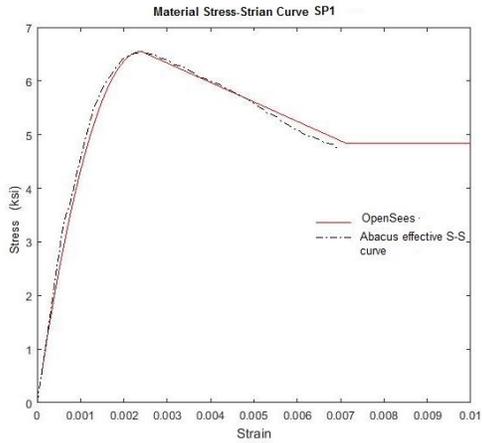
(a)
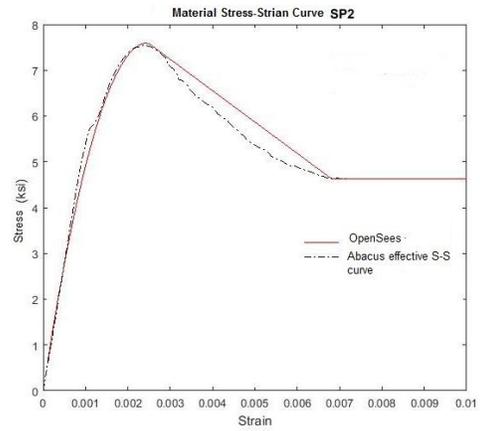
(b)
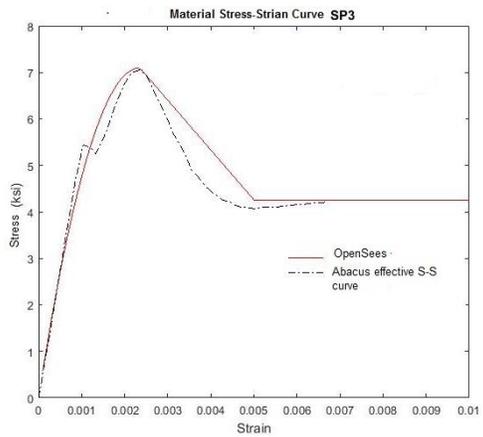
(c)
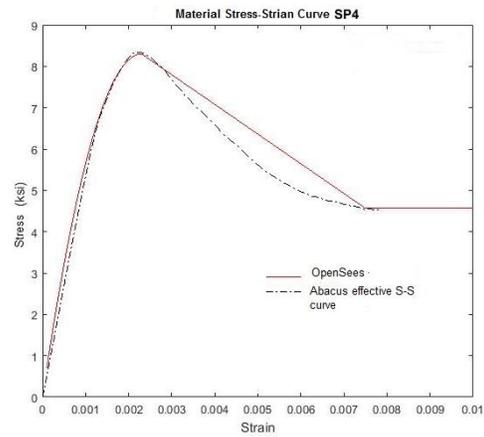
(d)
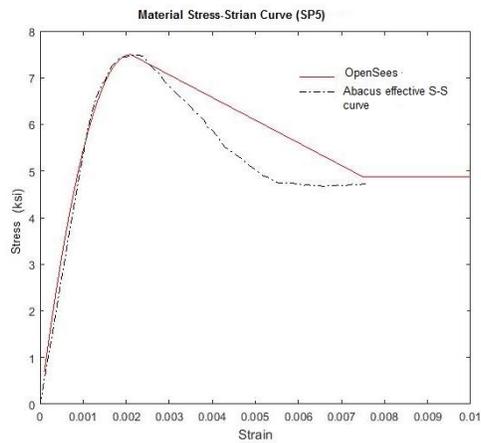
(e)

Figure 7.3. Comparison between concrete effective stress-strain curves in OpenSees to material models developed in Abaqus (a) SP1; (b) SP2; (c) SP3; (d) SP4; (e) SP5 (Soheil et al., Broberg et al. 2019)

Table 7-3. Concrete material parameters for assumed stress-strain curves

	SP1	SP2	SP3	SP4	SP5
F_{pc} (ksi)	6.5	7.8	8.7	8.4	7.4
e_{psc0}	0.0023	0.0025	0.0026	0.0026	0.0024
F_{pcu} (ksi)	3.9	4.7	5.3	5.1	4.4
e_{psu}	0.0071	0.0071	0.0071	0.0071	0.0071
E_{ts}	4566	4996	5292	5190	4865

7.4 Element Distribution

The OpenSees model was developed using the assumed material model discussed previously. The test results of planar walls showed that the inelastic behavior of composite walls was limited to a height of half of the wall width. The OpenSees model was divided into the nonlinear and elastic region where the nonlinear effect was limited to half of the wall length from the base and the rest of the wall was assumed elastic. Three elements were used in the plastic hinge zone. Three elastic elements were used for the rest of the wall above the nonlinear range.

7.5 OpenSees model and Test Data Comparison

Based on the material models and element distribution, the OpenSees models were created to replicate the behavior of the test walls. Figure 7.4 shows the comparison of force versus displacement curve of the SP1 test specimen to the behavior obtained from OpenSees models with an effective stress-strain curve and assumed the stress-strain curve, respectively. The OpenSees material model was based on the assumed stress-strain curves (Figure 7.1) mentioned above. The proposed stress-strain curve provided a conservative estimate in terms of strength compared to the effective stress-strain curve as seen in Figure 7.4. The use of the proposed curve is justified as it limits the capacity and performance as well as helps to significantly reduce the computation time required to run a large number of analyses. Figure 7.5 shows the comparison of the force-displacement curve of the OpenSees model and the test specimens SP2, SP3, SP4, and SP5. The benchmarking results suggest that the proposed material models used to develop the OpenSees model provides conservative behavior and would result in more critical performance factors. The

actual structure wall have slightly better performance than the behavior showcased by the OpenSees model using proposed steel and concrete material behavior.
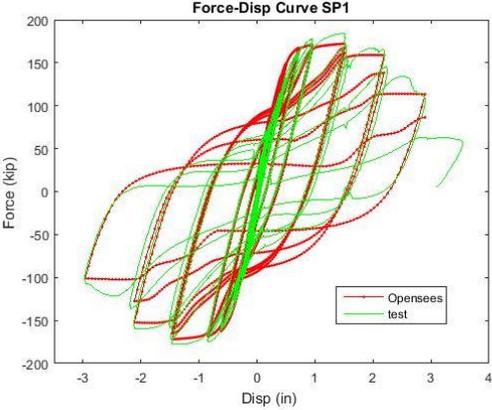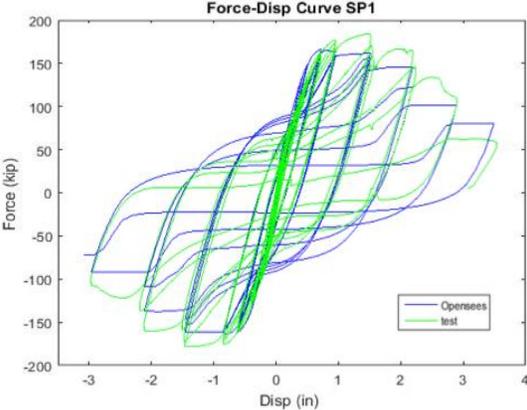
(a)   (b)

Figure 7.4. Force versus displacement curves for SP1. (a) Matching effective stress-strain curves; (b) Matching assumed stress-strain curves (Broberg et al. 2019)
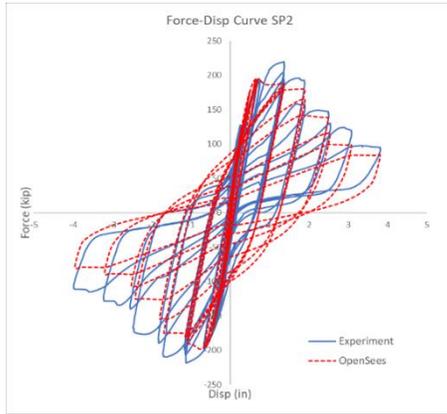
(a)
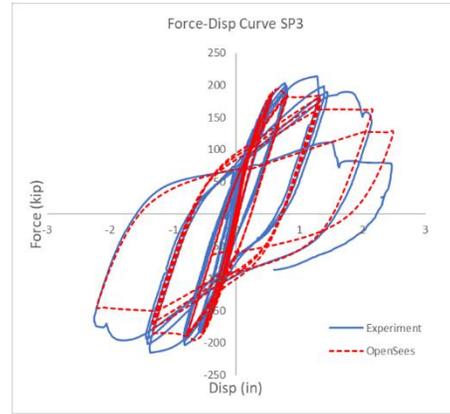
(b)
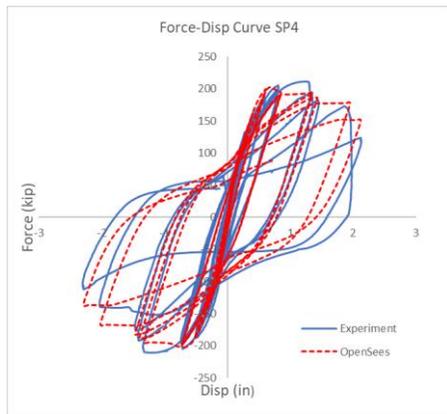
(c)
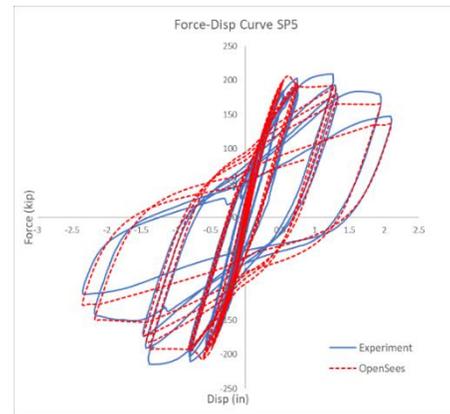
(d)

Figure 7.5. Force-Displacement comparison using assumed effective stress-strain curves for
(a) SP2; (b) SP3; (c) SP4; (d) SP5 (Broberg et al. 2019)

8 OPENSEES MODEL

This chapter presents the details of the OpenSees FEA fiber model build for planar and C-shaped composite walls. This model was used for nonlinear and dynamic analyses and, ultimately, to evaluate the performance of the archetype structures.

8.1 Steel and Concrete Material Parameters

As discussed in Section 7.3, the steel faceplates and closure plates were modeled using the *ReinforcingSteel* material model and the infill concrete was modeled using the *Concrete02* material model. These material models are implemented in a 2D finite element OpenSees model. The material stress-strain curves discussed in Chapter 7 were used to model steel and concrete behavior. The steel material strength, buckling, and fatigue parameters are listed in Table 8-1. A yield strength, F_y, of 50 ksi and ultimate strength, F_u, of 65 ksi was used. This model implemented the specified yield (F_y) and ultimate strength (F_u) and did not use expected values (i.e. $R_y F_y$). Figure 8.1 shows the steel material model used to model the OpenSees wall. The concrete material parameters used to model the infill concrete are listed in Table 8-2. The compressive strength of concrete, f'_c, was taken as 6 ksi with residual stress capacity of $0.6f'_c$. Figure 8.2 shows the concrete material model used to model the OpenSees wall.

| (a) | (b) |
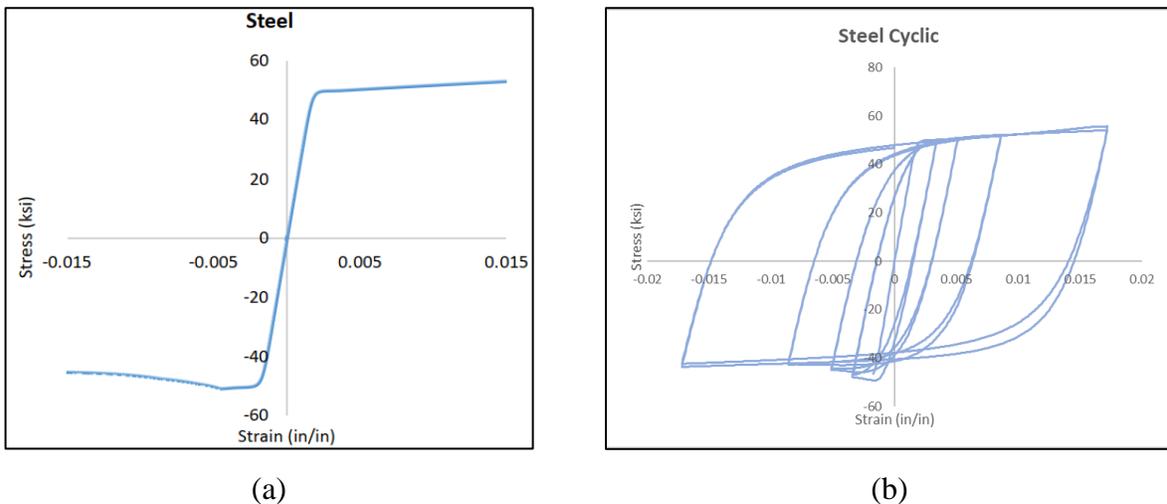
Figure 8.1. Steel material behavior (a) Monotonic stress-strain curve; (b) Cyclic behavior

Table 8-1. Steel material parameters used for OpenSees wall model

Parameter	Symbol	Value
Modulus of elasticity	E (ksi)	29000
Hardening ratio	b	0.01
Initial strain hardened tangent	E_{sh} (ksi)	290
Yield stress in tension	F_y (ksi)	50.0
Ultimate stress in tension	F_u (ksi)	65.0
Strain at the start of strain hardening	e_{sh}	0.003
Strain at peak stress	e_{ult}	0.1
Buckling Parameters		
Slenderness Ratio	L_{sr}	10
Buckled stress-strain curve Amplification factor	beta	1
Buckling reduction factor	r	0.65
Buckling constant	gamma	0.5
Fatigue Parameters		
Coffin-Manson Constant	C_f	0.6
Coffin Manson Constant	alpha	0.5
Cyclic strength reduction factor	C_d	0.35

Table 8-2. Concrete material parameters used for OpenSees wall model

Parameter	Symbol	Value
Compressive strength	f'_c (ksi)	-6
Strain at compressive strength	e_{c0}	-0.002
Initial modulus of concrete	E_c (ksi)	$57 \times \sqrt{f'_c}$
Concrete crushing strength	f'_{cu} (ksi)	3.6
Ratio of unloading and loading slope	lambda	0.1
Strain at concrete crushing	e_{final}	-0.008
Tension Parameters		
Tensile strength	f'_t (ksi)	$-0.1 \times f'_c$
Strain at the tensile strength	e_t	0.00008
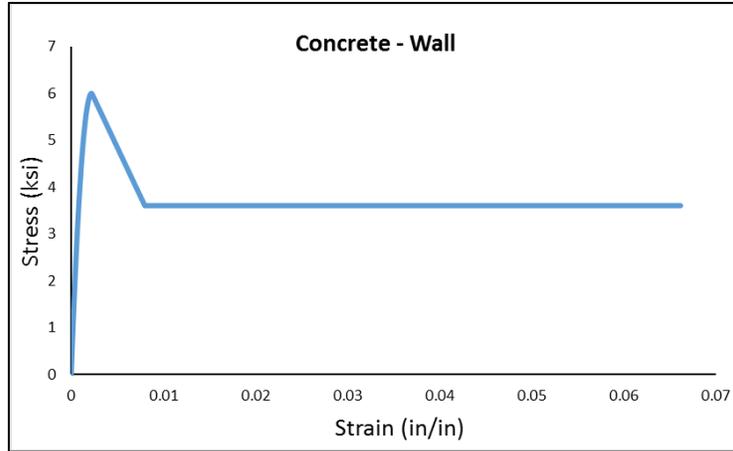
Figure 8.2. Concrete material behavior

8.2 Fiber Model

The steel and concrete material models mentioned in Section 8.1 were used to create a 2D fiber-based model for the archetype structure. This model consisted of nonlinear fiber elements for the base of the wall and elastic elements for the remainder of the wall. Figure 8.3 depicts the OpenSees model configuration used to model the 6-story archetype structure. This model is divided into two main components: (1) the composite wall fiber element and (2) the P-Delta column.

(a) (b)
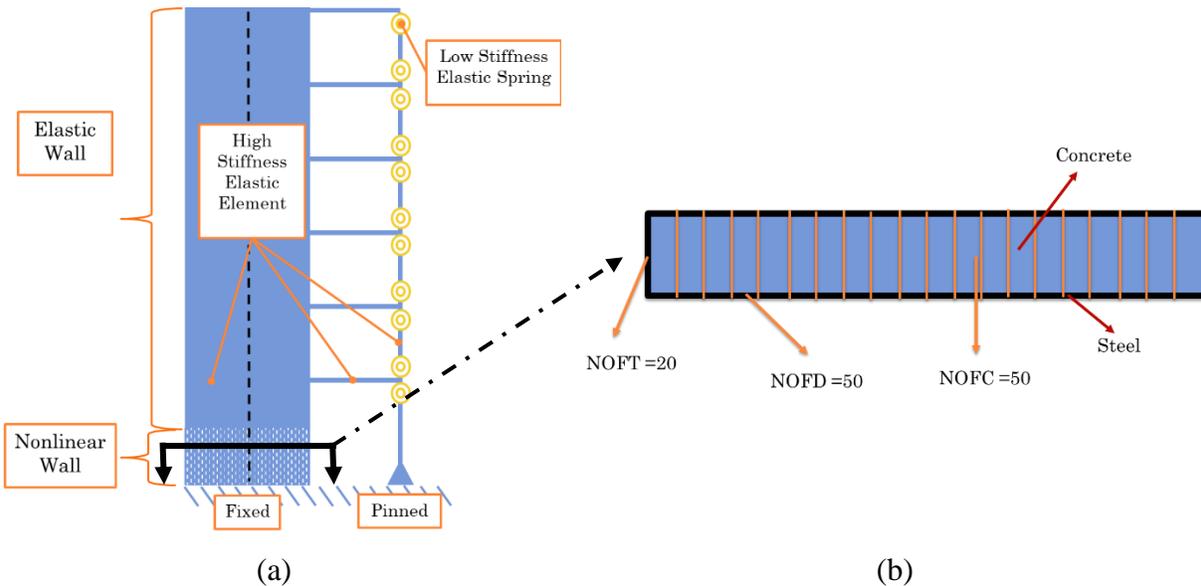
Figure 8.3. OpenSees model for 6 story archetype structure (a) Elevation view; (b) Wall cross-section

8.2.1 Wall Element

As shown in Figure 8.3, the OpenSees model has nonlinear fiber elements defined at the base and elastic elements at the top. The wall was fixed at the base. The nonlinear wall elements extended to the minimum of half of the wall length or the height of the first story (17ft). The nonlinear fiber cross-section was developed using the nominal properties of steel and concrete materials discussed in Section 8.1. Figure 8.3b shows the cross-section and fiber distribution of the nonlinear wall elements. Four displacement-based fiber elements at an equal distance were used to model the nonlinear part of the wall. The rest of the composite wall was modeled using the elastic elements. The elastic elements used the effective stiffness EI_{eff} as estimated in Section 3.3.3. The gross properties of the composite wall were used to define the axial and shear stiffness of the elastic element. One elastic element at each floor was used to model the elastic portion. The tributary mass was applied at each story level.

8.2.2 P-Delta Columns

The P-delta columns were used to represent the weight of the remainder of the building. The configuration of the p-delta column used in the OpenSees model is shown in Figure 8.3. The P-delta columns elements are high stiffness elastic elements. The two P-delta elements were connected to each other using two low stiffness elastic spring elements. The low stiffness springs prevented any transfer of moment from one P-delta column element to the other. The P-delta column was pinned at the base of the structure to prevent the P-delta columns from contributing to the moment resistance of the system. The P-delta column elements were connected to the wall elements using elements with high elastic stiffness. The gravity load was applied to the P-delta columns at the nodes of each story level.

9 PLANAR COMPOSITE WALLS ANALYSIS AND RESULTS

This chapter presents the nonlinear static pushover and incremental dynamic analysis study conducted on the planar composite walls. It also summarizes the results of collapse assessment and performance evaluation of the planar walls.

9.1 General

Section 2.4.3 discusses the key components which are required to perform collapse assessment of the composite wall system. The details of each of the four planar composite walls archetypes are discussed in Chapter 5. The design and sizing details of planar walls archetype are discussed in Table 5-1 and Table 5-2. Planar composite wall archetypes. The calibrated steel and concrete material models used for the OpenSees analysis are described in Chapters 6 and 7. The details of the OpenSees fiber model used for the nonlinear analyses are described in Chapter 8. Chapter 9 presents the nonlinear analysis and the collapse assessment of the planar wall archetypes.

9.2 Nonlinear Pushover (Static) Analysis

The nonlinear static pushover analyses to estimate the overstrength factor, Ω_0, and period-based ductility, μ_t, was conducted in compliance with FEMA P695 approach as described in Section 2.4.1. The results of the pushover analyses of 3-story, 6-story, 9-story, and 12-story archetypes are presented below. Figure 9.1 to Figure 9.4 provide base shear versus IDR plot, base shear versus maximum IDR plot, and moment versus roof displacement plot for the 3-story, 6-story, 9-story, and 12-story archetypes, respectively.

(a)

(b)

(c)
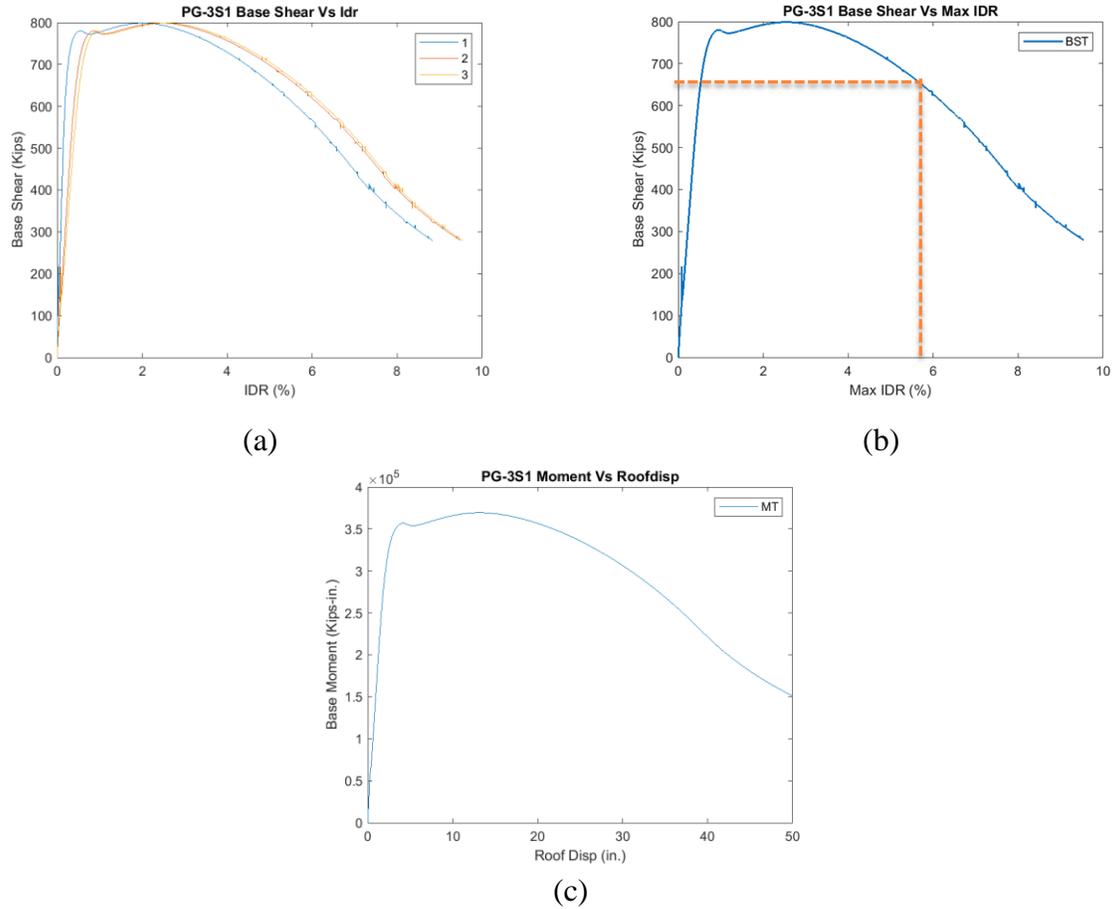
Figure 9.1. Pushover analysis results for 3-story archetype (a) Base shear vs. IDR; (b) Base shear vs. maximum IDR; (c) Moment vs. roof displacement

(a)

(b)
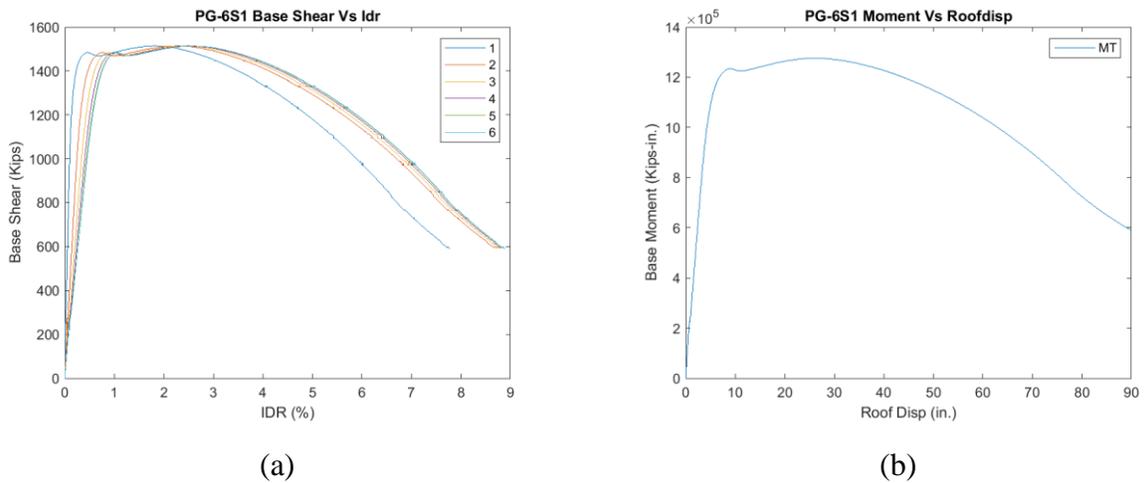
Figure 9.2. Pushover analysis results for 6-story archetype (a) Base shear vs. IDR; (b) Moment vs. roof displacement
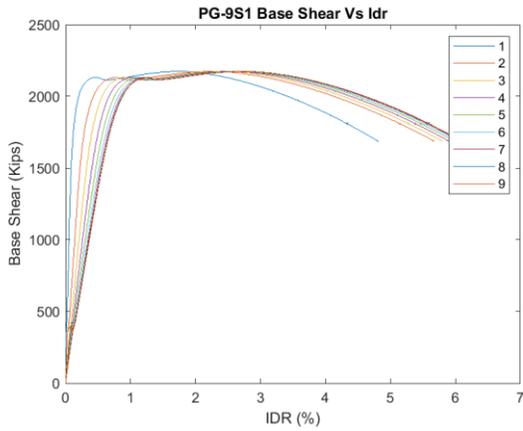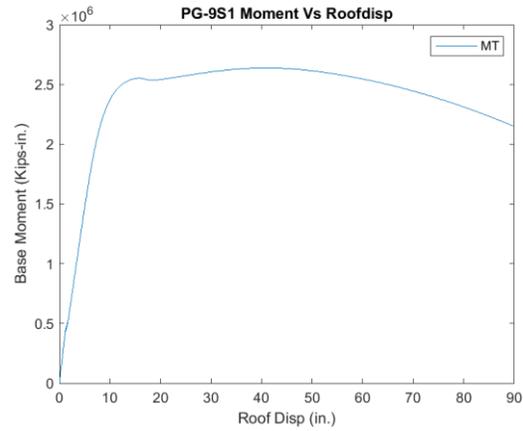
(a)   (b)

Figure 9.3. Pushover analysis results for 9-story archetype (a) Base shear vs. IDR; (b) Moment vs. roof displacement
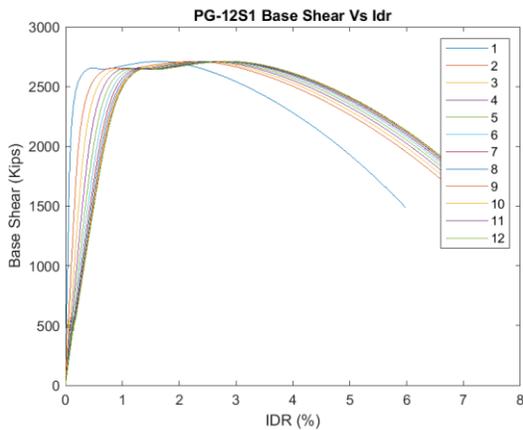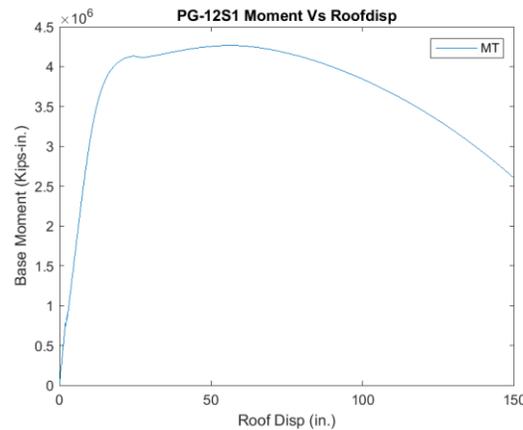
(a)   (b)

Figure 9.4. Pushover analysis results for 12-story archetype (a) Base shear vs. IDR; (b) Moment vs. roof displacement

Figure 9.5 shows base shear versus roof displacement plots for the 3-story, 6-story, 9-story, and 12-story archetypes. It also provides the estimate of maximum base shear, V_{max}, ELF base shear demand, V_{ELF}, and ultimate roof displacement, δ_u (at 80% remaining capacity). These values are then used to calculate the overstrength factor, Ω_0, and period-based ductility, μ_t.
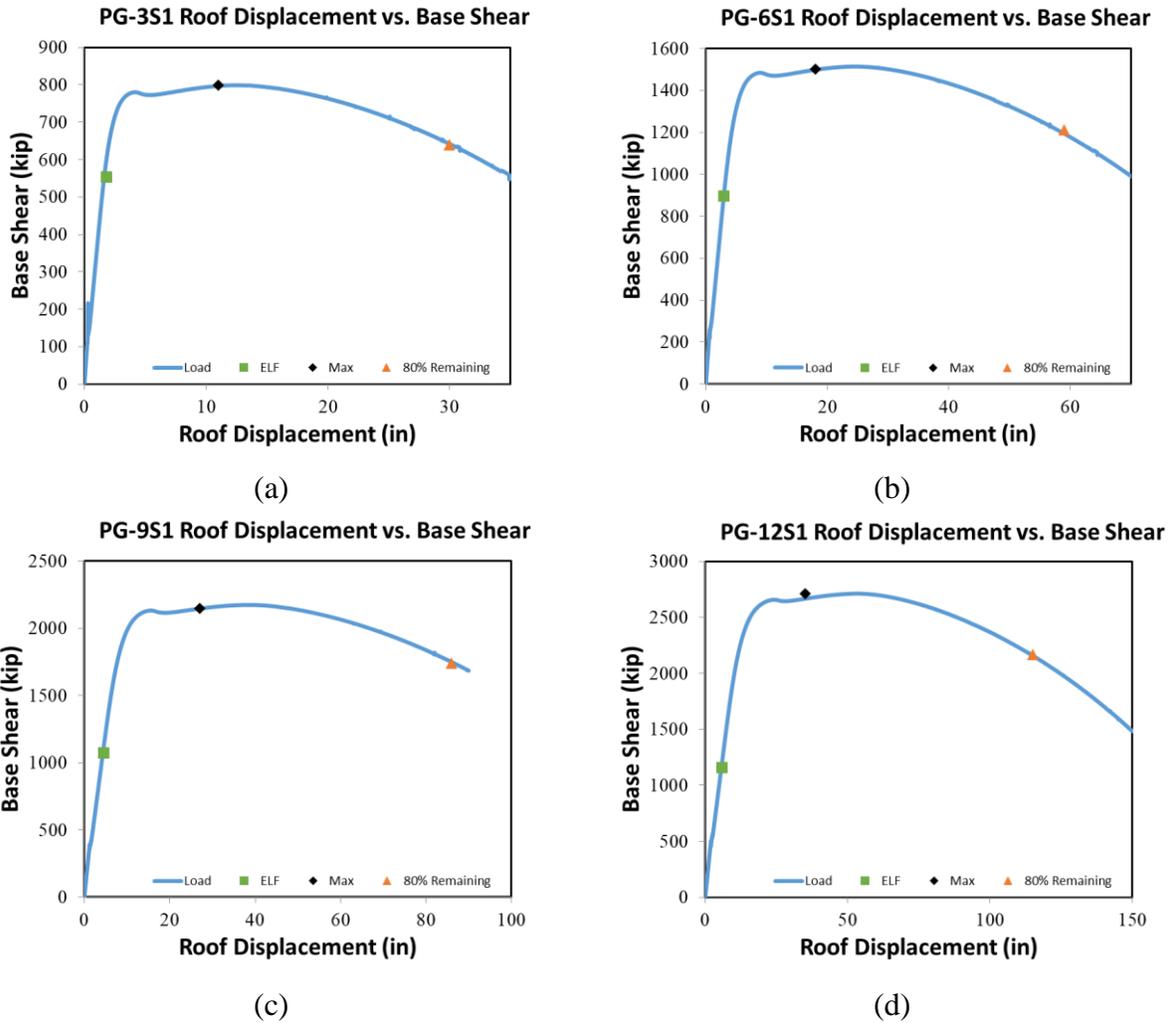
Figure 9.5. Maximum base shear capacity, ELF displacement and ultimate displacement (a) 3S1; (b) 6S1; (c) 9S1; (d) 12S1

The nonlinear pushover analysis results of the planar archetypes are presented in Table 9 1. The maximum base shear, V_{max}, ELF base shear demand, V_{ELF}, increased from 3S1 to 12S1. The ultimate roof displacement, δ_u, and the yield roof displacement, δ_y, also increased from 3S1 to 12S1. The overstrength factor, Ω, increased from 3S1 to 12S1. These is consistent with the increase in the flexural wall strength margin observed in Table 5-3. The period-based ductility which is the ratio of ultimate roof displacement to yield roof displacement decreased from 3S1 to 12S1 as the rate of increase to the ultimate roof displacement was less than that of yield roof displacement. Similar behavior is observed for C-shaped archetype which is discussed in Chapter 10.

Table 9-1. Pushover analysis results for planar archetype structures

Structure	V_{ELF}, (kips)	V_{max}, (kips)	$\delta_{y, eff}$, in	δ_u, in	Overstrength, Ω	Period-based ductility, μt
3S1	553	799	1.2	30	1.44	25.1
6S1	897	1514	2.4	58	1.69	24.1
9S1	1074	2175	4.4	86	2.02	19.7
12S1	1160	2710	6.7	115	2.34	17.2
				Avg	1.87	21.5

9.3   Incremental Dynamic Analysis

The incremental dynamic analyses (IDA), as described in Section 2.4.2, are conducted in compliance with the approach prescribed in FEMA P695 methodology. IDA is used to determine the median collapse intensity, S_{CT}, and collapse margin ratio, *CMR*. The IDA analyses are performed for 44 ground motion specified in FEMA P695. An example of the incremental dynamic analysis of the 6-story archetype for the 1994 Northridge earthquake (NGA record seq. no. 953) is presented here to describe the process used to estimate the collapse margin ratio. This process is repeated for all ground motion records for each archetype structure and the results are summarized later in this section. Figure 9.6 shows the variation of roof displacement and inter-story drift ratio of the 6-story archetype structure when it is subjected to the scaled 1994 Northridge ground motion record. This scaled ground motion resulted in a maximum IDR of 0.8% at the top level of the wall as marked in Figure 9.6a. The ground motion record is scaled up, and the analysis is repeated until the defined collapse level is reached. The maximum archetype structure IDR caused by the given ground motion record is obtained for each of the scaling intensity. Figure 9.7 shows the plot between the scale factor and the maximum inter-story drift. Figure 9.8 shows the plot between the spectral acceleration and the maximum inter-story drift.

The process is repeated for all other far-field ground motions, and the spectral acceleration vs. the maximum inter-story drift ratio for each of the 44 far-field ground motion is obtained. Figure 9.9 illustrates the combined spectral acceleration vs. maximum IDR plot for all of the 44 ground motion records. The median spectral acceleration collapse intensity is then obtained as the spectral acceleration resulting in the collapse of the archetype structure for half of the ground motion

76

records, i.e. 22 of 44 records for a given collapse criterion (i.e. 3%). The median collapse intensity for a 3% collapse criterion was determined to be 2.0 and is represented by the red line in Figure 9.9.
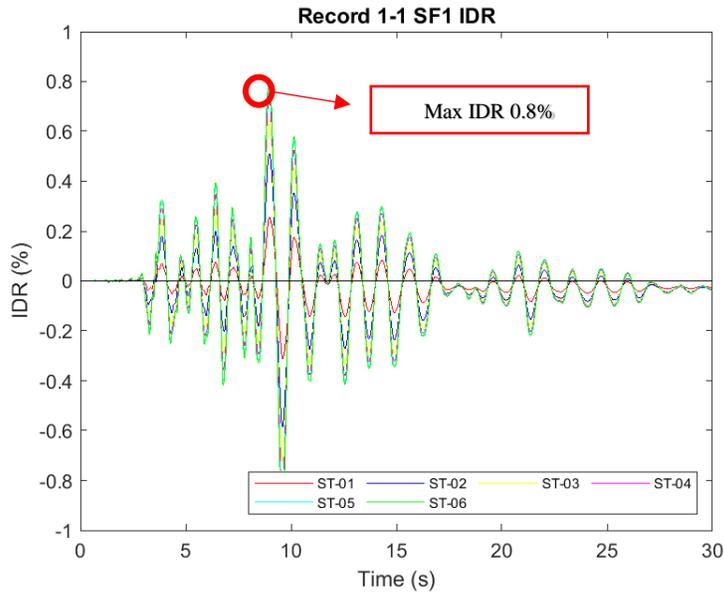
(a)
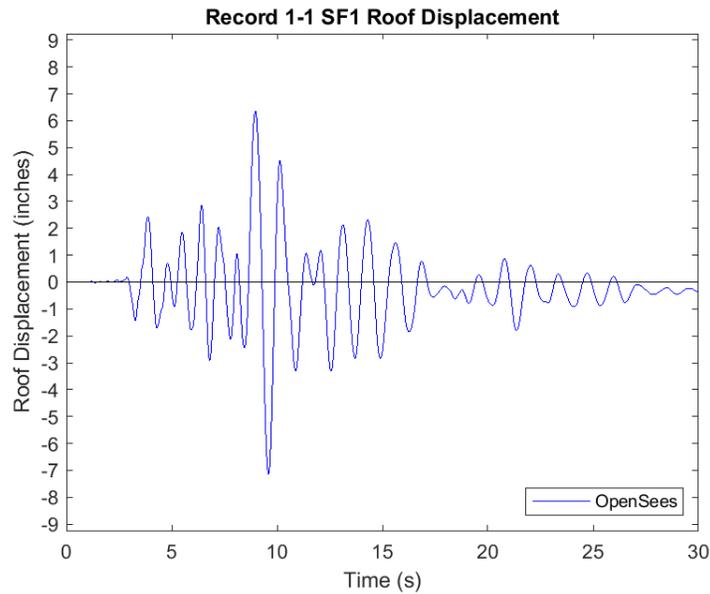
(b)

Figure 9.6. Response history analysis for 6-story archetype (a) IDR vs. time (s); (b) Roof displacement vs. time
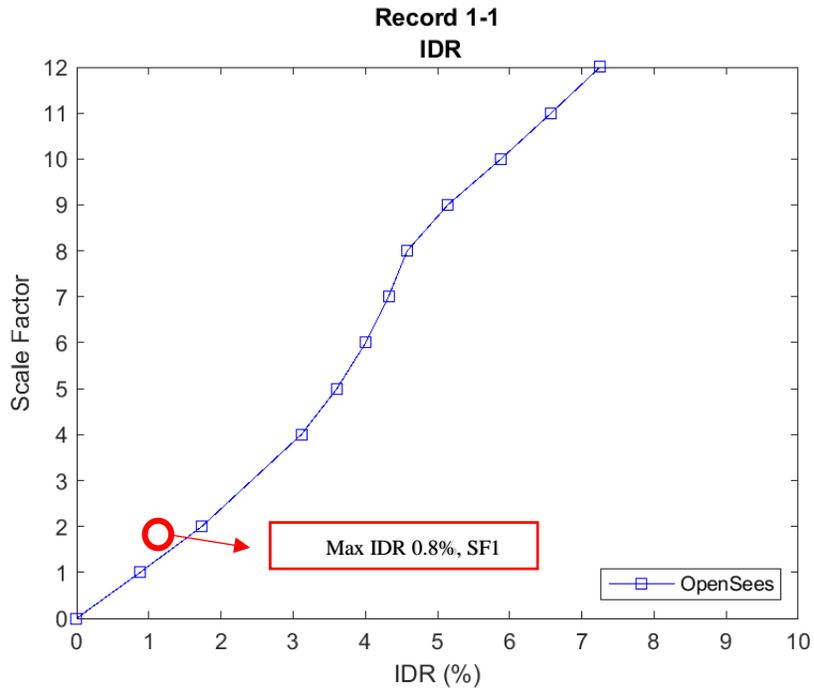
Figure 9.7. 6-story archetype scale factor vs. IDR
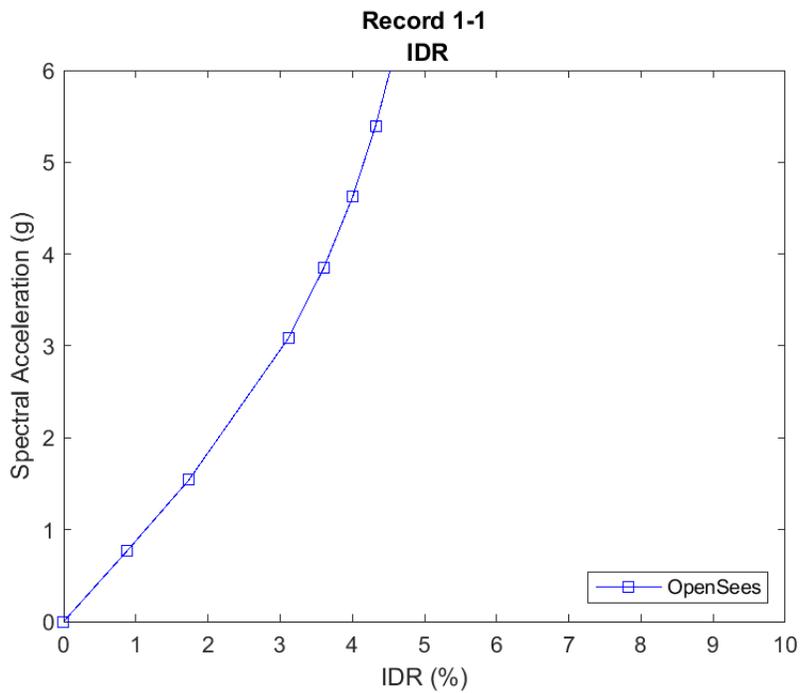
Figure 9.8. 6-story archetype spectral acceleration vs. IDR
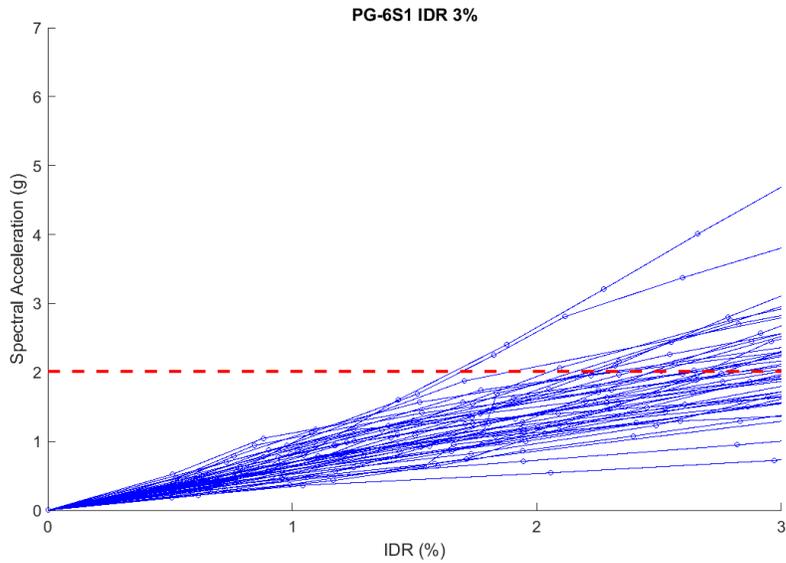
Figure 9.9. 6-story archetype IDA plot, spectral acceleration vs. IDR

The whole procedure mentioned above is repeated for all the other archetypes.

Figure 9.10 to Figure 9.14 illustrates the spectral acceleration vs. maximum inter-story drift ratio plot and cumulative failure probability vs. spectral acceleration for 3-story, 6-story, 9-story, and 12-story. These figures are provided considering different levels of collapse criterion.

(a)

(b)
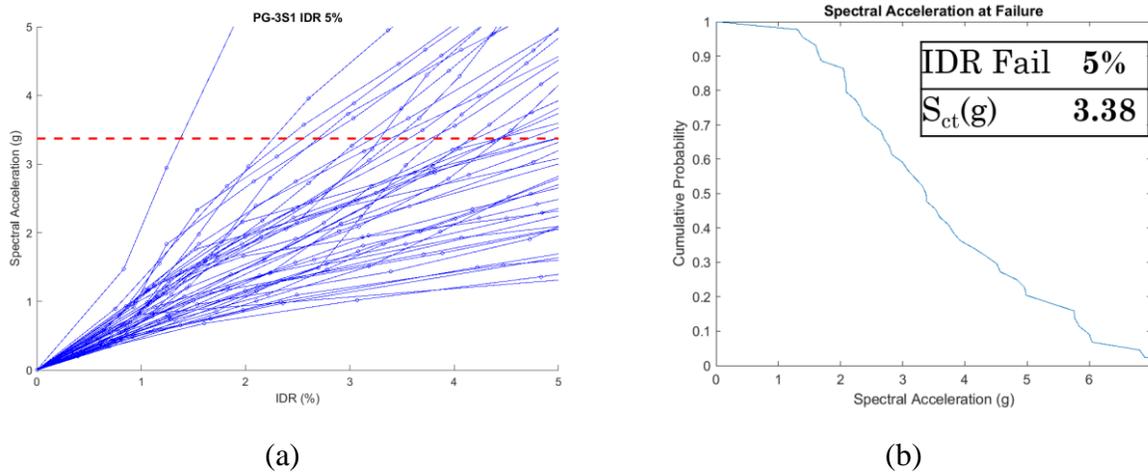
Figure 9.10. IDA Plot for 3-story archetype with 5% collapse criterion (a) Spectral acceleration vs. IDR; (b) Cumulative probability of failure vs. spectral acceleration
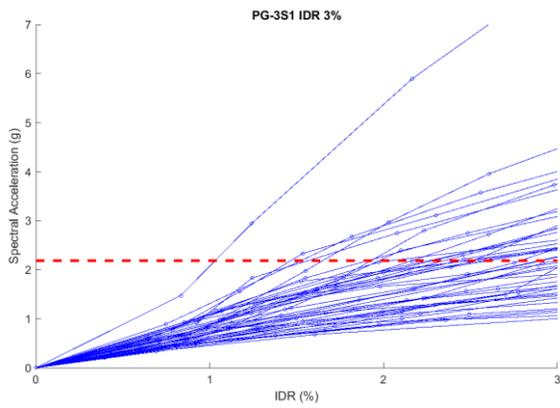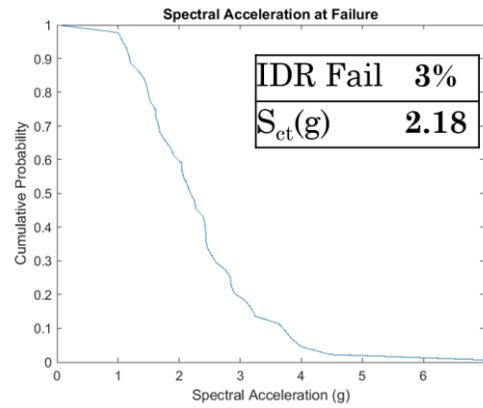
(a)	(b)

Figure 9.11. IDA plot for 3-story archetype with 3% collapse criterion (a) Spectral acceleration vs. IDR; (b) Cumulative probability of failure vs. spectral acceleration
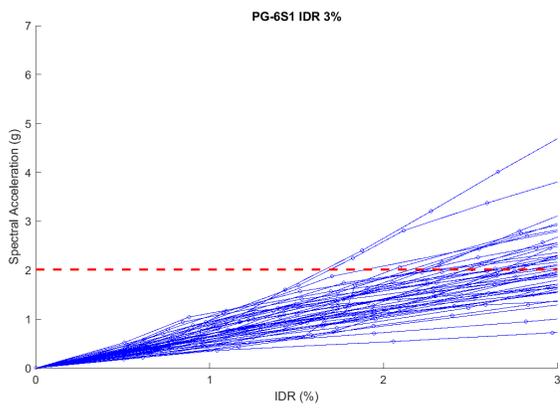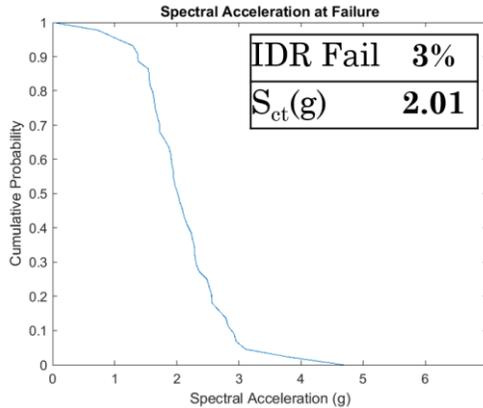
(a)	(b)

Figure 9.12. IDA plot for 6-story archetype with 3% collapse criterion (a) Spectral acceleration vs. IDR; (b) Cumulative probability of failure vs. spectral acceleration

| (a) | (b) |
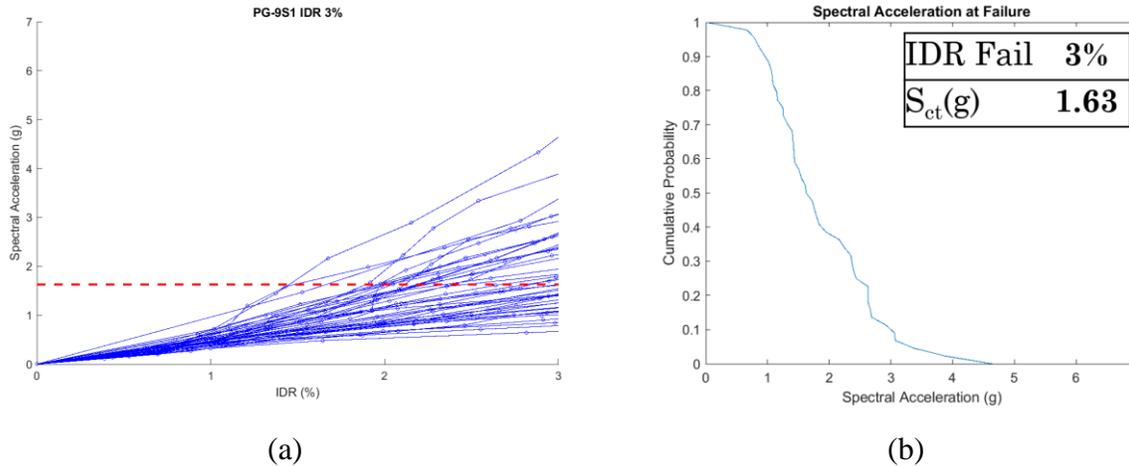
Figure 9.13. IDA plot for 9-story archetype with 3% collapse criterion (a) Spectral acceleration vs. IDR; (b) Cumulative probability of failure vs. spectral acceleration

| (a) | (b) |
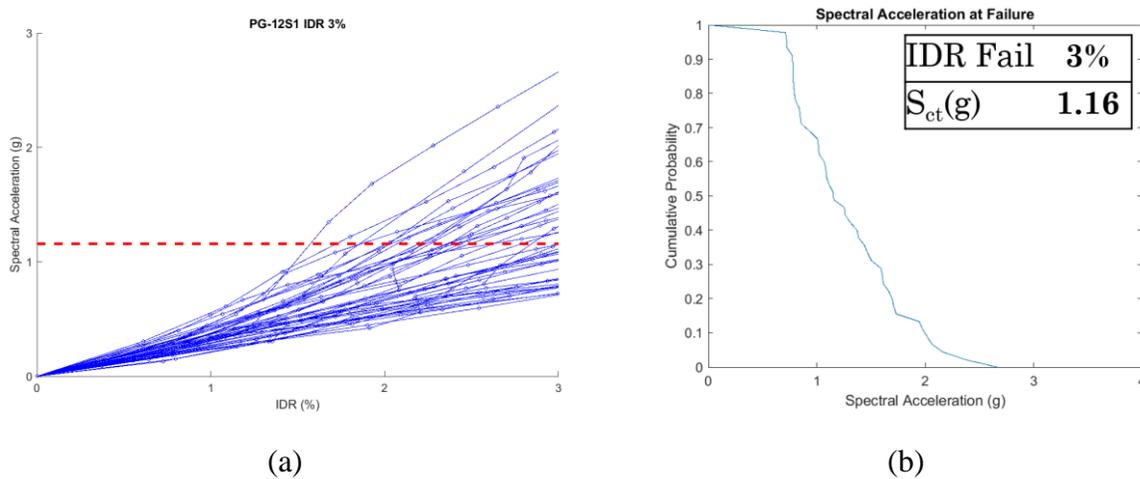
Figure 9.14. IDA plot for 12-story archetype with 3% collapse criterion (a) Spectral acceleration vs. IDR; (b) Cumulative probability of failure vs. spectral acceleration

9.4 Performance Evaluation

The performance of planar composite walls is assessed according to FEMA P695 methodology as described in Section 2.4**.** It is used to check the validity of the seismic performance factors used to design the archetypes. The median spectral acceleration collapse intensity, S_{CT}, collapse margin ratio, *CMR*, and adjusted collapse margin ratio, *ACMR* were calculated and summarized in Table 9-2. The value of the adjusted collapse margin ratio, *ACMR*, is then compared to the acceptable

81

value of adjusted collapse margin ratio at 10% probability of failure, $ACMR_{10\%}$ (Table 2-1), for the level of uncertainty, β_T, considered as good.

Table 9-2. Performance evaluations results for planar archetype structures

Structure	OS Period (s)	S_{ct} (g)	S_{mt} (g)	CMR	ACMR (μ_T>3)	ACMR (μ_T=3)
3S1	0.7	2.2	1.4	1.58	2.16	1.90
6S1	1.0	2.0	0.9	2.12	3.08	2.64
9S1	1.3	1.6	0.7	2.39	3.72	3.09
12S1	1.7	1.2	0.5	2.24	3.61	2.96
				Avg	3.14	2.65

As seen in Table 9-2 calculated *ACMR* values (μ_T>3) for all planar composite wall archetype are greater than the required acceptable value of $ACMR_{10\%}$ of 1.96. This suggests that the seismic performance factors selected to design the required archetype provide the required level of seismic resistance and collapse prevention. The median collapse intensity, S_{ct}, decreased from 3S1 to 12S1. The MCE ground motion spectral acceleration, S_{MT}, also decreased from 3S1 to 12S1 resulting in increase of collapse margin ratio, *CMR,* from 3S1 to 12S1. The *ACMR* values increased as the number of stories increased. This suggests that a taller structure has better seismic performance and collapse prevention than a shorter structure. The performance results of C-shaped archetype is summarized in Chapter 10.

10 C-SHAPED COMPOSITE WALLS ANALYSIS AND RESULTS

This chapter presents the nonlinear static pushover and incremental dynamic analysis study conducted on the C-shaped composite walls. It also summarizes the results of collapse assessment and performance evaluation of the C-shaped composite walls.

10.1 General

Three C-shaped archetypes (15-story, 18-story, and 22-story) were analyzed as part of the study. The details of composite walls dimensions, floor plans, and archetype structure are presented in Section 5.2. The material properties and finite element models used for the nonlinear analysis are presented in Chapters 7 and 8. The procedure similar to the planar wall was used to analyze the performance of C-shaped walls. The results of this chapter are also applicable for archetypes with an I-shaped configuration. Since only uncoupled direction was considered and the 2D FEA model was used for analysis, the effects of torsion were neglected for the study.

10.2 Nonlinear Static (Pushover) Analysis

The nonlinear pushover analysis of the C-shaped composite wall was conducted in compliance with FEMA P695 approach as described in Section 2.4.1. The results of the pushover analyses of 15-story, 18-story, and 22-story archetypes are presented below. Figure 10.1 to Figure 10.3 provide base shear vs. IDR plot, base shear vs. maximum IDR plot, and moment vs. roof displacement plot for the 15-story, 18-story, and 22-story archetypes.
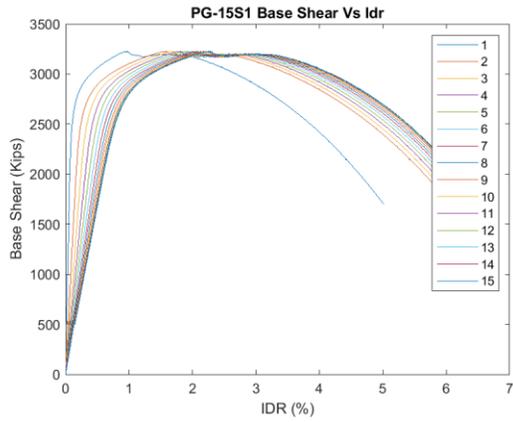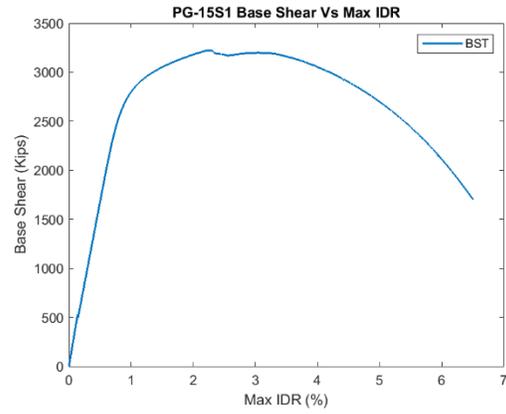
(a)   (b)
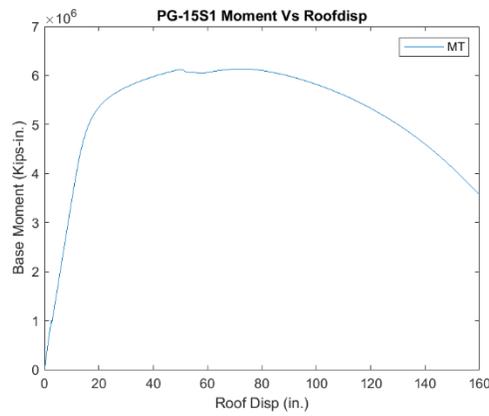
(c)

Figure 10.1. Pushover analysis results for 15-story archetype (a) Base shear vs. IDR; (b) Base shear vs. maximum IDR; (c) Moment vs. roof displacement
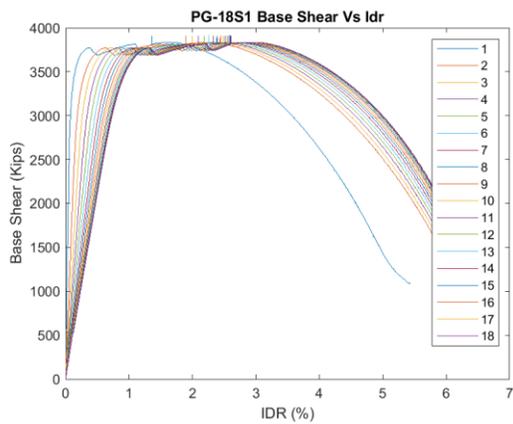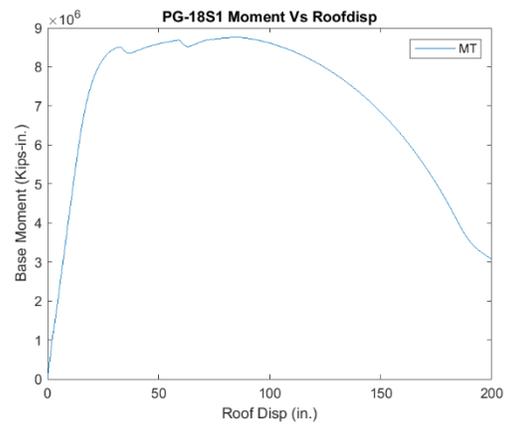
(a)   (b)

Figure 10.2. Pushover analysis results for 18-story archetype (a) Base shear vs. IDR; (b) Moment vs. roof displacement

84
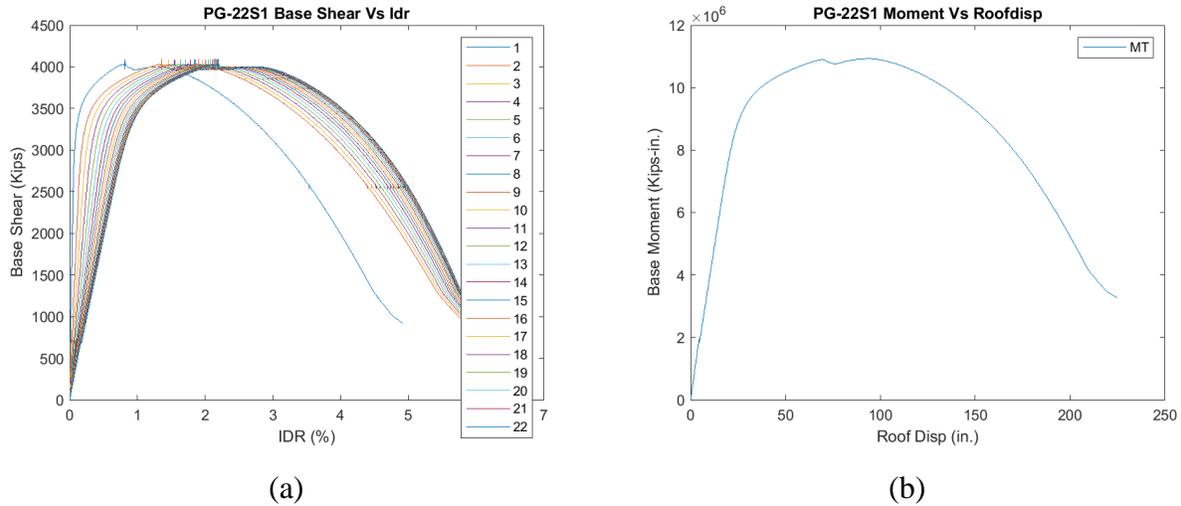
Figure 10.3. Pushover analysis results for 22-story archetype (a) Base shear vs. IDR; (b) Moment vs. roof displacement

The nonlinear pushover analysis results of the planar archetypes are presented in Table 10-1.

Table 10-1. Pushover analysis results for C-shaped archetype structures

Structure	V_{ELF}, (kips)	V_{max}, (kips)	$\delta_{y, eff}$, in	δ_u, in	Overstrength, Ω	Period-based ductility, μt
15S1	1230	3230	9.7	125	2.63	12.9
18S1	1470	3910	11.3	140	2.66	12.4
22S1	1485	4090	16.1	150	2.75	9.3
				Avg	2.68	11.5

Figure 10.4 shows base shear vs. roof displacement plots for the 15-story, 18-story, and 22-story archetypes. It also provides the estimate of maximum base shear, V_{max}, ELF base shear demand, V_{ELF}, and ultimate roof displacement, δ_u (at 80% remaining capacity). These values are then used to calculate the overstrength factor, Ω_0, and period-based ductility, μ_t.
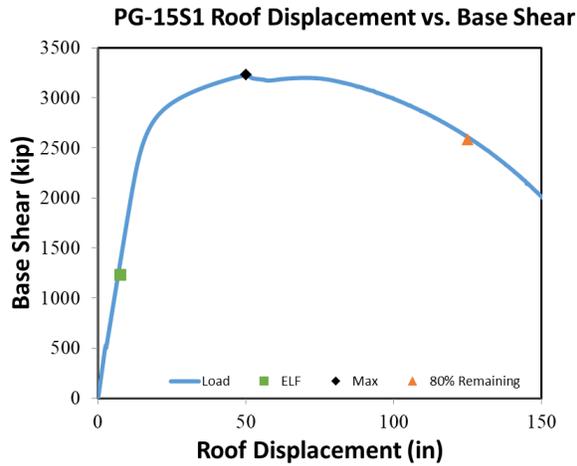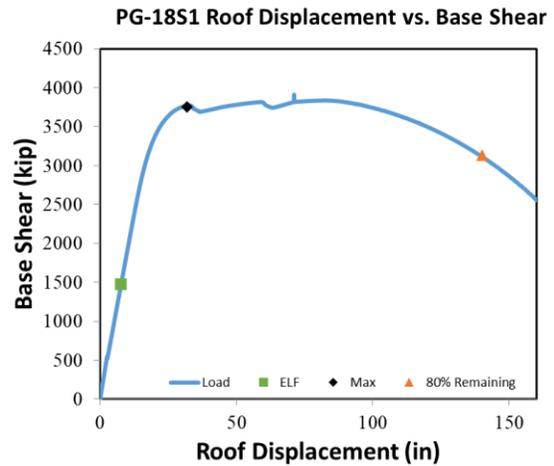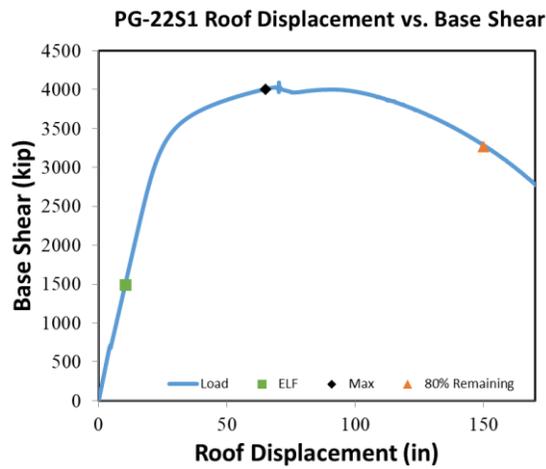
Figure 10.4. Maximum base shear capacity, ELF base shear, and ultimate displacement (a) 15S1; (b) 18S1; (c) 22S1

10.3 Incremental Dynamic Analysis

The incremental dynamic analysis for C-shaped composite walls archetypes is conducted in compliance with the approach prescribed in FEMA P695 methodology as described in Section 2.4.2. Steps similar to the steps explained in Section 9.3 are used to create the spectral acceleration vs. maximum inter-story drift curve and hence create the IDA plots and estimate median collapse intensity. A conservative collapse criterion of 3% was used for C-shaped medium-rise walls.

86

Figure 10.5 to Figure 10.7 illustrate the spectral acceleration vs. maximum inter-story drift ratio plot and cumulative failure probability vs. spectral acceleration for 15-story, 18-story, and 22-story. It also lists down the median collapse intensity for the 3% collapse criterion.

(a)	(b)
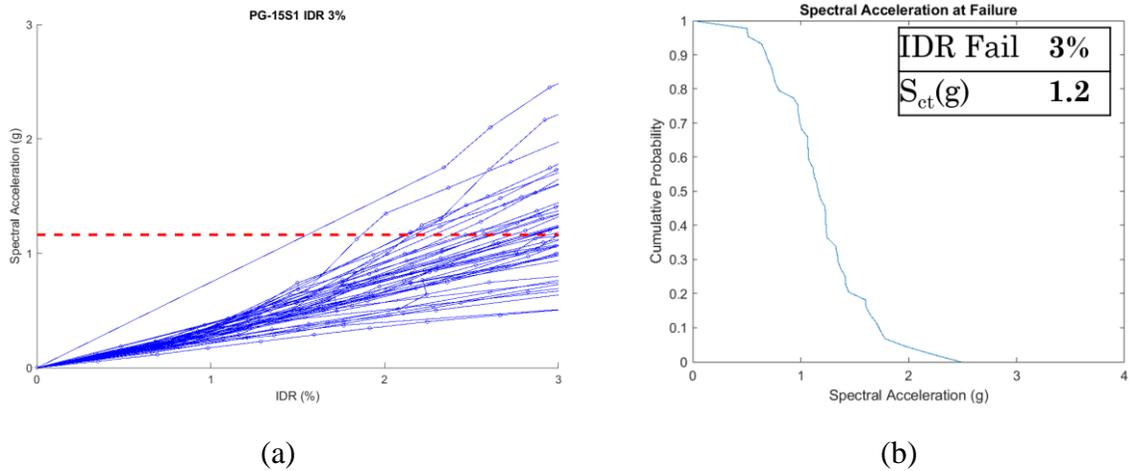
Figure 10.5. IDA plot for 15-story archetype with 3% collapse criterion (a) Spectral acceleration vs. IDR; (b) Cumulative probability of failure vs. spectral acceleration

(a)	(b)
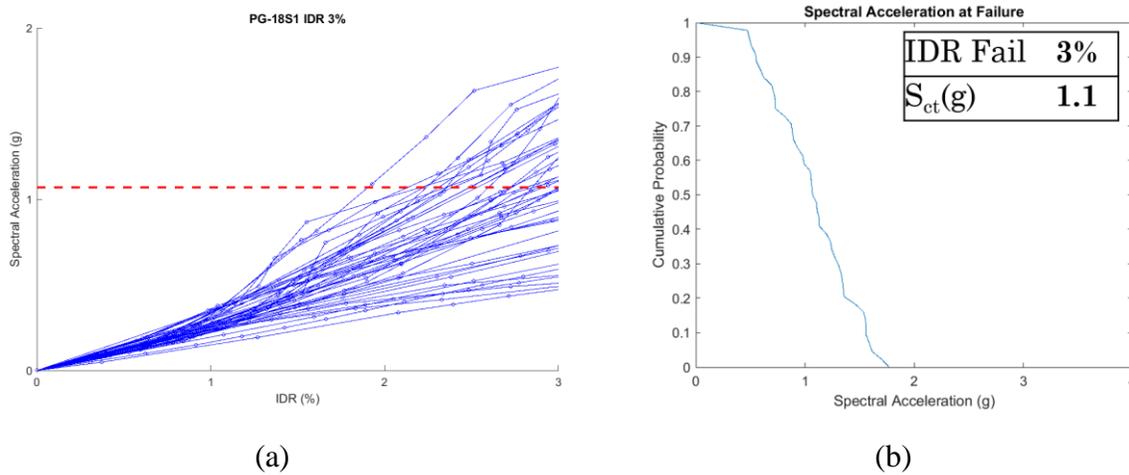
Figure 10.6. IDA Plot for 18-story archetype with 3% collapse criterion (a) Spectral acceleration vs. IDR; (b) Cumulative probability of failure vs. spectral acceleration

(a)   (b)
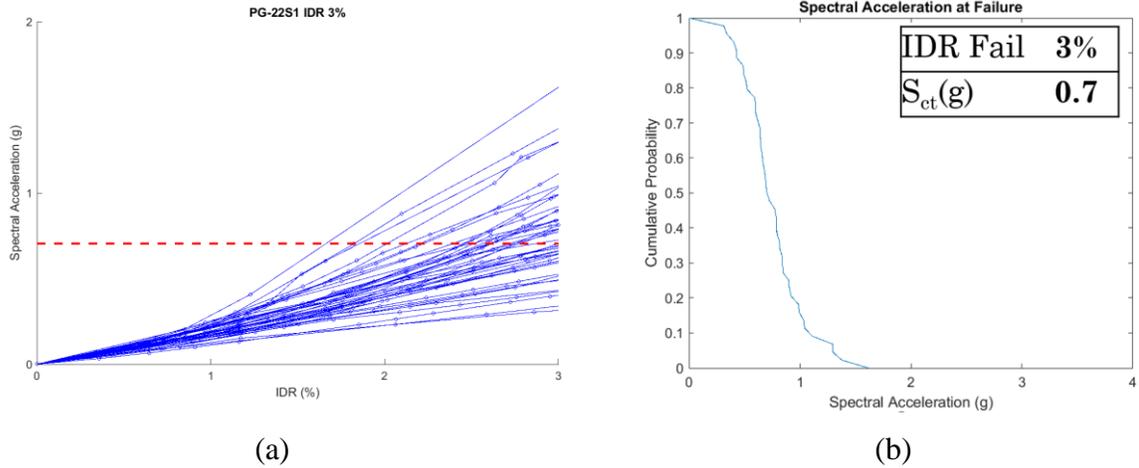
Figure 10.7. IDA Plot for 22-story archetype with 3% collapse criterion (a) Spectral
acceleration vs. IDR; (b) Cumulative probability of failure vs. spectral acceleration

10.4 Performance Evaluation

The performance of C-shaped composite walls was assessed according to the FEMA P695
methodology as described in Section 2.4. The validity of the seismic performance factors used to
design the archetype is evaluated in this section. The collapse margin ratio, *CMR*, and adjusted
collapse margin ratio, *ACMR*, are presented in Table 10-2. The value of the adjusted collapse
margin ratio, *ACMR*, is then compared to the acceptable value of adjusted collapse margin ratio at
10% probability of failure, *ACMR$_{10\%}$* provided in Table 2-1.

Table 10-2. Performance evaluation results for C-shaped archetype structures

PG	OS Period (s)	S_{ct} (g)	S_{mt} (g)	CMR	ACMR (μ_t>3)	ACMR (μ_t=3)
15S1	2.0	1.2	0.4	2.62	4.22	3.46
18S1	2.4	1.1	0.4	2.82	4.53	3.72
22S1	2.9	0.7	0.3	2.29	3.68	3.02
				Avg	4.14	3.40

The calculated *ACMR* values (μ_t>3) for all planar composite wall archetypes are greater than the
required acceptable value of *ACMR$_{10\%}$* of 1.96. This suggests that the seismic performance factors
selected to design the archetype provide a sufficient level of seismic resistance and collapse
prevention. The average *ACMR* value for the taller C-shaped archetype is found out to greater than

the average *ACMR* value for smaller planar archetype structures. This suggests that the taller structure have better seismic performance compared to the shorter structure.

11 WALLS WITHOUT CLOSURE FLANGE PLATES

This chapter presents the details of planar composite walls without boundary elements (without closure plates) as shown in Figure 11.1. The infill concrete is confined by steel faceplates. Closure plates in C-PSW/CF walls discussed earlier provide additional confinement to the infill concrete and reduce the effects of steel faceplate fracture and buckling. The closure plate also prevents concrete from spalling near the toes of the composite walls. Closure plates also eliminate the requirement of formwork during construction. Walls without closure plates lack all these benefits. This leads to the question of the adequacy of walls without boundary elements compared to walls with a boundary element. This chapter presents the FEMA P695 based study for the walls without closure plates.
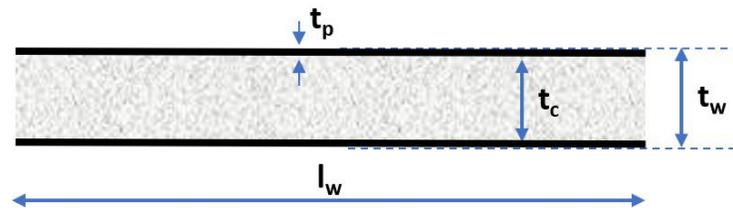
Figure 11.1. Planar composite plate shear wall without closure plate

11.1 Material Models and Model Benchmarking

As discussed earlier, the closure plate enhances the confinement in the infill concrete provided by the faceplates. The properties of walls without closure plates differ from the properties of walls with closure plates. Kurt et al. (2016), from his experiments on walls without closure plates, observed flexural cracking of concrete followed by local buckling of steel faceplates. Further increase in the drift on the test specimen leads to crushing and spalling of concrete and eventually results in ductile fracture of the steel faceplates near the base. The level of confinement observed in the infill concrete also varied along the length of the walls. The concrete near the toes of the walls had a lesser degree of confinement compared to the concrete present on the center of the wall. The overall behavior of infill concrete was in between a confined model used for walls with closure plate and unconfined concrete. For this reason, two different material models for concrete and steel were selected to create the OpenSees model. The first model was based on the Tao concrete model (confined concrete model) and the second model was based on the Popovics

concrete model (unconfined concrete model). The steel behavior was then adjusted to achieve proper benchmarking with the experimental results. Figure 11.2 presents the concrete and steel effective stress-strain curve for the first model. Figure 11.3 presents the concrete and steel effective stress-strain curve for the second model.

(a) (b)
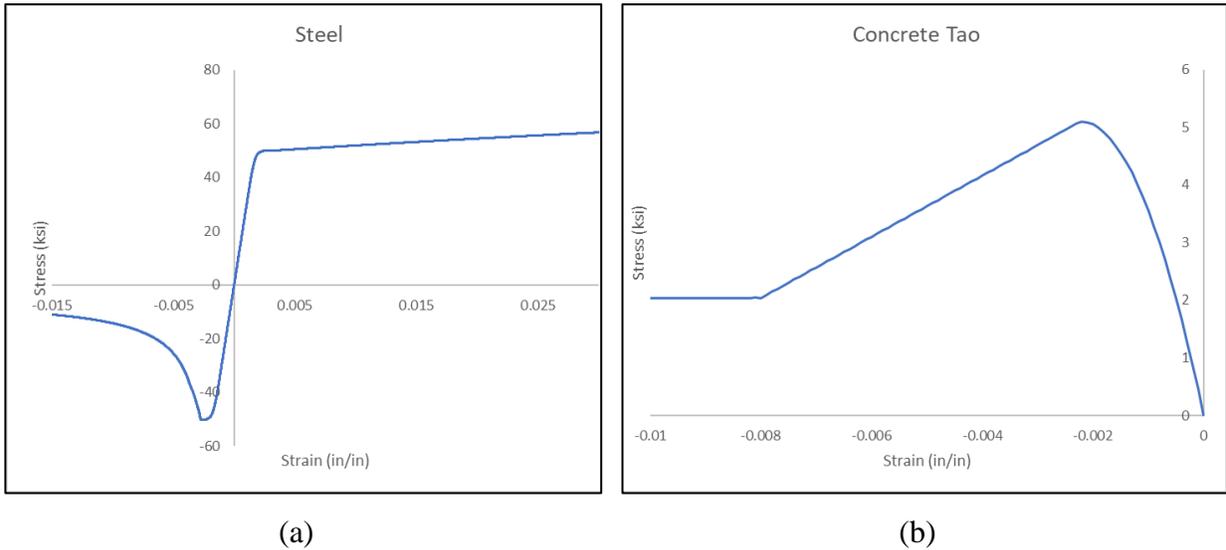
Figure 11.2. Effective stress-strain curve for the first case with the Tao confined concrete model (a) Steel stress vs. strain; (b) Confined concrete stress vs. strain

(a) (b)
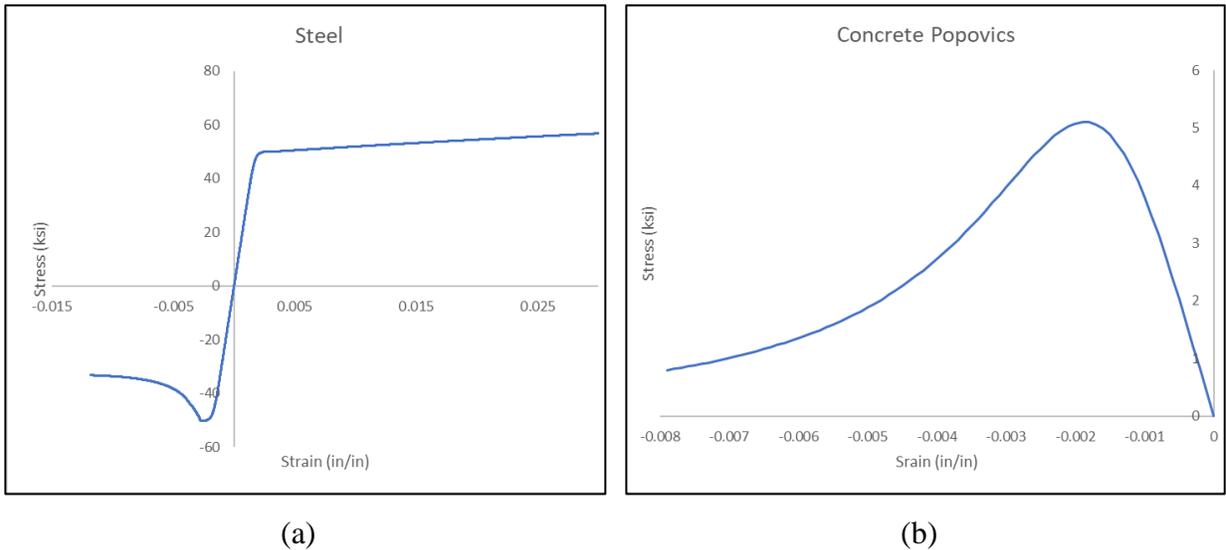
Figure 11.3. Effective stress-strain curve for the second case with the Popovics unconfined concrete model (a) Steel stress vs. strain; (b) Unconfined concrete stress vs. strain

Figure 11.4 compares the experimental results with the two OpenSees models. The overall behavior and seismic behavior of these walls is in between the results obtained from the two models.

(a)   (b)
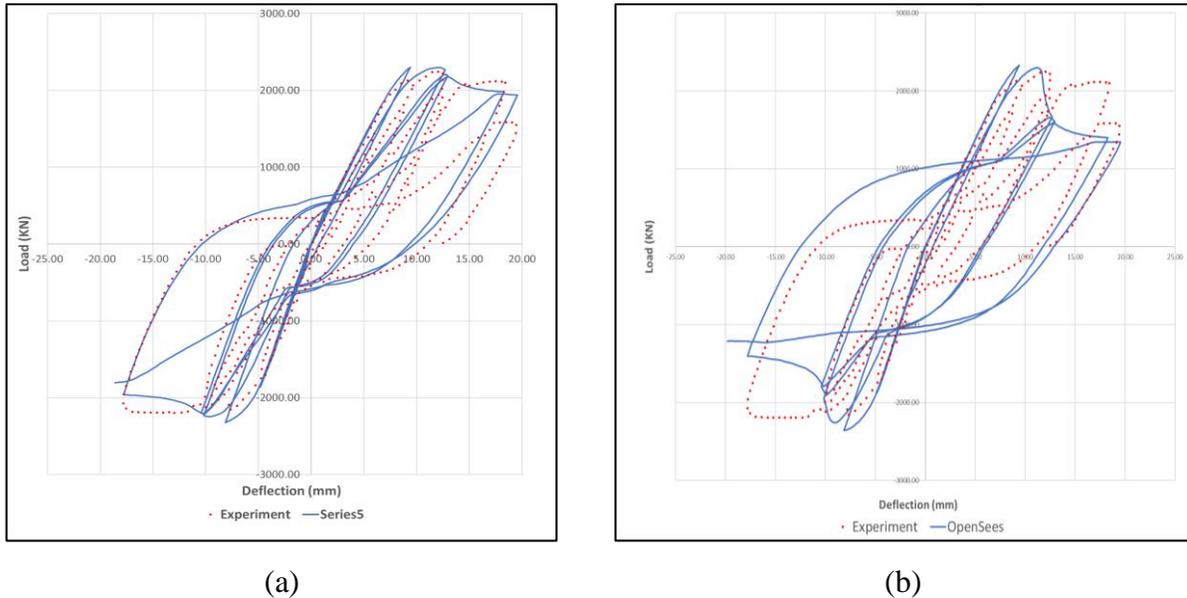
Figure 11.4. Experiment result vs. OpenSees model (a) First model (Tao concrete); (b) Second model (Popovics concrete)

11.2 Archetype Models

This section presents the development of the archetype model for walls without closure plates. As observed from the results of planar composite walls (with closure plates) archetype, 3-story and 6-story structure had the lowest value of adjusted collapse margin ratio, *ACMR*. The *ACMR* value increased as the number of stories (i.e. the height of the structure) increased. Higher *ACMR* values correspond to better seismic performance and lower probability of collapse. For this reason, the most critical cases of 3-story and 6-story archetype structure were considered for analysis.

Experiment results by Kurt et al. (2016) indicated that local buckling of steel and crushing of unconfined concrete occurred at almost the same instant. The crushing of concrete resulted in spalling hence eventual degradation in flexural strength. Therefore, for these walls flexural capacity was taken as the yield moment capacity, M_{yc}, instead of the plastic moment capacity, M_p, used for walls with closure plates. The yield moment capacity, M_{yc}, is found using the stress block

shown in Figure 11.5 based on the lower bound plasticity theorem. For this, the concrete behavior was assumed linear elastic with the compressive stress limited to $0.70f'_c$. The estimate of the neutral axis location, c, and the corresponding yield moment capacity, M_{yc}, is given by Equation 11.1 and 11.2 respectively.
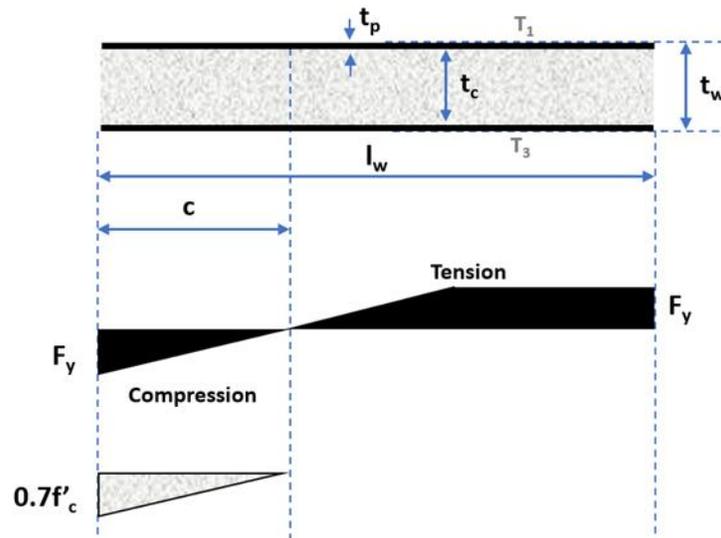
Figure 11.5. Stress distribution assumed to calculate the yield moment (Kurt et al. 2016)

$$c = \frac{2t_p F_y l_w}{0.35 t_c f'_c + 4 t_p F_y} \tag{11.1}$$

$$M_{yc} = \frac{0.7 f'_c t_c c^2}{3} + F_y t_p \left(\frac{4}{3}c^2 - 2l_w c + l_w^2\right) \tag{11.2}$$

where t_c is the thickness of concrete, t_p is one faceplate thickness and l_w is the length of the wall

A floor plan and story height similar to the 3-story and 6-story planar archetypes was used for the archetype structures without closure plates.

Table 11-1 summarizes the dimensions and additional details of the wall used for the two archetypes.

Table 11-1. Planar composite wall archetypes

Case	No. of Stories	Wall Thickness, in	Wall Length, ft	Plate Thickness, in	Wall Strength Margin		Max IDR (%)
					$\phi M_{n,wall}/M_{u,wall}$	$\phi V_{n,wall}/4V_{u,wall}$	
1	3	12	15	4/16	1.15	1.83	2.0
2	6	16	25	5/16	1.22	2.20	2.0

11.3 Nonlinear Pushover (Static) Analysis

The nonlinear pushover analysis of the wall without closure plates was conducted in compliance with FEMA P695 approach as described in Section 2.4.1. The results of the pushover analyses of 3-story and 6-story archetypes without closure plates are presented below. Figure 11.6 to Figure 11.8 provides base shear versus IDR plots and moment versus roof displacement plots for the 3-story (Tao model - 3WF1 and Popovics model – 3WF2) and 6-story (Tao model - 6WF1) archetypes. The pushover results show that both walls with the Tao concrete model and the Popovics concrete model have a sudden drop in base shear carrying capacity just after reaching the peak capacity. The sudden drop is then followed with a gradual decrease in the capacity resulting from buckling and fracture of steel fibers. These walls have lower ductility compared to walls with the closure plate. The effective flexural stiffness of the walls without closure plates is nearly equal to that of the walls with closure plates. This is because of the similar initial behavior of both the walls with and without closure plate. The main difference between the two wall systems is in the post-peak behavior once the concrete reaches its peak.
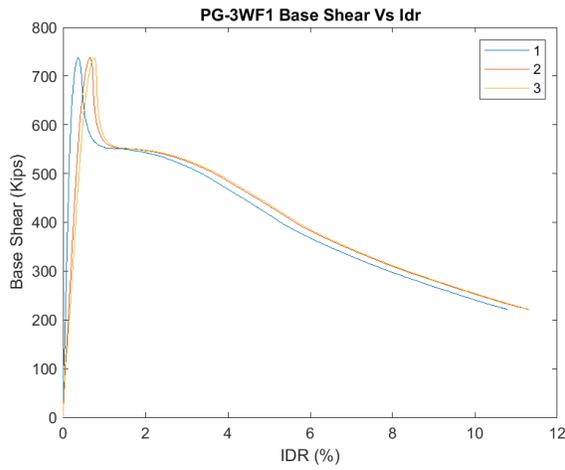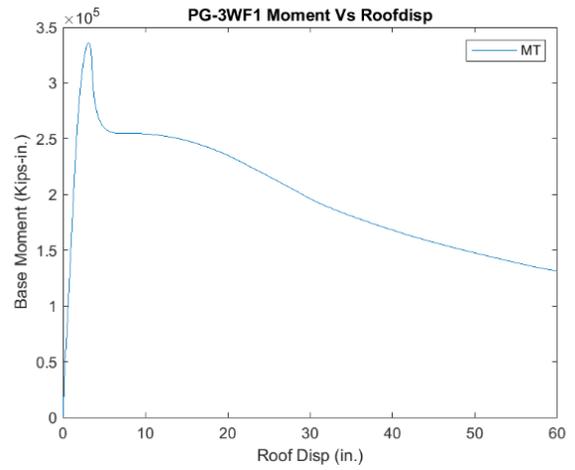
(a)	(b)

Figure 11.6. Pushover analysis results for 3-story archetype (3WF1 – Tao concrete model) (a) Base shear vs. IDR; (b) Moment vs. roof displacement
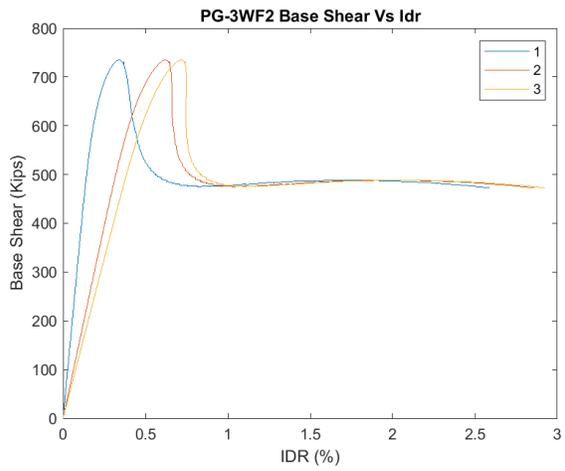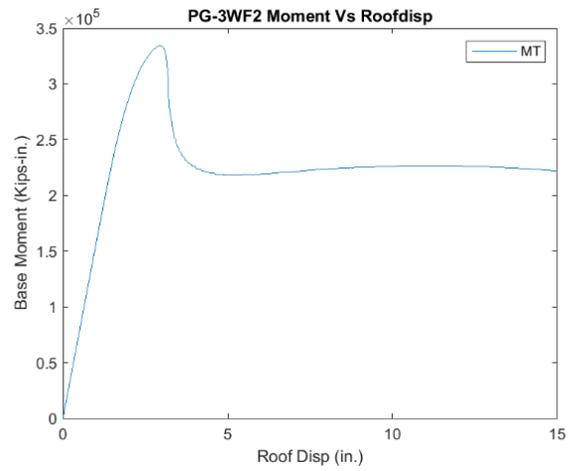
(a)	(b)

Figure 11.7. Pushover analysis results for 3-story archetype (3WF2 – Popovics concrete model) (a) Base shear vs. IDR; (b) Moment vs. roof displacement
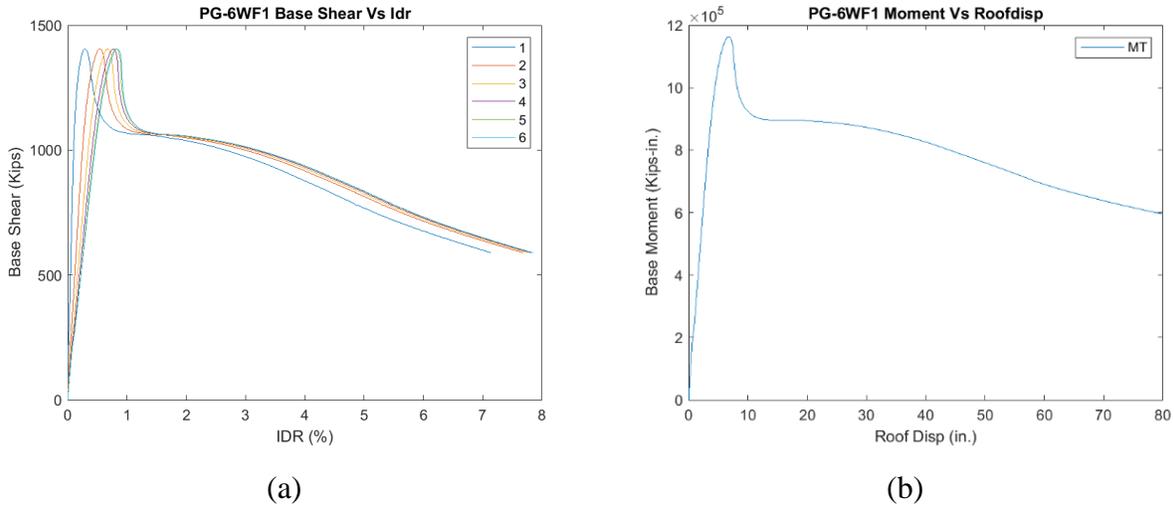
Figure 11.8. Pushover analysis results for 6-story archetype (6WF1 – Tao concrete model) (a) Base shear vs. IDR; (b) Moment vs. roof displacement

Figure 11.9 shows base shear vs. roof displacement plots for the 3-story and 6-story archetypes. It also provides the estimate of maximum base shear, V_{max}, ELF base shear demand, V_{ELF}, and ultimate roof displacement, δ_u (at 80% remaining capacity). These values are then used to calculate the overstrength factor, Ω_0, and period-based ductility, μ_t.
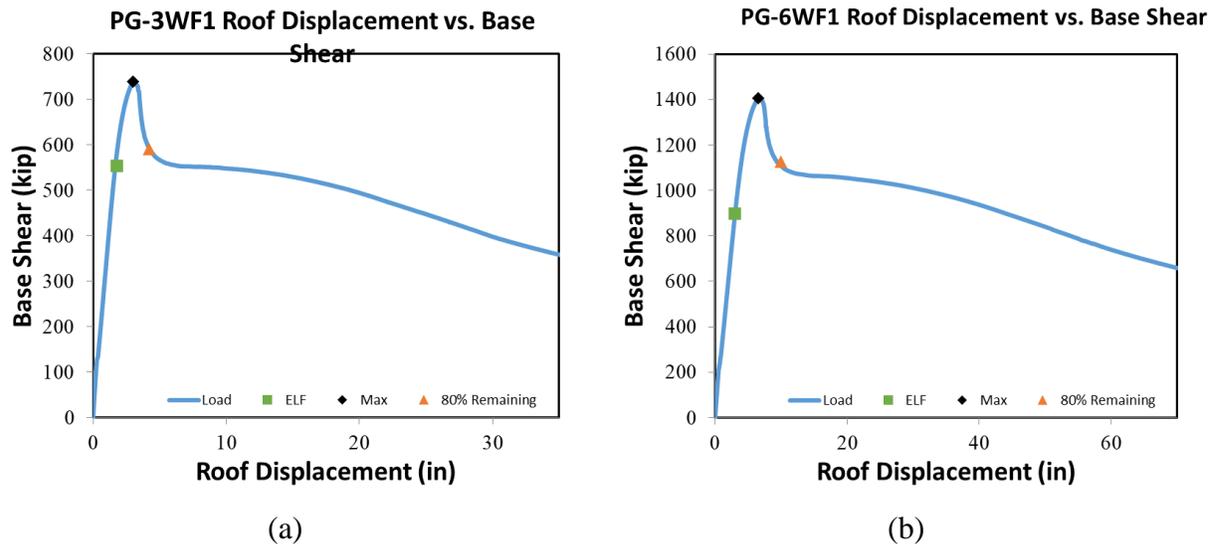
Figure 11.9. Maximum base shear capacity, yield displacement, and ultimate displacement (a) 3WF1; (b) 6WF1

96

The nonlinear pushover analysis results of the planar archetypes are presented in Table 11-2. The 80% drop in strength occurred immediately after the peak was reached. This drop in strength resulted in a lower value of ultimate displacement and hence lower period-based ductility. The period-based ductility calculated for walls without closure plate ranged from 2.9 to 3.8 while the same factor ranged from 17.2 to 25.1 for planar walls with closure plates.

Table 11-2. Pushover analysis results for planar archetype structures

Structure	V_{ELF}, (kips)	V_{max}, (kips)	$\delta_{y, eff}$, in	δ_u, in	Overstrength, Ω	Period-based ductility, μt
3WF1	554	739	1.2	4.2	1.33	3.6
3WF2	554	735	1.2	3.4	1.33	2.9
6WF1	897	1405	2.5	9.6	1.57	3.8
				Avg	1.41	3.4

11.4 Incremental Dynamic Analysis

The incremental dynamic analysis for walls without closure plate is conducted in compliance with the approach prescribed in FEMA P695 methodology as described in Section 2.4.2. The steps similar to the steps explained in Section 9.3 are used to create the spectral acceleration vs. maximum inter-story drift curve and hence create the IDA plots and estimate median collapse intensity. Figure 11.10 to Figure 11.12 illustrates the spectral acceleration vs. maximum inter-story drift ratio plot and cumulative failure probability vs. spectral acceleration for 3WF1, 3WF2, and 6WF1. The median collapse intensity for the 3% collapse criterion is also listed.
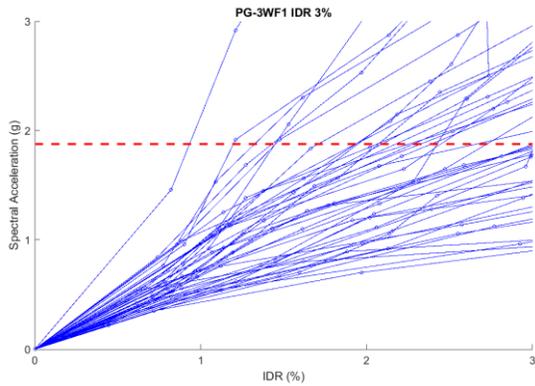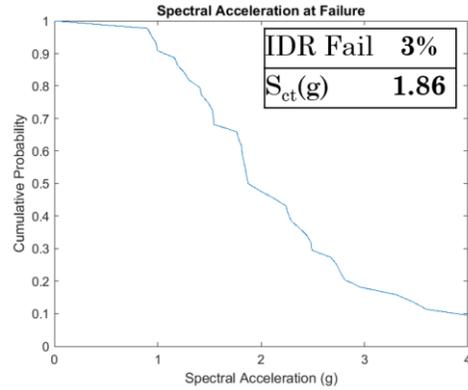
(a)   (b)

Figure 11.10. IDA plot for 3WF1 with 3% collapse criterion (a) Spectral acceleration vs. IDR;
(b) Cumulative probability of failure vs. spectral acceleration
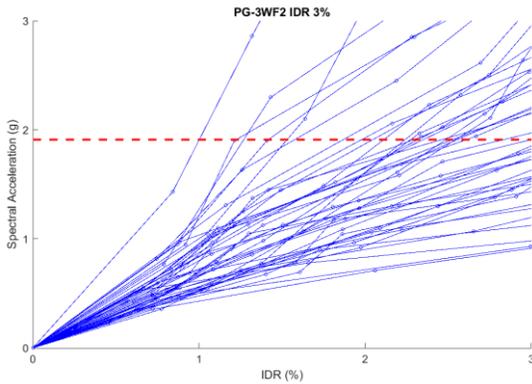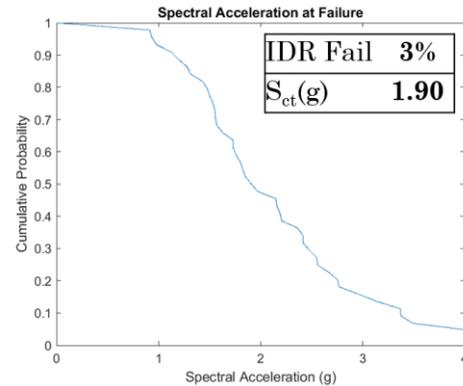
(a)   (b)

Figure 11.11. IDA plot for 3WF2 with 3% collapse criterion (a) Spectral acceleration vs. IDR;
(b) Cumulative probability of failure vs. spectral acceleration
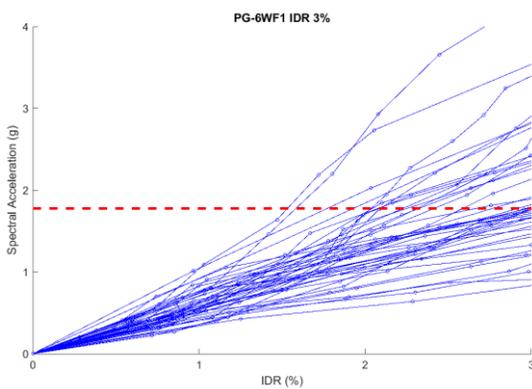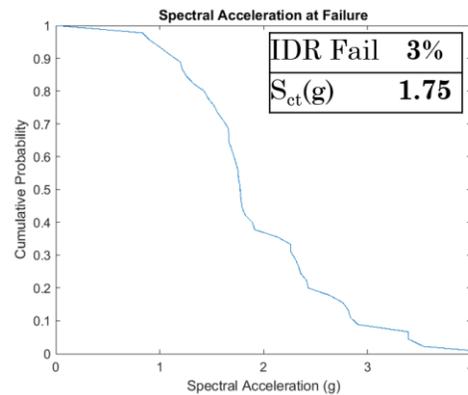
(a)   (b)

Figure 11.12. IDA plot for 6WF1 with 3% collapse criterion (a) Spectral acceleration vs. IDR;
(b) Cumulative probability of failure vs. spectral acceleration

98

11.5 Performance Evaluation

The performance of the walls without closure plates is assessed according to the FEMA P695 methodology as described in Section 2.4. The validity of the seismic performance factors used to design the archetype is evaluated in this section. The collapse margin ratio, *CMR*, and adjusted collapse margin ratio, *ACMR*, are presented in Table 11-3. The value of the adjusted collapse margin ratio, *ACMR*, is then compared to the acceptable value of adjusted collapse margin ratio at 10% probability of failure, $ACMR_{10\%}$ provided in Table 2-1.

Table 11-3. Performance evaluations results for C-shaped archetype structures

Structure	OS Period (s)	S_{ct} (g)	CMR	ACMR (μ_t=3)
3WF1 (Tao)	0.64	1.9	1.34	1.62
3WF2 (Popovics)	0.65	1.9	1.38	1.66
6WF1	0.99	1.8	1.93	2.40
			Avg	1.89

The calculated *ACMR* values for all 3-story wall archetype is smaller than the required acceptable value of $ACMR_{10\%}$. This suggests that the 3-story archetype does not pass the required ACMR criteria and the selected seismic performance factors do not provide enough seismic performance and collapse prevention capacity. The 6-story had acceptable *ACMR* value for 3% drift collapse criteria. Experimental results from Kurt indicate that the specimen undergoes concrete crushing and faceplate fracture below a 2% drift ratio. Table 11-4 and Table 11-5 present the variation of adjusted collapse margin ratio for different levels of collapse criteria.

The 6-story archetype does not satisfy the $ACMR_{10\%}$ requirement for a 2% drift limit taken as collapse criteria. This suggests that the seismic performance factors selected to design a wall without closure plates do not provide the required level of seismic resistance and collapse prevention.

Overall considering the results of performance evaluation and ease of construction provided by the inclusion of closure plates, it is recommended that that the boundary elements or closure plates is

provided for all wall panels. If walls without closure plates are used, it is recommended to use more conservative values seismic performance factors.

Table 11-4. Performance evaluation results for C-shaped archetype structures

Structure	IDR Collapse	S_{ct} (g)	CMR	ACMR ($u_t > 8$)	ACMR ($u_t = 3$)
3WF1	2.0%	1.4	1.00	1.36	1.20
3WF1	2.5%	1.7	1.21	1.65	1.46
3WF1	3.0%	2.0	1.43	1.96	1.72
3WF1	4.0%	2.6	1.85	2.53	2.23
3WF1	5.0%	3.2	2.28	3.11	2.74

Table 11-5. Performance evaluation results for C-shaped archetype structures

Structure	IDR Collapse	S_{ct} (g)	CMR	ACMR ($u_t > 8$)	ACMR ($u_t = 3$)
6WF1	2.0%	1.3	1.39	2.02	1.73
6WF1	2.5%	1.5	1.69	2.47	2.12
6WF1	3.0%	1.8	1.93	2.81	2.40
6WF1	4.0%	2.3	2.49	3.62	3.11
6WF1	5.0%	2.6	2.88	4.20	3.60

12 STIFFNESS AND SEISMIC PERFORMANCE FACTOR ESTIMATES AND VALIDATION

This chapter presents the estimation of cracked section flexural stiffness for the C-PSW/CF. It also presents the validation of the trial seismic performance factors used to design the C-PSW/CF archetype structure.

12.1 Flexural Stiffness Estimate

The effective flexural stiffness defined in Section 3.3.3 was used to design the planar and C-shaped C-PSW/CF archetype structure. Planar wall C-PSW/CF archetype design used an effective stiffness calculated using the cracked transformed section properties corresponding to 60% of the nominal flexural capacity. Effective flexural stiffness calculated using Equation 3.1 was used to design the C-shaped C-PSW/CF archetypes. The stiffness depends on the total overturning moment applied on the walls due to the equivalent lateral loads. As the height of the composite walls increases, the wall design becomes more drift critical and the flexural overstrength also becomes larger. The lower overturning moment relative to wall strength for taller structures will result in less cracking in the concrete. The cracked properties also vary along with the height of the wall due to lower moment demands at upper levels. Figure 12.1 shows an example of the ratio of the overturning moment and design strength along the height of the wall for an 18-story archetype. The 18-story archetype structure does not reach 60% of the nominal moment and should have more stiffness then what is estimated corresponding to 60% of the nominal flexural capacity.

The use of different stiffnesses along with the height of the structure and for different archetypes increases the complexity of the design procedure. For this reason, a simple equation for stiffness estimation is provided (see Equation 3.1). This equation is based on the stiffness calculated for the cracked reinforced concrete wall per Table 6.6.3.1.1(a) of ACI 318-14. A nonlinear model as shown in Figure 8.3 was used to validate for the above equation. Nonlinear wall elements as discussed in Section 8 were used for the entire structure instead of a small region near the base of the wall. Equivalent lateral forces as calculated in Section 4.2 were applied to the nonlinear model to obtain the maximum IDR. This model was compared to a full elastic model with an effective elastic stiffness, EI_1, which would result in the same maximum IDR calculated from the fully

nonlinear model. Table 12-1 compares the effective elastic stiffness, *EI₁*, and stiffness calculated using Equation 3.1.
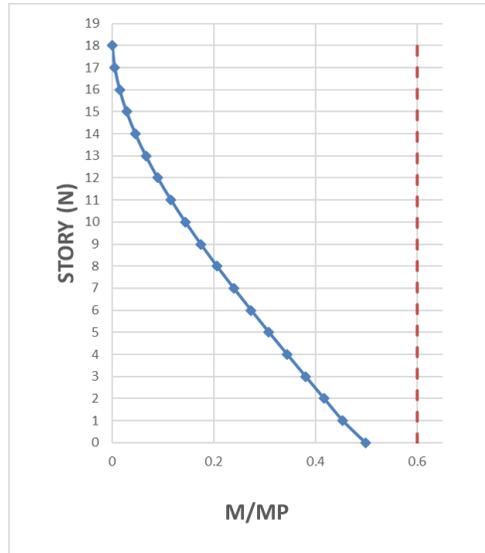
Figure 12.1. Ratio of the overturning moment and design strength for the 18-story archetype

Table 12-1. Effective stiffness estimate for C-PSW/CF archetype structures

		EI_1	EI_{eff}	
Case	Wall	Effective EI (Fiber)	$E_sI_s+0.35E_cI_c$	EI_1/EI_{eff}
1	3S1	1.6E+10	1.7E+10	0.92
2	6S1	9.7E+10	1.0E+11	0.97
3	9S1	2.6E+11	2.6E+11	1.01
4	12S1	5.1E+11	5.1E+11	0.99
5	15S1	7.1E+11	6.8E+11	1.04
6	18S1	1.3E+12	1.1E+12	1.16
7	22S1	1.8E+12	1.6E+12	1.10
			Average	1.03

As seen in Table 12-1, the average effective stiffness estimated using the nonlinear fiber model equates well with the stiffness calculated using Equation 3.1. Hence, Equation 3.1 reasonably estimates the effective flexural stiffness for the composite walls system. The use of different

stiffness along the height of the walls is permitted using a thorough cracked transformed section analysis. The gravity loads due to the tributary floor area result in $0.05A_gf_c$ to $0.07A_gf_c$ axial force in the wall. This axial force increases the overall effective stiffness by 10-20% for the archetype structures. Considering slightly less relative effective stiffness for the 3-story of 0.92, the increase in effective stiffness due to the tributary axial force is neglected to maintain a more conservative design procedure.

12.2 Response Modification Factor, *R*

The response modification factor is defined at the ratio of the elastic base shear demand to the design base shear. A response modification factor, *R*, of 6.5 was used to design the C-PSW/CF archetype. This report validates the use of a response modification factor of 6.5 using FEMA P695 based nonlinear static and dynamic analysis. This analysis was conducted on both planar and C-shaped C-PSW/CFs. FEMA P695 methodology requires the adjusted collapse margin ratio, *ACMR,* to be greater than two performance criteria, namely for individual archetypes ($ACMR_{20\%}$) and performance groups ($ACMR_{10\%}$). If these two criteria are satisfied, then the trial factor R factor used to design the archetype is deemed acceptable. Chapters 9 and 10 discussed the incremental dynamic analysis and performance evaluation conducted on planar C-PSW/CF and C-shaped C-PSW/CF, respectively. Table 9-2 and Table 10-2 summarizes the results of the performance evaluation conducted on these walls. The adjusted collapse margin ratio, *ACMR,* was greater than the required $ACMR_{10\%}$ and $ACMR_{20\%}$ value for all the planar and C-shaped C-PSW/CF. This justifies the use of an R factor of 6.5 for planar and C-shaped C-PSW/CFs. The same study was conducted for walls without a closure plate and discussed in Chapter 11. The *ACMR* values of walls without closure plates did not satisfy the 10% collapse $ACMR_{10\%}$ requirement. Hence, a lower R factor is recommended to design of walls without closure plates. This additional study on walls without closure plates was not performed but would require designing structures with a lower R factor until an acceptable seismic performance is reached.

12.3 Deflection Amplification Factor, C_d

A deflection amplification factor, C_d, of 5.5 was used to design the C-PSW/CF archetypes. The C_d factor depends on the ratio of nonlinear displacement to the elastic displacement of the system. The maximum IDR of a nonlinear at the Design Basis Earthquake (DBE) level was found for each

of the C-PSW/CF archetype structure for all the 44 ground motion responses. The mean and 90th percentile IDR values were calculated from these results. Table 12-2 lists the average IDR, IDR_{DBE_Avg}, and 90th percentile maximum IDR, $IDR_{DBE\_90\%}$ for each structure. The table also lists the elastic drift, IDR_{ELF}, from the equivalent lateral force loading on the composite walls.

Table 12-2. Deflection amplification factor, C_d, estimate for C-PSW/CF archetype structures

Archetype	IDR_{DBE_Mean}	$IDR_{DBE\_90\%}$	IDR_{MCE}	IDR_{ELF}	$C_{d\_DBE\_Mean}$	$C_{d\_DBE\_90\%}$
3S1	1.36	1.96	2.04	0.30	4.5	6.5
6S1	1.19	1.67	1.78	0.30	4.0	5.6
9S1	1.17	1.70	1.75	0.30	3.8	5.6
12S1	1.24	1.79	1.85	0.29	4.2	6.1
15S1	1.11	1.52	1.67	0.35	3.2	4.4
18S1	1.11	1.60	1.67	0.36	3.1	4.4
22S1	1.22	1.61	1.83	0.37	3.3	4.4
				Average	3.7	5.3

The average deflection amplification factor, $C_{d\_DBE\_Mean}$, for the mean DBE response was calculated as 3.7 and $C_{d\_DBE\_90\%}$ for the 90th percentile DBE response was found out to be 5.3. The deflection amplification factor calculated for the 90th percentile DBE response compares well with 5.5 value used for the design of archetype. Drift calculations do not incorporate a safety factor similar to the resistance factor for strength-based limits; therefore, the Cd used in the design should be a lower-bound value. Using the 90th percentile result captures this conservatism while also following the observed structural response. The average value of C_d for the 90th DBE response was calculated as 5.3, which is close to a C_d value of 5.5 as assumed in the design procedure.

12.4 Overstrength Factor, Ω_0

The overstrength provides a ratio of the maximum base shear resistance to the design base shear. The design procedure of uncoupled composite walls does not require the use of the overstrength factor apart from the usual safety factor and material overstrength. The design of the C-PSW/CF archetype structures was drift-governed and large sizes of walls were used to limit the IDR to 2% for equivalent lateral forces. This design limit resulted in an inherent overstrength strength in the system. The overstrength factor generally increased as the height of the structure increased with

the largest overstrength observed for the 22-story archetype. The overstrength factors listed in Table 9-1 and Table 10-1 were determined using nominal material properties and do not account for additional material strength above the minimum yield capacity. A separate nonlinear static analysis using expected steel strength was conducted on the planar and C-shaped and the results are summarized in Table 12-3. Here, Ω_1 is the overstrength of the system using nominal properties and Ω_2 is the overstrength with a steel overstrength, R_y, of 1.1.

Table 12-3. Overstrength for planar and C-shaped archetype structures. Ω_1 considers nominal material properties and Ω_2 considers the expected strength of steel.

PG	Planar C-PSW/CF				C-shaped C-PSW/CF			Avg
	3S1	6S1	9S1	12S1	15S1	18S1	22S1	
Overstrength, Ω_1	1.44	1.69	2.02	2.34	2.63	2.66	2.75	2.22
Overstrength, Ω_2	1.54	1.81	2.18	2.52	2.80	2.82	2.92	2.37

13 POST PROCESSING RESULTS

This chapter discusses the behavior of planar and C-shaped C-PSW/CF at three different levels of seismic hazard. The behavior of each archetype was analyzed at the Design Basis Earthquake (DBE) level, the Maximum Considered Earthquake (MCE) level, and the collapse criterion (3% maximum IDR). The study was conducted for three different ground motions corresponding to the 25th, 50th (median), and 75th percentile response at failure. The global response was captured in moment and base shear as a function of time plots, and the local behavior was considered by looking at the moment versus rotation demand and curvature for the base of the wall, and stress-strain response of extreme fibers of the wall at the base.

13.1 Planar Walls

The nonlinear time history response of planar walls is assessed in this section. An example of post-processing conducted is presented in detail for the 3-story archetype, and then tabulated results for all planar archetypes are listed in Table 13-1 to Table 13-4. Figure 13.1 shows the spectral acceleration (SA) versus maximum IDR plot and the ground motion responses selected corresponding to the 25th, 50th (median), and 75th percentile spectral acceleration at 3% IDR. For the 3-story archetype, 25th percentile, 50th percentile, and 75th percentile response correspond to a record from the Chi-Chi, Taiwan (PEER-NGA Record CHICHI/CHY101-E), Northridge (NORTHR/MUL279), and Cape Mendocino (CAPEMEND/RIO270), respectively.
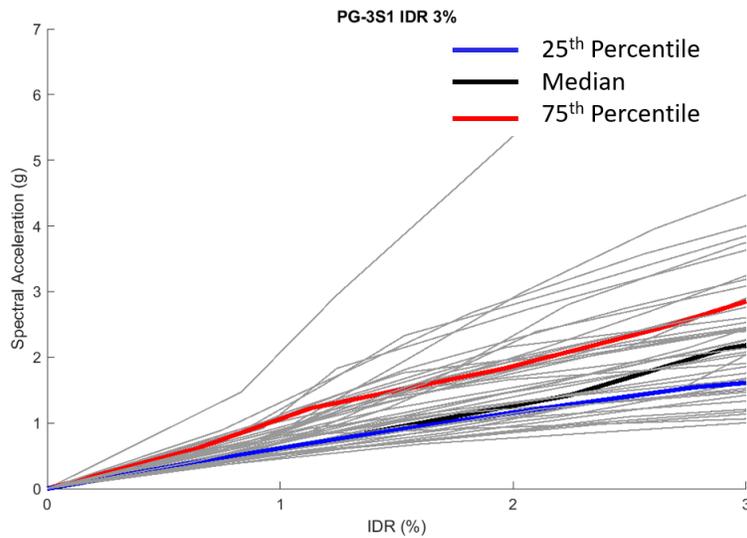
Figure 13.1. Spectral acceleration (g) vs. IDR (%) for 3-story archetype highlighting three selected ground motions

The median response was used to calculate the collapse margin ratio and evaluate the performance of the building. Collapse criterion of 3% and 5% maximum IDR were also considered for the 3-story and 6-story archetypes to examine the behavior of the wall at high levels of drift. For the 3-story archetype, the MCE level earthquake is reached at a ground motion scale factor of 2.4 and the DBE level earthquake at a scale factor of 1.6 (two-thirds of MCE level). These ground motion scale factors are applied to the normalized record set detailed in FEMA P695. The ground motions are normalized based on the peak ground velocity. This process is described in detail in FEMA P695 Appendix A.8. The 3% and 5% IDR were observed at different scale factors depending on the drift experienced by the archetype structures. Figure 13.2 shows the normalized moment at the base of the 3-story archetype wall at DBE, MCE, 3% IDR and 5% IDR for the median SA ground motion. Figure 13.3 shows the normalized moment at the base of the 3-story archetype wall at 3% IDR hazard level for the 25th percentile and 75th percentile ground motion response.
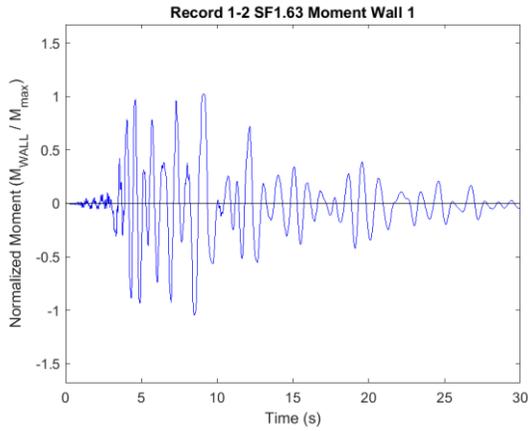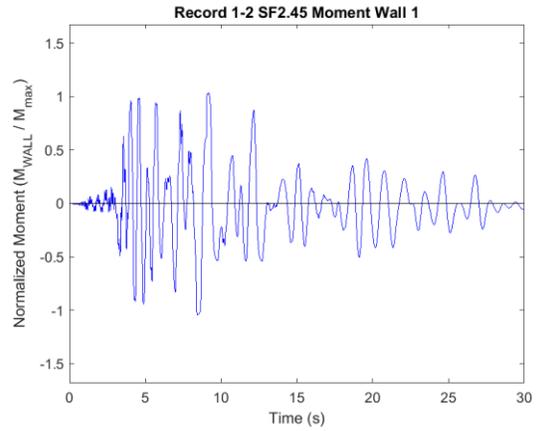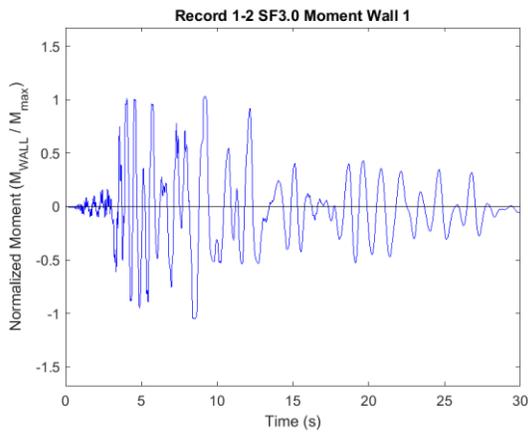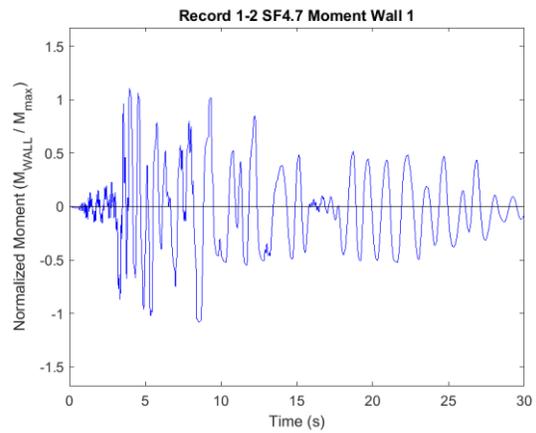
Figure 13.2. Normalized moment vs. time of 3-story archetype for median response for different hazard levels (a) DBE level; (b) MCE level; (c) 3% IDR; (d) 5% IDR
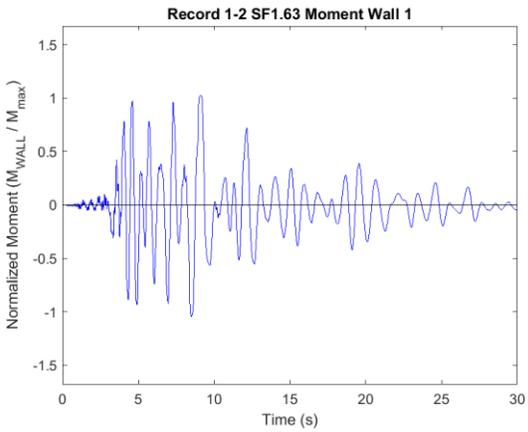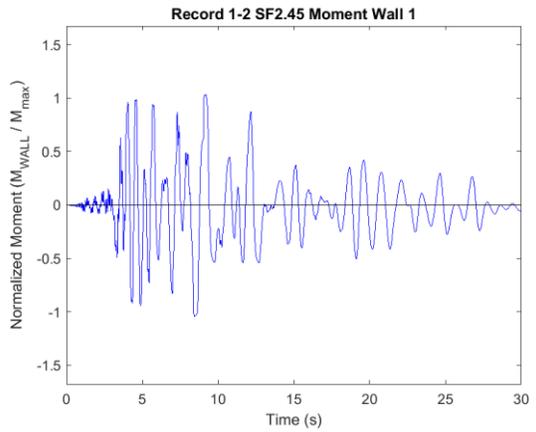
Figure 13.3. Normalized moment vs. time of 3-story archetype at 3% IDR hazard level (a) 25th percentile; (b) 75th percentile ground motion response

The 3-story structure nearly reaches yield moment at the base for DBE and yields for MCE, 3% IDR and 5% IDR hazard levels. The yielding spreads through the cross-section along the height resulting in plastic hinge formation near the base of the wall. This plastic hinge at the base acts as the main source of energy dissipation. Figure 13.4 shows the variation of the normalized moment versus change in rotation along the height of the nonlinear zone of the 3-story archetype at a 3% IDR hazard level. Here, element 1 represents the lowermost element near the base and elements 2, 3 and 4 are subsequently present along the nonlinear wall height.
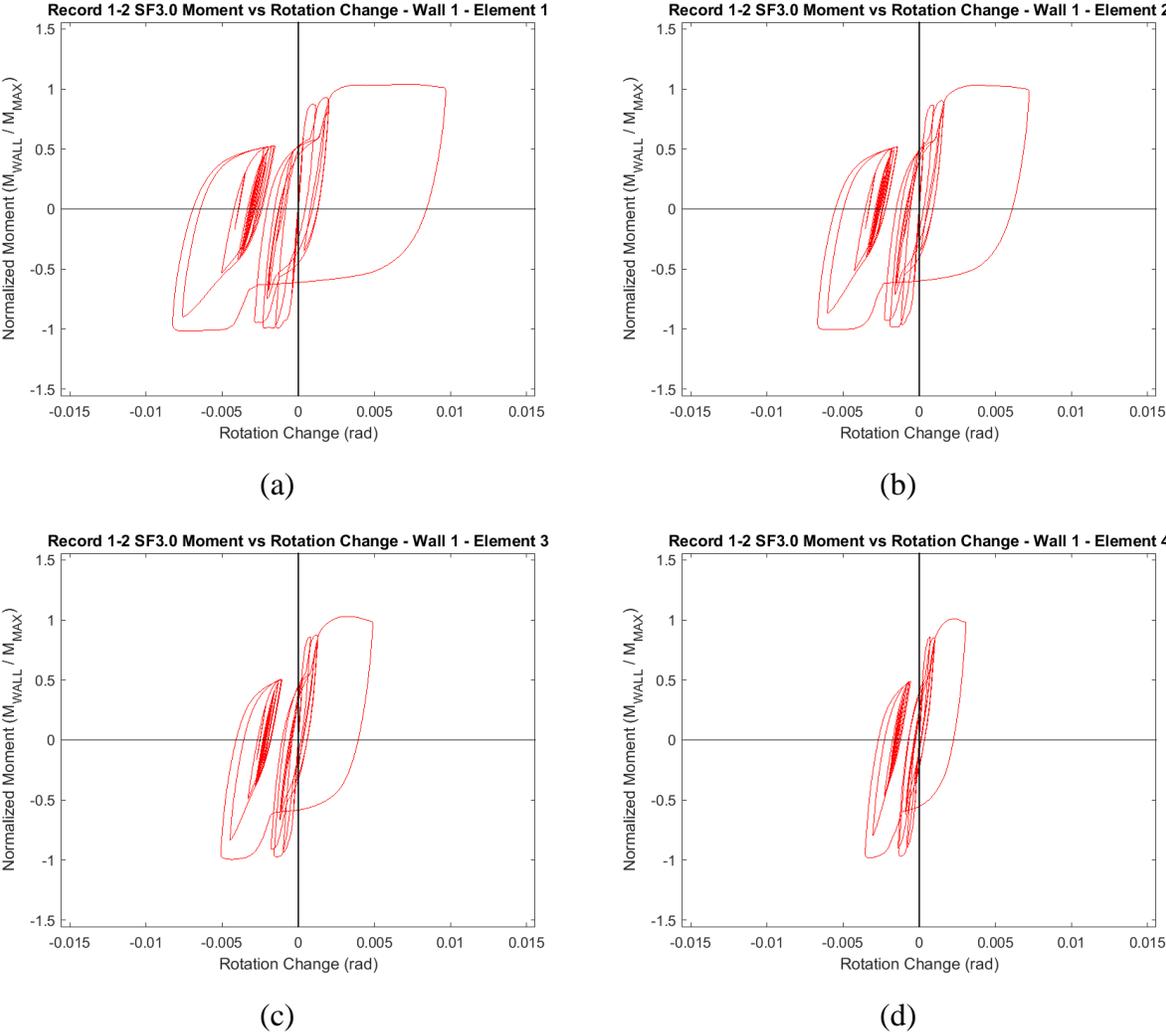
Figure 13.4. Normalized moment vs. change in rotation of 3-story archetype for median response at 3% IDR (a) Element 1; (b) Element 2; (c) Element 3; (d) Element 4

The change in rotation demand decreased along the height of the structure with the highest amount of change in rotation in element 1 and lowest in element 4. Figure 13.5 shows the variation in the behavior of element 1 at the median response for the different hazard levels.

(a)

(b)

(c)

(d)
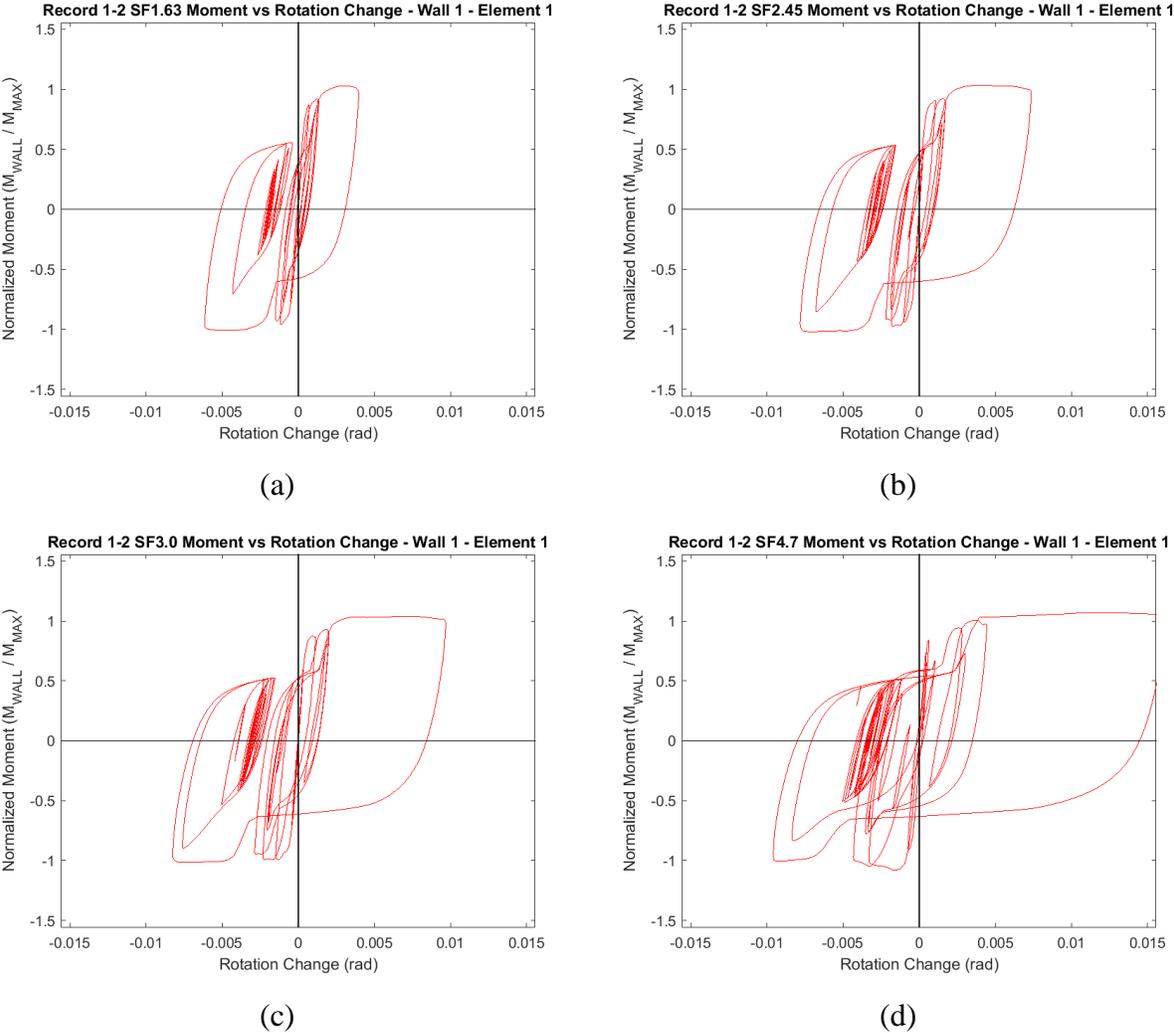
Figure 13.5 Normalized moment vs. change in rotation for element 1 of 3-story archetype at median response (a) DBE; (b) MCE; (c) 3% IDR; (d) 5% IDR

Element 1 has a low rotational demand (less than 0.008 rad) for the DBE and MCE hazard levels but starts to see high rotational demand (more than 0.01 rad) at 3% IDR and 5% IDR. To prevent the collapse of the wall, the total rotation of the base of the wall should not exceed 0.04 rad. Figure 13.6 shows the variation of total plastic hinge rotational demand for different hazard levels at the median ground response. Here the total rotational demand represents the sum of the change in

rotation for all four elements (i.e. element 1, element 2, element 3, and element 4) present in the nonlinear zone of the wall.
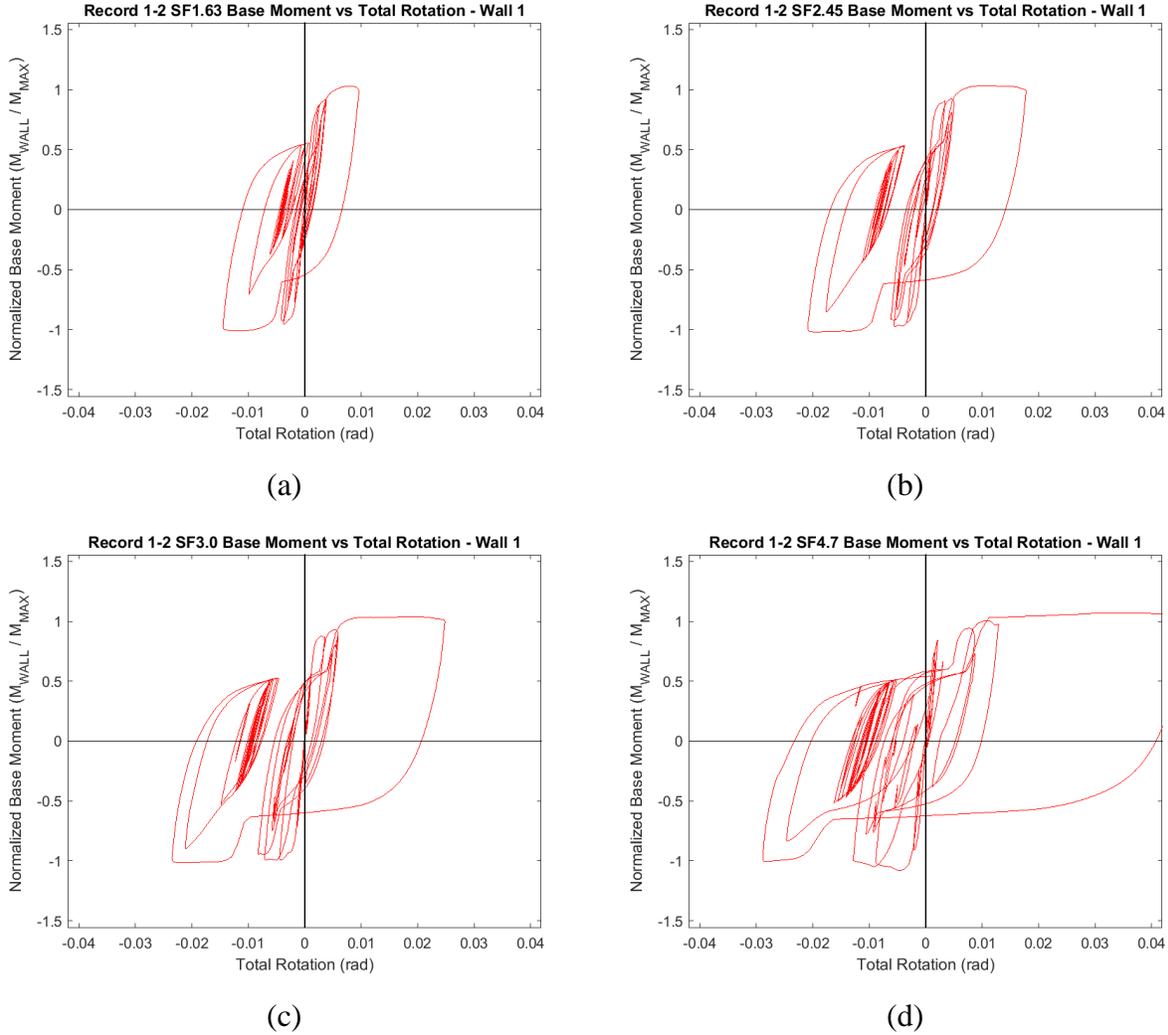
Figure 13.6. Normalized moment vs. total plastic rotation of 3-story archetype for the median response (a) DBE level; (b) MCE level; (c) 3% IDR; (d) 5% IDR

The walls have a total plastic rotation of 0.015 rad, 0.021 rad, 0.024 rad, and 0.046 rad for DBE, MCE, 3% IDR, and 5% IDR hazard levels, respectively. Figure 13.7 shows the variation of total plastic hinge rotation for the three different ground motion responses at a 3% IDR collapse level. The archetype wall has a nearly equivalent plastic rotation for all three ground motion responses as the collapse criterion was fixed at 3% IDR level. Since both, the walls work as an individual

seismic force-resisting system, the same amount of inter-story drift results in a nearly identical value of maximum rotation at the base for a given archetype structure.

(a)

(b)

(c)
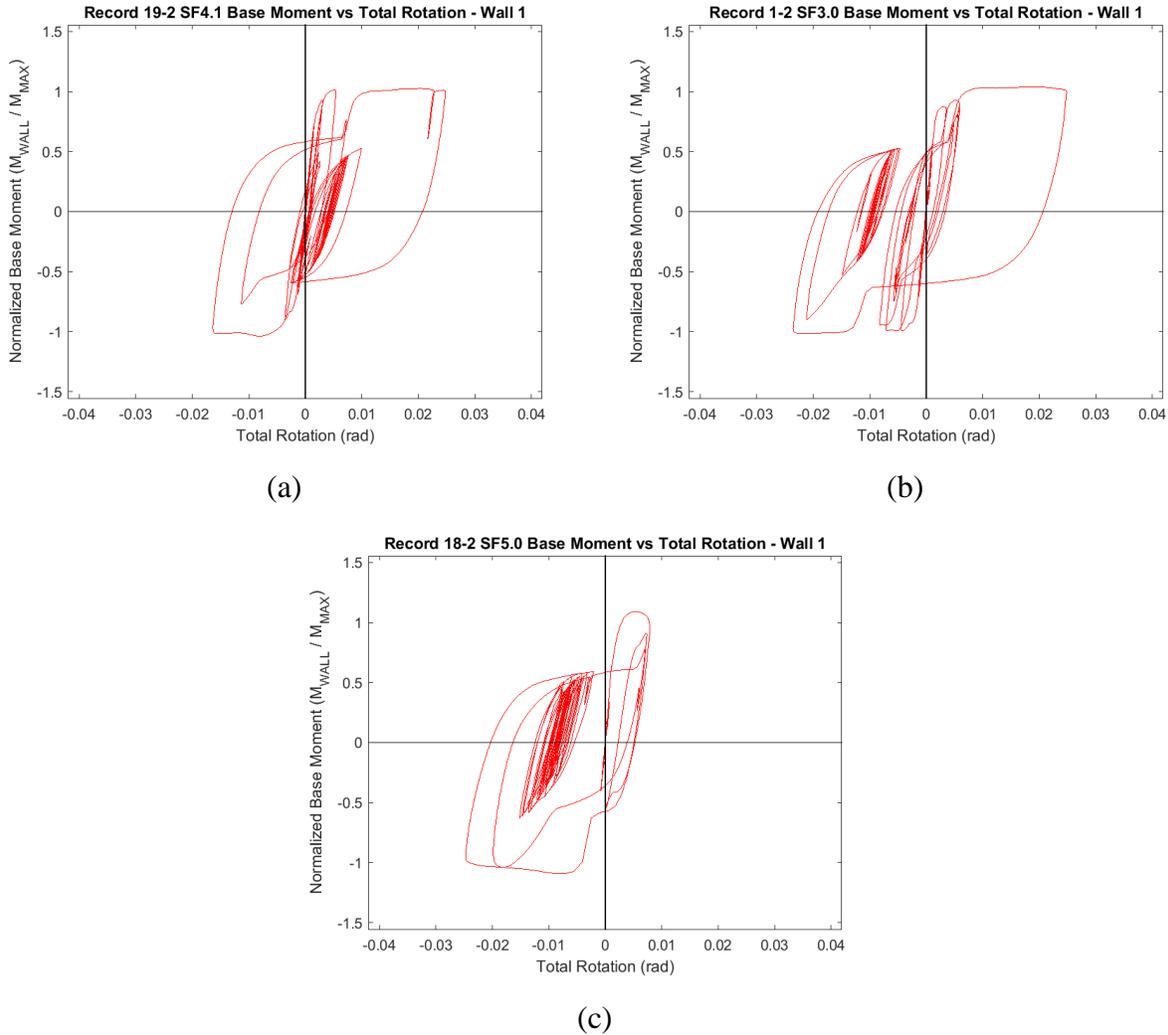
Figure 13.7. Normalized moment vs. total plastic rotation of 3-story archetype at 3% IDR hazard level for (a) 25th percentile ground motion response; (b) Median ground motion response; (c) 75th percentile ground motion response

The stress-strain curve for the extreme steel fiber in element 1 (i.e. outer edge of the closure plate) of the 3-story archetype for median ground motion response is presented in Figure 13.8. The maximum tensile strain of 0.039 in/in, 0.049 in/in, 0.057 in/in, and 0.091 in/in was observed at the DBE, MCE, 3% IDR, and 5% IDR hazard levels, respectively. The maximum tensile strain at 5% IDR level reached close to the strain limit of 0.1in/in defined in the OpenSees model. A minimum

compressive strain of -0.013 in/in, -0.018 in/in, -0.024 in/in, and -0.045 in/in was observed at the DBE, MCE, 3% IDR, and 5% IDR hazard level, respectively.

n(a)   (b)

(c)   (d)
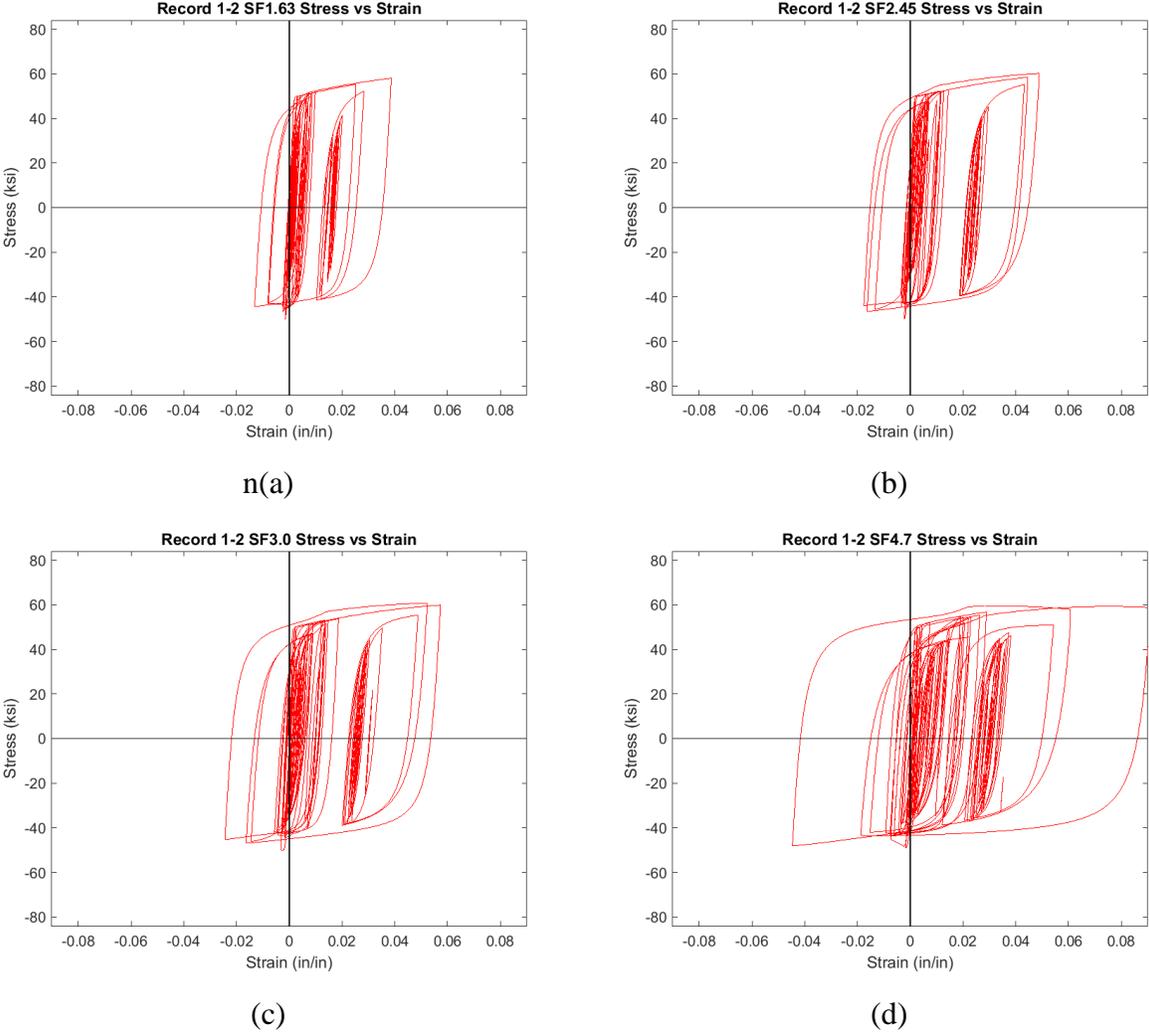
Figure 13.8. Stress-strain curve for extreme steel fibers of 3-story archetype at the median response (a) DBE level; (b) MCE level; (c) 3% IDR; (d) 5% IDR hazard levels

The post-processing results including global response and local response of 3-story, 6-story, 9-story, and 12-story archetype structures are summarized in Table 13-1 to Table 13-4, respectively. The table lists each structure's response including the maximum inter-story drift ratio, maximum total rotation at the base, and maximum tensile and minimum compression strain (element 1 outermost steel fiber). The archetype responses are listed for the 25th percentile, 50th percentile,

and 75th percentile ground motion records at the hazard DBE and MCE hazard levels and 3% and 5% collapse criteria.

Table 13-1. Post-processing results for 3-story planar archetype structure

Percentile SA @ 3% IDR	Ground Motion (PEER-NGA Record)	Hazard Level	Scale Factor	SA (g)	IDR (%)	Max Base Rot (rad)	Max Tensile Strain E1 (in/in)	Min Comp Strain E1 (in/in)
25% Response	19-2 (CHICHI/ CHY101-E)	DBE	1.6	0.6	1.0	0.006	0.019	-0.005
		MCE	2.4	0.9	1.6	0.025	0.068	-0.026
		3% IDR	4.1	1.6	2.9	0.025	0.068	-0.026
		5% IDR	5.4	2.1	4.9	0.045	0.122	-0.055
50% Response	1-2 (NORTHR/ MUL279)	DBE	1.6	1.2	1.7	0.015	0.039	-0.013
		MCE	2.4	1.9	2.6	0.021	0.049	-0.018
		3% IDR	3.0	2.1	2.9	0.024	0.057	-0.024
		5% IDR	4.7	3.2	4.9	0.046	0.091	-0.045
75% Response	18-2 (CAPEMEND/ RIO270)	DBE	1.6	0.9	0.9	0.005	0.013	-0.003
		MCE	2.4	2.3	1.4	0.010	0.025	-0.009
		3% IDR	5.0	3.0	3.1	0.025	0.049	-0.020
		5% IDR	11.4	7.0	5.0	0.040	0.076	-0.043

Table 13-2. Post-processing results for 6-story planar archetype structure

Percentile SA @ 3% IDR	Ground Motion (PEER-NGA Record)	Hazard Level	Scale Factor	SA (g)	IDR (%)	Max Base Rot (rad)	Max Tensile Strain E1 (in/in)	Min Comp Strain E1 (in/in)
25% Response	9-1 (KOCAELI/ DZC180)	DBE	1.70	0.53	0.71	0.003	0.006	-0.002
		MCE	2.55	0.81	1.18	0.007	0.016	-0.006
		3% IDR	5.20	1.64	2.97	0.022	0.055	-0.024
		5% IDR	7.2	2.27	5	0.045	0.104	-0.043
50% Response	4-1 (HECTOR/ HEC000)	DBE	1.70	0.52	1.15	0.007	0.017	-0.005
		MCE	2.55	0.8	1.43	0.008	0.020	-0.005
		3% IDR	6.20	1.93	2.87	0.022	0.053	-0.019
		5% IDR	10.1	3.15	4.9	0.041	0.088	-0.039
75% Response	13-1 (LOMAP/ CAP000)	DBE	1.70	0.83	1.7	0.012	0.033	-0.012
		MCE	2.55	1.25	2.1	0.015	0.040	-0.015
		3% IDR	5.10	2.5	2.9	0.022	0.052	-0.022
		5% IDR	8.5	4.97	5.1	0.041	0.080	-0.039

Table 13-3. Post-processing results for 9-story planar archetype structure

Percentile SA @ 3% IDR	Ground Motion (PEER-NGA Record)	Hazard Level	Scale Factor	SA (g)	IDR (%)	Max Base Rot (rad)	Max Tensile Strain E1 (in/in)	Min Comp Strain E1 (in/in)
25% Response	22-1 (SFERN/ PEL090)	DBE	1.67	0.72	1.47	0.008	0.020	-0.006
		MCE	2.51	1.08	2.58	0.017	0.041	-0.015
		3% IDR	2.80	1.21	2.92	0.021	0.047	-0.018
50% Response	3-1 (DUZCE/ BOL000	DBE	1.67	0.41	0.92	0.003	0.005	-0.002
		MCE	2.51	0.61	1.32	0.006	0.012	-0.004
		3% IDR	6.60	1.62	2.98	0.020	0.047	-0.019
75% Response	1-2 (NORTHR/ MUL279)	DBE	1.67	0.72	1.43	0.008	0.016	-0.005
		MCE	2.51	1.3	2.4	0.010	0.021	-0.007
		3% IDR	5.50	2.4	2.93	0.023	0.043	-0.017

Table 13-4. Post-processing results for 12-story planar archetype structure

Percentile SA @ 3% IDR	Ground Motion (PEER-NGA Record)	Hazard Level	Scale Factor	SA (g)	IDR (%)	Max Base Rot (rad)	Max Tensile Strain E1 (in/in)	Min Comp Strain E1 (in/in)
25% Response	10-1 (KOCAELI/ ARC000)	DBE	1.93	0.12	0.36	0.001	0.001	-0.001
		MCE	2.89	0.17	0.55	0.001	0.002	-0.001
		3% IDR	14.20	0.84	3.00	0.022	0.051	-0.020
50% Response	11-2 (LANDERS/ YER360)	DBE	1.93	0.27	0.77	0.002	0.004	-0.001
		MCE	2.89	0.40	1.06	0.004	0.008	-0.002
		3% IDR	8.10	1.13	2.91	0.022	0.046	-0.019
75% Response	2-1 (NORTHR/ LOS000)	DBE	1.93	0.57	1.35	0.006	0.012	-0.003
		MCE	2.89	0.76	1.83	0.008	0.017	-0.005
		3% IDR	6.20	1.63	3.04	0.017	0.038	-0.016

Table 13-5 shows the maximum tensile strain and maximum compression strain observed in element 2 (E2), element 3 (E3), and element 4 (E4) for the 6-story archetype structure. It also shows the average maximum tensile strain and compressive strain observed over the entire nonlinear range, i.e. E1 to E4. It can be observed that the absolute value of both maximum tensile strain and maximum compression strain decreases as we move from the element 1 (E1) to element 4 (E4). The average maximum tensile strain for 3% IDR hazard level was found out to be around

0.034 and the average maximum compression strain for 3% IDR hazard level was found out to be around -0.014.

Table 13-5. Maximum strains for 6-story planar archetype structure

Percentile SA @ 3% IDR	Hazard Level	Maximum Tensile Strain (in/in)			Maximum Compressive Strain (in/in)			Average Max (E1, E2, E3, E4)	
		E2	E3	E4	E2	E3	E4	Tensile (in/in)	Comp. (in/in)
25% Response (9-1)	DBE	0.005	0.004	0.003	-0.002	-0.002	-0.001	0.005	-0.002
	MCE	0.011	0.008	0.006	-0.004	-0.003	-0.002	0.010	-0.004
	3% IDR	0.040	0.026	0.016	-0.016	-0.010	-0.005	0.034	-0.014
	5% IDR	0.079	0.058	0.039	-0.030	-0.020	-0.012	0.070	-0.026
50% Response (4-1)	DBE	0.013	0.009	0.006	-0.003	-0.002	-0.002	0.011	-0.003
	MCE	0.015	0.011	0.008	-0.004	-0.003	-0.002	0.014	-0.003
	3% IDR	0.040	0.028	0.020	-0.012	-0.007	-0.004	0.035	-0.011
	5% IDR	0.070	0.053	0.040	-0.028	-0.018	-0.011	0.063	-0.024
75% Response (13-1)	DBE	0.022	0.014	0.009	-0.007	-0.004	-0.003	0.019	-0.006
	MCE	0.028	0.018	0.011	-0.008	-0.005	-0.003	0.024	-0.008
	3% IDR	0.039	0.031	0.024	-0.014	-0.008	-0.006	0.036	-0.013
	5% IDR	0.065	0.051	0.041	-0.029	-0.021	-0.015	0.059	-0.026

13.2 C-Shaped Walls

This section summarizes the post-processing results of C-shaped walls. An example of post-processing conducted is presented in detail for the 3-story archetype and then tabulated results for all planar archetypes are listed in Table 13-6 to Table 13-8. Figure 13.9 shows the SA versus maximum IDR plot and the three ground motion responses selected corresponding to the 25th, 50th (median), and 75th percentile spectral acceleration at 3% IDR. For the 15-story archetype, 25th percentile, 50th percentile, and 75th percentile response corresponds to a record from the Superstition Hills (PEER-NGA Record SUPERST/B-ICC000), Friuli, Italy (FRIULI/A-TMZ000), and Loma Prieta (LOMAP/CAP090), respectively. For the 15-story archetype, the MCE level earthquake was observed at the scale factor 3.1 and the DBE level earthquake. The 3% IDR was observed at different scale factors depending on the response of the archetype structures.
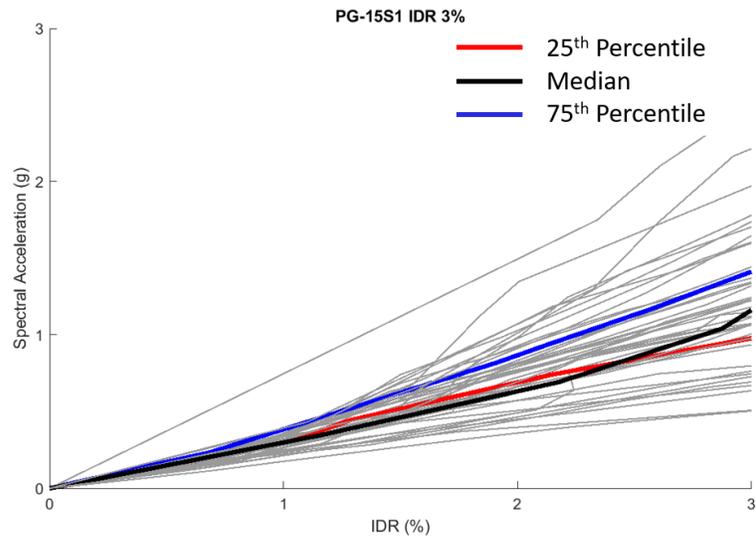
Figure 13.9. Spectral acceleration (g) vs. IDR (%) highlighting 25th percentile, 50th percentile, and 75th percentile ground motion response

Figure 13.10 to Figure 13.12 shows the normalized moment at the base of the 15-story archetype wall at DBE and 5% IDR for the median, 25th percentile, and the 75th percentile ground motion.
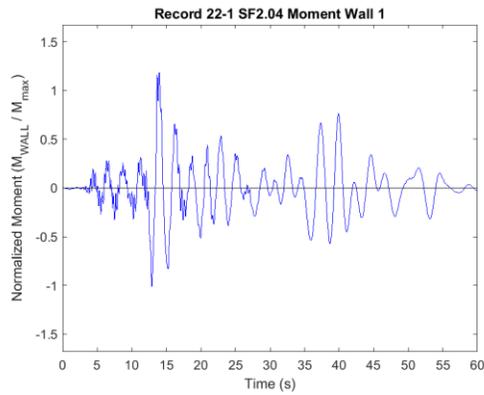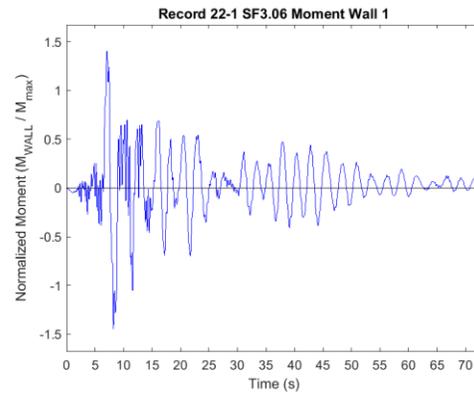
(a)   (b)

Figure 13.10 Normalized moment vs. time of 15-story archetype for median response (a) DBE level; (b) 3% IDR
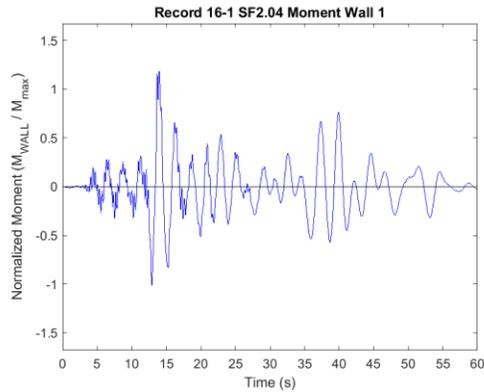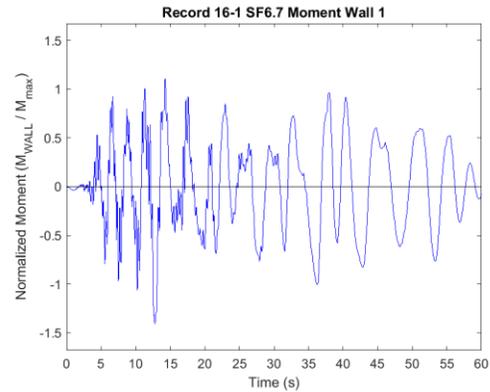
(a)   (b)

Figure 13.11 Normalized moment vs. time of 15-story archetype for 25th percentile response (a) DBE level; (b) 3% IDR
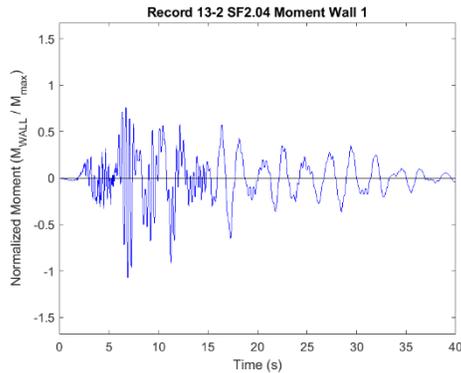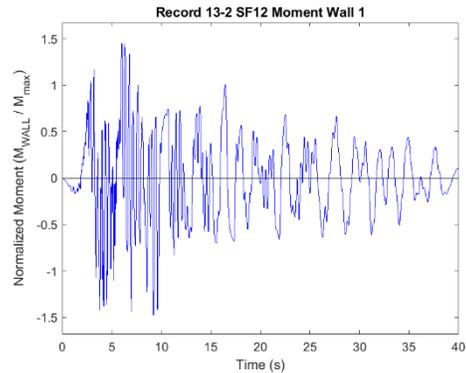
(a)   (b)

Figure 13.12 Normalized moment vs. time of 15-story archetype for 75th response (a) MCE level; (b) 3% IDR

Figure 13.13 shows the variation of total plastic hinge rotational demand at different hazard levels for the 75th percentile ground response. The maximum plastic rotation of 0.003 rad, 0.009 rad, and 0.012 rad were observed for the 75th percentile ground motion response at DBE level, MCE level and 3% IDR collapse level, respectively. Overall less plastic rotation was observed for taller C-shaped walls compared to the shorter planar wall archetype (approximately 20% difference). The archetype structure reached the yield point for the DBE level earthquake and for the remainder of the hazard levels.
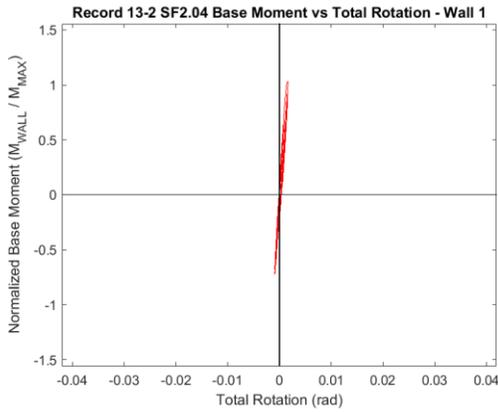
(a)
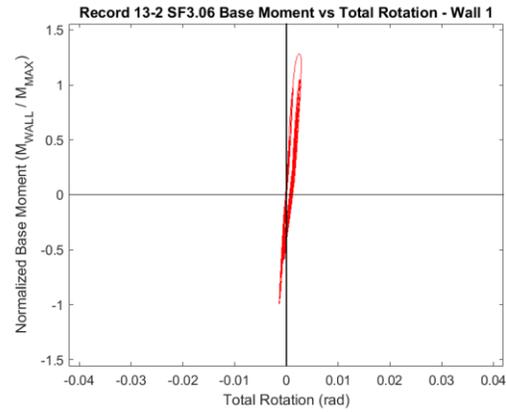
(b)
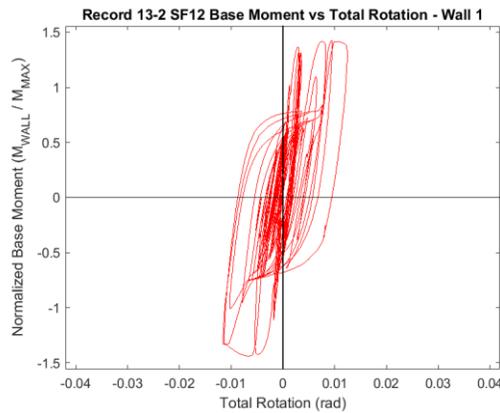
(c)

Figure 13.13. Normalized moment vs. total plastic rotation of 15-story archetype for the 75th percentile response (a) DBE level; (b) MCE level; (c) 3% IDR

The stress-strain curve of extreme steel fiber (i.e. extreme flange plate) of 15-story archetype for the 75th percentile ground motion response is presented in Figure 13.14. The maximum tensile strain of 0.006 in/in, 0.020 in/in, and 0.029 in/in was observed at the DBE, MCE, and 3% IDR hazard level, respectively. The minimum compressive strain of -0.002 in/in, -0.004 in/in, and -0.012 in/in was observed at the DBE, MCE, and 3% IDR hazard level, respectively. The absolute value maximum tensile and compressive strain observed for the C-shaped archetypes were comparatively less than that of planar archetype for similar hazard levels.

119
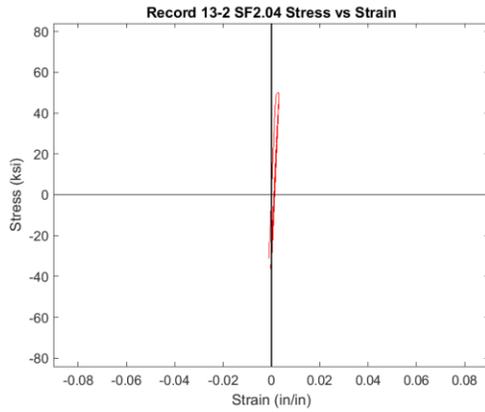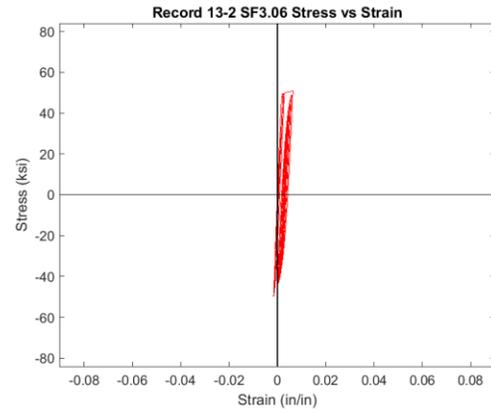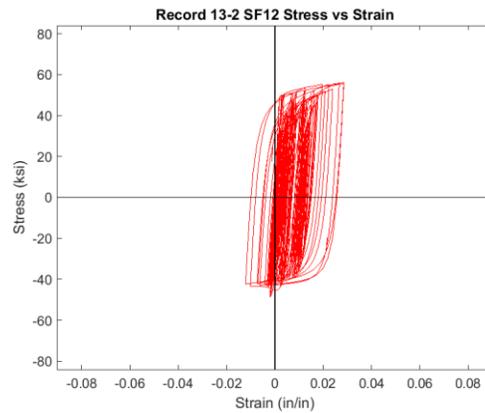
Figure 13.14. Stress-strain curve for extreme steel fibers of 15-story archetype for the 75th percentile response at (a) DBE level; (b) MCE level; (c) 3% IDR

The post-processing results including global response and local response of 15-story, 18-story, and 22-story archetype structures are summarized in Table 13-6 to Table 13-8, respectively. The behavior of archetypes at 25th percentile, 50th percentile, and 75th percentile at the hazard levels of DBE, MCE, 3% IDR (collapse criterion) and 5% IDR are presented in these tables.

Table 13-6. Post processing results for 15-story C-shaped archetype structure

Percentile SA @ 3% IDR	Ground Motion (PEER-NGA Record)	Hazard Level	Scale Factor	SA (g)	IDR (%)	Max Base Rot (rad)	Max Tensile Strain E1 (in/in)	Min Comp Strain E1 (in/in)
25% Response	16-1 (SUPERST/ B-ICC000)	DBE	2.04	0.30	1.02	0.003	0.007	-0.001
		MCE	3.06	0.45	1.31	0.005	0.011	-0.002
		3% IDR	6.70	1.00	3.04	0.016	0.032	-0.011
50% Response	22-1 (SFERN/ PEL090)	DBE	2.04	0.71	2.21	0.009	0.020	-0.004
		MCE/3% IDR	3.06	1.04	2.87	0.014	0.029	-0.005
		5% IDR	8.10	2.81	5.91	0.043	0.069	-0.034
75% Response	13-2 (LOMAP/ CAP090)	DBE	2.04	0.24	0.70	0.003	0.006	-0.002
		MCE	3.06	0.36	0.98	0.009	0.020	-0.004
		3% IDR	12.00	1.40	2.98	0.012	0.029	-0.012

Table 13-7. Post processing results for 18-story C-shaped archetype structure

Percentile SA @ 3% IDR	Ground Motion (PEER-NGA Record)	Hazard Level	Scale Factor	SA (g)	IDR (%)	Max Base Rot (rad)	Max Tensile Strain E1 (in/in)	Min Comp Strain E1 (in/in)
25% Response	11-1 (LANDERS/ YER270)	DBE	2.15	0.30	1.10	0.003	0.007	-0.002
		MCE	3.23	0.45	1.51	0.005	0.013	-0.003
		3% IDR	6.30	0.88	2.80	0.018	0.046	-0.019
50% Response	17-1 (SUPERST/ B-POE270)	DBE	2.15	0.37	1.40	0.005	0.016	-0.004
		MCE	3.23	0.59	1.97	0.009	0.024	-0.009
		3% IDR	5.60	1.05	2.92	0.017	0.039	-0.018
75% Response	4-2 (HECTOR/ HEC090)	DBE	2.15	0.32	1.25	0.003	0.009	-0.002
		MCE	3.23	0.48	1.56	0.006	0.016	-0.004
		3% IDR	9.20	1.38	3.07	0.019	0.042	-0.018

Table 13-8. Post processing results for 22-story C-shaped archetype structure

Percentile SA @ 3% IDR	Ground Motion (PEER-NGA Record)	Hazard Level	Scale Factor	SA (g)	IDR (%)	Max Base Rot (rad)	Max Tensile Strain E1 (in/in)	Min Comp Strain E1 (in/in)
25% Response	16-1 (SUPERST/ B-ICC000)	DBE	2.47	0.20	1.05	0.002	0.005	-0.001
		MCE	3.70	0.29	1.52	0.004	0.012	-0.002
		3% IDR	7.50	0.54	2.85	0.017	0.045	-0.013
50% Response	7-2 (KOBE/ NIS090)	DBE	2.47	0.22	1.32	0.003	0.009	-0.002
		MCE	3.70	0.33	1.77	0.006	0.015	-0.005
		3% IDR	8.10	0.73	3.08	0.016	0.038	-0.017
75% Response	9-2 (KOCAELI/ DZC270)	DBE	2.47	0.25	1.02	0.002	0.005	-0.001
		MCE	3.70	0.33	1.46	0.003	0.009	-0.001
		3% IDR	10.30	0.92	3.04	0.013	0.035	-0.007

14 SUMMARY AND CONCLUSION

Composite plate shear walls – concrete filled (C-PSW/CF) are highly efficient and effective seismic force-resisting system. This system along with the coupled composite wall system is transforming the construction of tall buildings. The system significantly reduces construction duration compared to the traditional reinforced concrete systems. The system has many of the benefits of reinforced concrete walls in terms of strength and stiffness without having problems with rebar congestion. C-PSW/CF construction does not require complex formwork which adds to the time and cost of onsite construction. Overall, this system provides a viable alternative for traditional reinforced concrete walls seismic resisting system.

As presented in this report, a study based on FEMA P695 methodology was conducted to quantify the seismic response of the C-PSW/CF system. This study validates the seismic performance and collapse assessment of C-PSW/CF. The details on the seismic design philosophy of C-PSW/CF are outlined in Chapters 3 and 4. Four planar C-PSW/CF (3-story, 6-story, 9-story, and 12-story) and three C-shaped (15-story, 18-story, and 22-story) C-PSW/CF archetypes were designed using a seismic response modification factor, R, of 6.5 and a deflection amplification factor, C_d, of 5.5. The details of the seven archetypes were presented in Section 5. OpenSees was used to develop a 2D fiber-based nonlinear finite element model (see Section 6). The OpenSees models accounted for the steel and concrete material properties, and the model was benchmarked using experimental test results conducted on composite walls (See Section 7 and 8). Nonlinear static and dynamic analyses were conducted using the above OpenSees model. The results of the nonlinear analysis were used to evaluate the performance of the C-PSW/CF system (see Sections 9 and 10) designed using the seismic performance factors mentioned above. After nonlinear analysis, post processing of structural response was performed to further understand the wall behavior and material response under time history analysis. All planar and C-shaped C-PSW/CF archetype reached a 3% inter-story drift before collapse for each of the 44 ground motions. Collapse and a large amount of base rotation were observed before 5% inter-story drift for some of the analyses. Hence, a conservative value of 3% IDR (less than the actual collapse point) was assumed as the collapse criterion.

In general, a larger value of the collapse margin ratio was observed for taller structures. The adjusted collapse margin ratio, *ACMR,* (period-based ductility, $\mu_t = 3$) was 1.90, 2.64, 3.09, 2.96, 3.46, 3.72, and 3.02 for the 3, 6, 9, 12, 15, 18 and 22 story archetypes, respectively. The *ACMR* using the actual period-based ductility was found to be 2.16, 3.08, 3.72, 3.61, 4.22, 4.53, and 3.68 for the 3, 6, 9, 12, 15, 18 and 22 story archetypes, respectively. These values were compared to the *ACMR$_{10\%}$* collapse criterion of 1.96 and *ACMR$_{20\%}$* collapse criterion of 1.56 for the total system collapse uncertainty, β_{TOT}, as "good".

The overstrength factor, Ω_o, was calculated in two ways. First, the overstrength factor was calculated using nominal material properties. These values ranged from 1.44 to 2.75 for the given archetypes. Then the overstrength factor, Ω_o, was calculated using expected steel behavior (yield strength of R_yF_y). The overstrength strength calculated using these materials ranged from 1.54 to 2.92. The overstrength factor for planar and C-shaped archetype is summarized in Table 12-3. As the overstrength factor is intended to quantify the inherent overdesign in the structure, an overstrength factor, Ω_o, of 2.5 is recommended as the overstrength factor for the archetype structures.

The deflection amplification factors, C_d, found for the planar and C-shaped archetypes are summarized in Table 12-2. The average deflection amplification factor was 5.3. This value was calculated at the 90th percentile confidence level for the design basis earthquake. This value compares well with the current ASCE7-16 C_d factor of 5.5. Therefore, the Cd factor is recommended to remain at 5.5.

A study was also conducted for walls without closure plates (see Chapter 11). The period-based ductility of these walls was found to be considerably lower than the planar walls with closure plates. The adjusted collapse margin ratio found for walls without closure plates did not satisfy the required collapse prevention criterion. Hence, a more conservative value for the response modification factor is required to design walls without closure plates. Considering the many drawbacks of using C-PSW/CF walls without closure plates, the use of this type of wall should be limited and used only when the inclusion of closure plate or boundary elements is not possible.

Based the findings of this study, walls with half-circular and full-circular boundary elements should have similar, if not better performance, to walls with rectangular boundary elements as the inclusion of these closure plates increases the concrete confinement without introducing potential areas of undesired stress concentrated like the corners of rectangular closure plates. In the future, FEMA P695 study on C-PSW/CF walls with half-circular or full-circular boundary elements could be conducted to verify appropriate seismic performance factors for these wall elements.

REFERENCES

AISC341 (2016). *"Seismic provisions for structural steel buildings."*, ANSI/AISC 341-16, American Institute of Steel Construction, Inc., Chicago, Illinois.

AISC (2013). "Steel Construction Manual." *American Institute of Steel Construction*, ANSI/AISC, American Institute of Steel Construction, Inc., Chicago, Illinois.

AISC (2019). "Speedcore." *Retrieved from* https://www.aisc.org/why-steel/innovative-systems/SpeedCore/*, 07/10/2019*.

Alzeni, Y., and Bruneau, M. (2014). "Cyclic Inelastic Behavior Of Concrete Filled Sandwich Panel Walls Subjected To In-Plane Flexure." *MCEER Report, The State University of New York at Buffalo.*

Alzeni, Yasser, and Michel Bruneau. "In-plane cyclic testing of concrete-filled sandwich steel panel walls with and without boundary elements." *Journal of Structural Engineering* 143, no. 9 (2017): 04017115.

ASCE (2016). *Minimum design loads for buildings and other structures.*, American Society of Civil Engineers Inc., Chicago, Illinois.

Brown, J., and Kunnath, S. K. (2000). "Low-cycle fatigue behavior of longitudinal reinforcement in reinforced concrete bridge columns." *MCEER Report, The State University of New York at Buffalo*.

Broberg, M.R., Shafaei, S., Seo, J., Varma, A.H., Agrawal, S. (2019). "Introduction to Seismic Analysis of Coupled Composite Plate Shear Walls -- Concrete-Filled (CC-PSW/CF)." SSRC Conferences, April 2-5.

Broberg M., Kizilarslan, E., Shafaei, S., Varma, A.H., Bruneau, M., (2019). "Non-linear Inelastic Behavior of Coupled Composite Plate Shear Walls—Concrete Filled (Coupled-CPSW/CF)." *Engineering Journal*, AISC, In Preparation

Bruneau, M., Varma, A.H., Broberg, M.R., Shafaei, S., Seo, J., "R-Factors for Coupled Composite Plate Shear Walls / Concrete Filled (CC-PSW/CF)." Charles Pankow Foundation & American Institute of Steel Construction

Bhardwaj, S., A. Wang, and Amit H. Varma. "Slenderness requirements for CF-CPSW: the effects of concrete casting." In *Proceedings of the Eighth International Conference on Thin-Walled Structures–ICTWS 2018: at Lisbon, Portugal. July 24-27*. 2018.

Chang, G., and Mander, J. B. (1994). "Seismic energy based fatigue damage analysis of bridge columns: part 1-evaluation of seismic capacity." *MCEER Report, The State University of New York at Buffalo*.

CIS (2017). "SAP2000: integrated finite element analysis and design of structures." *Computers and Structures, Berkeley, California*.

Coffin, J. L. F. (1954). "A study of the effects of cyclic thermal stresses on a ductile metal." *trans. ASME*, 76, 931-950.

Coffin, L. (1971). "A note on low cycle fatigue laws(Plastic strain range-fatigue life behavior as two slope relationship, considering low cycle fatigue laws in terms of crack propagation mode change)." *Journal of Materials*, 6, 388-402.

Dhakal, R. P., and Maekawa, K. (2002). "Modeling for postyield buckling of reinforcement." *Journal of Structural Engineering*, 128(9), 1139-1147.

Ezzeldin, M., Wiebe, L., and El-Dakhakhni, W. (2016). "Seismic collapse risk assessment of reinforced masonry walls with boundary elements using the FEMA P695 methodology." *Journal of Structural Engineering*, 142(11), 04016108.

FEMA (2009). "FEMA P695: Quantification of Building Seismic Performance Factors." *Applied Technology Council. Federal Emergency Management Agency*.

Filiatrault, A., and Christovasilis, I. "Example application of the FEMA P695 (ATC-63) Methodology for the collapse performance evaluation of wood light-frame systems." *Proc., 9th US National & 10th Canadian Conference on Earthquake Engineering*.

Fiorino, L., Shakeel, S., Macillo, V., and Landolfo, R. (2017). "Behaviour factor (q) evaluation the CFS braced structures according to FEMA P695." *Journal of Constructional Steel Research*, 138, 324-339.

Gogus, A., and Wallace, J. W. (2015). "Seismic safety evaluation of reinforced concrete walls through FEMA P695 methodology." *Journal of Structural Engineering*, 141(10), 04015002.

Gomes, A., and Appleton, J. (1997). "Nonlinear cyclic stress-strain relationship of reinforcing bars including buckling." *Engineering Structures*, 19(10), 822-826.

Kaufmann, E., Metrovich, B., and Pense, A. (2001). "Characterization of cyclic inelastic strain behavior on properties of A572 Gr. 50 and A913 Gr. 50 rolled sections." *ATLSS Report No. 01-13*.

Kechidi, S., Bourahla, N., and Castro, J. M. (2017). "Seismic design procedure for cold-formed steel sheathed shear wall frames: Proposal and evaluation." *Journal of Constructional Steel Research*, 128, 219-232.

Kircher, C., Deierlein, G., Hooper, J., Krawinkler, H., Mahin, S., Shing, B., and Wallace, J. (2010). "Evaluation of the FEMA P-695 Methodology for Quantification of Building Seismic Performance Factors| NIST." Grant/Contract Reports (NISTGCR) - 10-917-8.

Kizilarslan, E., Kenarangi, H., and Bruneau, M. (2019). "Cyclic Behavior of C-Shaped Composite Plate Shear Walls – Concrete Filled." *Journal of Structural Engineering, ASCE, In preparation*.

Kunnath, S. K., Heo, Y., and Mohle, J. F. (2009). "Nonlinear uniaxial material model for reinforcing steel bars." *Journal of Structural Engineering*, 135(4), 335.

Kuşyılmaz, A., and Topkaya, C. (2016). "Evaluation of seismic response factors for eccentrically braced frames using FEMA P695 methodology." *Earthquake Spectra*, 32(1), 303-321.

Manson, S. (1965). "Fatigue: a complex subject—some simple approximations." *Experimental mechanics*, 5(4), 193-226.

Masroor, A., and Mosqueda, G. (2015). "Assessing the collapse probability of base-isolated buildings considering pounding to moat walls using the FEMA P695 methodology." *Earthquake Spectra*, 31(4), 2069-2086.

Mathworks (1992). "Matlab, User's Guide." *Inc., Natick, MA*, 1992.

McKenna, F., Mazzoni, S., and Fenves, G. (2016). "Open System for Earthquake Engineering Simulation (OpenSees) Software Version 2.2. 5." *University of California, Berkeley, CA. Available from http://opensees.berkeley.edu*.

Menegotto, M. "Pinto,(1973), PE, Method of Analysis for Cyclically Loaded Reinforced Concrete Plane Frames Including Changes in Geometry and Non-elastic Behavior of Elements Under Combined Normal Force and Bending." *Proc., IABSE Symposium on the Resistance and Ultimate Deformability of Structures Acted on by Well-Defined Repeated Loads, Lisbon*.

Miner, M. A. (1945). "Cumulative damage in fatigue." *J. Appl. Mech.*, 12, A159–A164.

Neuenhofer, A., and Filippou, F. C. (1997). "Evaluation of nonlinear frame finite-element models." *Journal of structural engineering*, 123(7), 958-966.

Nicknam, A. (2015). *Seismic analysis and design of buildings equipped with propped rocking wall systems*, ProQuest Dissertations Publishing, 2015. 3683065, The State University of New York at Buffalo.

Nie, J.-G., Hu, H.-S., and Eatherton, M. R. (2014). "Concrete filled steel plate composite coupling beams: Experimental study." *Journal of Constructional Steel Research*, 94, 49-63.

Panthaki, F. D. (1992). "Low cycle fatigue behavior of high strength and ordinary reinforcing steels." Doctoral dissertation, The State University of New York at Buffalo.

PEER (2005). "PEER NGA Database." *Pacific Earthquake Engineering Research Center (PEER), University of California, Berkeley, California <http://peer.berkeley.edu/nga/>*.

PEER, T. (2010). "Guidelines for performance-based seismic design of tall buildings." University of California Berkeley, USA.

Post, N. M. (2019). "Erector Proves Speed Predictions for Radical Steel Frame of Seattle's Rainier Square Tower." *Engineering News-Records*.

Purba, R., and Bruneau, M. (2014). "Seismic performance of steel plate shear walls considering two different design philosophies of infill plates. I: Deterioration model development." *Journal of Structural Engineering*, 141(6), 04014160.

Restrepo-Posada, J., Dodd, L., Park, R., and Cooke, N. (1994). "Variables affecting cyclic behavior of reinforcing steel." *Journal of Structural Engineering*, 120(11), 3178-3196.

Seo, Jungil, Amit H. Varma, Kadir Sener, and Deniz Ayhan. "Steel-plate composite (SC) walls: In-plane shear behavior, database, and design." *Journal of Constructional Steel Research* 119 (2016): 202-215.

Susantha, K., Ge, H., and Usami, T. (2001). "Uniaxial stress–strain relationship of concrete confined by various shaped steel tubes." *Engineering Structures*, 23(10), 1331-1347.

Shafaei, S., Varma, A. H., Broberg, M. R., Seo, J. " An Introduction to Numerical Modeling of Composite Plate Shear Walls / Concrete Filled (C-PSW/CF)." SSRC Conferences, April 2-5.

Shafaei, S., Seo, J., and Varma, A.H. (2019). "Cyclic Behavior of Planar Composite Plate Shear Walls –Concrete Filled." *Journal of Structural Engineering*, ASCE, In Preparation.

Shafaei. S., Wang, A., Varma, A.H., and Morgen, B. (2018). "Stability of Steel Modules During Construction." *Proceedings of the Annual Stability Conference*, Baltimore, MD, April 10-13, 2018.

Tao, Z., Wang, Z.-B., and Yu, Q. (2013). "Finite element modelling of concrete-filled steel stub columns under axial compression." *Journal of Constructional Steel Research*, 89, 121-131.

Vamvatsikos, D., and Cornell, C. A. (2002). "Incremental dynamic analysis." *Earthquake Engineering & Structural Dynamics*, 31(3), 491-514.

Varma, A., Seo, J., and Lai, Z. (2017). "On the Lateral Behavior of Concrete-Filled Composite Plate Shear Walls." *Proceedings of the 9th International Symposium on Steel Structures, Nov. 1-4, 2017*, 426-427.

Varma, Amit H., Soheil Shafaei, and Ron Klemencic. "Steel modules of composite plate shear walls: Behavior, stability, and design." *Thin-Walled Structures* 145 (2019): 106384.

Varma, A. H., S. R. Malushte, and Z. Lai. "Modularity & innovation using steel-plate composite (SC) walls for nuclear and commercial construction." In *Proceedings of the 11th International Conference on Advances in Steel and Concrete Composite Structures, Beijing, China*, pp. 3-5. 2015.

Wallace, J. et al. (2019). *R-Factor for Coupled Concrete Core Wall System.* Report to the Charles Pankow Foundation.

Zareian, F., Lignos, D., and Krawinkler, H. "Evaluation of seismic collapse performance of steel special moment resisting frames using FEMA P695 (ATC-63) methodology." *Proc., Structures Congress 2010*, 1275-1286.

Zhang, K., Varma, A. H., Malushte, S. R., and Gallocher, S. (2014). "Effect of shear connectors on local buckling and composite action in steel concrete composite walls." *Nuclear Engineering and Design*, 269, 231-239.

APPENDIX A – PLASTIC MOMENT AND STIFFNESS CALCULATION

Planar Walls
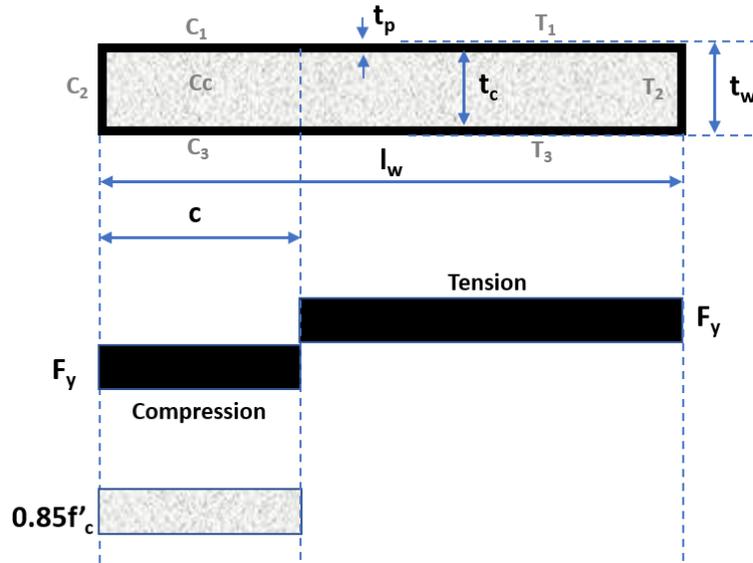
Figure 14.1. Stress distribution assumed in concrete infill and steel plates of Planar C-PSW/CFs for calculating the plastic moment capacity, M_p

Compression Block

$$C_1 = (c - t_p)t_p F_y \qquad \text{A.1a}$$

$$C_2 = t_p t_w F_y \qquad \text{A.1b}$$

$$C_3 = (c - t_p)t_p F_y \qquad \text{A.1c}$$

$$C_c = (c - t_p)t_{cw}(0.85 f_c') \qquad \text{A.1d}$$

$$C = C_1 + C_2 + C_3 + C_c \qquad \text{A.1e}$$

Tension Block

$$T_1 = (l_w - c - t_p)t_p F_y \qquad \text{A.2a}$$

$$T_2 = t_p t_w F_y \qquad \text{A.2b}$$

$$T_3 = (l_w - c - t_p)t_p F_y \qquad \text{A.2c}$$

$$T = T_1 + T_2 + T_3 \qquad \text{A.2d}$$

Here, assuming axial force equal to zero/negligible

$$C = T \qquad \text{A.3}$$

Solving the above equations we get,

Neutral axis, *c*

$$c = \frac{2l_w F_y t_p + 0.85 f_c' t_c t_p}{4F_y t_p + 0.85 f_c' t_c} \qquad \text{A.4}$$

Plastic Moment Capacity, *M_p*

$$M_p = \frac{(C_1 + C_3 + C_c)(c - t_p)}{2} + C_2\left(c - \frac{t_p}{2}\right) + (T_1 + T_3)\frac{(l_w - c - t_p)}{2} + T_2\left(l_w - c - \frac{t_p}{2}\right) \qquad \text{A.5}$$

Flexural Stiffness, *EI_eff*

$$I_s = \frac{2t_p(l_w - 2t_p)^3}{12} + 2t_p t_w\left(\frac{l_w - t_p}{2}\right)^2 \qquad \text{A.6a}$$

$$I_c = \frac{t_{cw}(l_w - 2t_p)^3}{12} \qquad \text{A.6b}$$

$$EI_{eff} = E_s I_s + 0.35 E_c I_c \qquad \text{A.7a}$$

or

$$EI_{eff} = \frac{M_{0.6}}{\varphi_{0.6}} \qquad \text{A.7b}$$

C-Shaped Walls
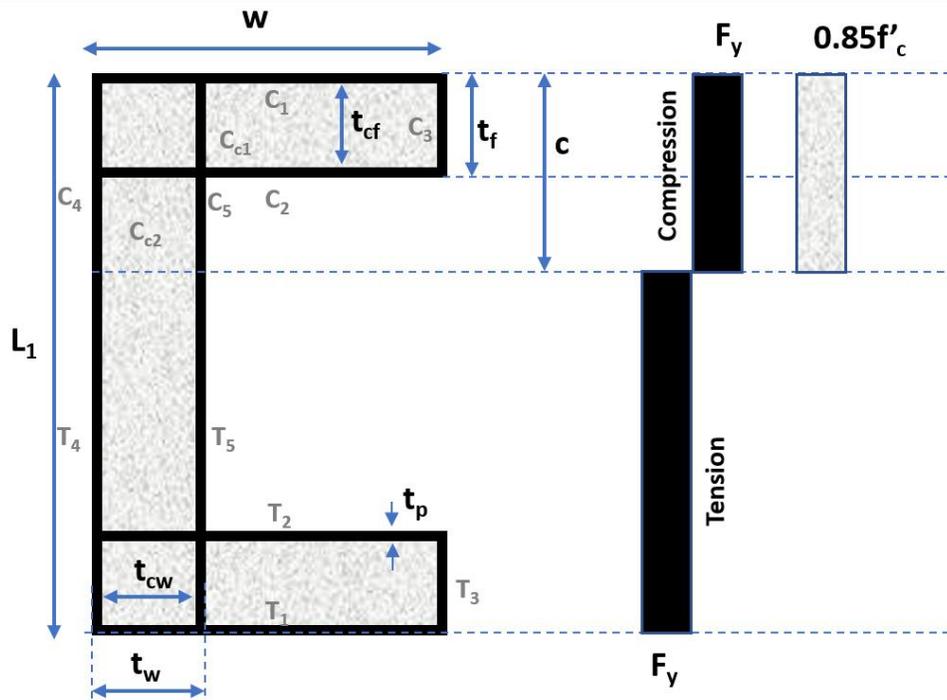
Figure 14.2. Stress distribution assumed in concrete infill and steel plates of C-Shaped C-PSW/CFs for calculating the plastic moment capacity, M_p

Compression Block

$$C_1 = (w - 3t_p)t_p F_y \qquad\qquad \text{A.8a}$$

$$C_2 = (w - 3t_p)t_p F_y \qquad\qquad \text{A.8b}$$

$$C_3 = t_f t_p F_y \qquad\qquad \text{A.8c}$$

$$C_4 = ct_p F_y \qquad\qquad \text{A.8d}$$

$$C_5 = ct_p F_y \qquad\qquad \text{A.8e}$$

$$C_{c1} = (w - 3t_p)(t_{cf})(0.85 f_c') \qquad\qquad \text{A.8f}$$

$$C_{c2} = (c - t_f)t_{cw}(0.85 f_c') \qquad\qquad \text{A.8g}$$

$$C = C_1 + C_2 + C_3 + C_4 + C_5 + C_{c1} + C_{c2} \qquad\qquad \text{A.8h}$$

$$w_c = w - 3t_p \qquad\qquad \text{A.9}$$

Tension Block

$$T_1 = (w - 3t_p)t_p F_y \qquad \text{A.10a}$$

$$T_2 = (w - 3t_p)t_p F_y \qquad \text{A.10b}$$

$$T_3 = t_f t_p F_y \qquad \text{A.10c}$$

$$T_4 = (l_1 - c)t_p F_y \qquad \text{A.10d}$$

$$T_5 = (l_1 - c)t_p F_y \qquad \text{A.10e}$$

$$T = T_1 + T_2 + T_3 + T_4 + T_5 \qquad \text{A.10f}$$

Here, assuming negligible axial force

$$C = T \qquad \text{A.11}$$

Solving the above equations, we get,

Neutral axis, c

$$c = \frac{2l_1 F_y t_p - 0.85 f_c'(t_{cf} w_c - t_{cw} t_f)}{4 F_y t_p + 0.85 f_c' t_{cw}} \qquad \text{A.12}$$

Plastic Moment Capacity, M_p

$$
\begin{aligned}
M_p = {} & C_1\left(c - \frac{t_p}{2}\right) + C_2\left(c - t_f + \frac{t_p}{2}\right) + C_3\left(c - \frac{t_f}{2}\right) + (C_4 + C_5)\frac{c}{2} + \\
& C_{c1}\left(c - \frac{t_f}{2}\right) + C_{c2}\left(\frac{c - t_f}{2}\right) + T_1\left(L_1 - c - \frac{t_p}{2}\right) + T_2\left(L_1 - c - t_f + \frac{t_p}{2}\right) + \\
& T_3\left(L_1 - c - \frac{t_f}{2}\right) + (T_4 + T_5)\frac{(L_1 - c)}{2}
\end{aligned}
\qquad \text{A.13}
$$

Flexural Stiffness, EI_{eff}

$$I_s = 2t_p w_c \frac{\left(L_1 - t_p\right)^2}{4} + 2t_p w_c \left(\frac{L_1 - 2t_f + t_p}{2}\right)^2 + 2t_p \frac{L_1^3}{12}$$

A.14a

$$I_c = \frac{2w_c t_{cf}^3}{12} + 2w_c t_{cf} \left(\frac{L_1 - t_f}{2}\right)^2 + t_{cw} \frac{\left(L_1 - 2t_f\right)^3}{12}$$

A.14b

$$EI_{eff} = E_s I_s + 0.35 E_c I_c$$

A.15a

or

$$EI_{eff} = \frac{M_{0.6}}{\varphi_{0.6}}$$

A.15b

137

APPENDIX B – EQUIVALENT LATERAL FORCE CALCULATIONS FOR 6-STORY ARCHETYPE

This appendix shows the equivalent lateral force calculation for the 6-story planar C-PSW/CF archetype.

Equivalent Lateral Force Calculations - 6-story Archetype

Step 1: Initial Parameters

Floor Plan

$N_{wall} := 2$ Number of walls in each direction

$w_{fl} := 0.12 ksf$ Floor dead load

$Fl_{width} := 205 ft$ Building width

$Fl_{depth} := 105 ft$ Building depth

$n_{fl} := 6$ Number of floors

$h_{typ} := 14 ft$ Typical floor height

$h_1 := 17 ft$ First floor height

$h_n := h_1 + h_{typ} \cdot (n_{fl} - 1) = 87 \cdot ft$ Total height of the building

$i := 1 .. n_{fl}$

$w_i := w_{fl} \cdot Fl_{width} \cdot Fl_{depth}$ Story weight

$w_1 = 2.58 \times 10^3 \cdot kip$

$W := \sum_{j=1}^{n_{fl}} w_j = 1.55 \times 10^4 \cdot kip$ Total weight

Step 2: Equivalent Lateral Force Analysis

Step 2-1: Develop response spectra

Calculated from D_{max}

The response spectra provided in FEMA P695 was used to select S_{DS} and S_{D1}

Response Spectra Parameters　　Site Class: D

$S_{DS} := 1.0$ 　　　　　　　　　　　　　　　　　　FEMA P695 Table 6-1,(ASCE7 11.4-3)

$S_{D1} := 0.6$ 　　　　　　　　　　　　　　　　　　FEMA P695 Table 6-1, (ASCE7 11.4-3)

Seismic Design Coefficients for C-PSW/CF walls

$R := 6.5$ 　　　　　　　　　　　　　　　　　　Response modification factor

$Cd := 5.5$ 　　　　　　　　　　　　　　　　　　Deflection amplification factor

$\Omega := 2.5$ 　　　　　　　　　　　　　　　　　　Overstrength factor

$I_e := 1$ 　　　　　　　　　　　　　　　　　　Importance factor

$\rho := 1$ 　　　　　　　　　　　　　　　　　　Seismic redundancy factor taken one for FEMA P695 study

Step 2-2: Estimate Fundamental Period (T)

$C_t := 0.02$ 　　　　　　　　　　　　　　　　　　Building period coefficient (ASCE 7 Table 12.8-2) selected considering "All other structural systems"

$x := 0.75$

$T_L := 8$ 　　　　　　　　　　　　　　　　　　Long Period

$T_o := 0.2 \cdot \dfrac{S_{D1}}{S_{DS}} = 0.12$ 　　　　　　　　　　0.2S_{DS}/S_{D1}, (ASCE7 Chapter 11)

$T_s := \dfrac{S_{D1}}{S_{DS}} = 0.6$ 　　　　　　　　　　S_{DS}/S_{D1}, (ASCE7 Chapter 11)

$T_a := C_t \cdot \left(\dfrac{h_n}{ft}\right)^x = 0.57$ 　　　　　　　　Approximate fundamental period

139

$$C_u := \begin{cases} 1.7 & \text{if } S_{D1} \le 0.15 \\ 1.6 & \text{if } 0.2 \ge S_{D1} \ge 0.15 \\ 1.4 & \text{if } S_{D1} \ge 0.3 \\ 1.5 & \text{if } 0.3 \ge S_{D1} \ge 0.2 \end{cases} = 1.4$$

Coefficients for upper limit period
(ASCE7-16 Table 12.8-1)
Interpolation may be required

$$T := C_u \cdot T_a = 0.8$$

Upper Limit Period
Sturcuture period is greater than
$C_u T_a$, so $C_u T_a$ is selected for design

Step 2-3: Seismic Response Coefficients (C_s)

$$C_{s\_cal} := \frac{S_{DS}}{\dfrac{R}{I_e}} = 0.15$$

(ASCE7 12.8-6)

(ASCE7 12.8-3)

$$C_{s\_max} := \begin{cases} \dfrac{S_{D1}}{T \cdot \dfrac{R}{I_e}} & \text{if } T \le T_L \\[4ex] \dfrac{S_{D1} \cdot T_L}{T^2 \cdot \dfrac{R}{I_e}} & \text{if } T \ge T_L \end{cases} = 0.12$$

$$C_{s1} := \max\left(0.044 \cdot S_{DS} \cdot I_e, 0.01, C_{s\_max}\right) = 0.12$$

(ASCE7 12.8-5)

$$C_s := \min\left(C_{s\_cal}, C_{s\_max}\right) = 0.12$$

Seismic response coefficient

Step 2-4: Base Shear Calculation

$$V := C_s \cdot W = 1.79 \times 10^3 \cdot \text{kip}$$

Base Shear

Step 2-5: Vertical Distribution of Seismic Forces

$$k := \begin{cases} \left[1 + \dfrac{(T - 0.5)}{2}\right] & \text{if } 0.5 \le T \le 2.5 \\ 1 & \text{if } T \le 0.5 \\ 2 & \text{if } T \ge 2.5 \end{cases} = 1.15$$

(ASCE7 12.8.3)

Story Elevations

$$ht_i := h_{typ} \qquad ht_1 := h_1$$

$$h_i := \sum_{j=1}^{i} ht_j \qquad h = \begin{pmatrix} 0 \\ 17 \\ 31 \\ 45 \\ 59 \\ 73 \\ 87 \end{pmatrix} ft$$

Story Elevations

Story Shear

$$Cv_i := \frac{w_i \cdot \left(\dfrac{h_i}{ft}\right)^k}{\displaystyle\sum_{j=1}^{n_{fl}} \left[w_j \cdot \left(\dfrac{h_j}{ft}\right)^k \right]}$$

Vertical distribution factor
(ASCE7 12.8-12)

$$Fx_i := V \cdot Cv_i \qquad Fx = \begin{pmatrix} 0 \\ 81 \\ 162 \\ 248 \\ 339 \\ 433 \\ 530 \end{pmatrix} \cdot kip$$

Story force (ASCE 7 12.8-11)

$$Fsum_i := \sum_{j=i}^{n_{fl}} Fx_j \qquad Fsum = \begin{pmatrix} 0 \\ 1794 \\ 1712 \\ 1550 \\ 1302 \\ 963 \\ 530 \end{pmatrix} \cdot kip$$

Story shear
(ASCE 7 12.8-13)

141

Step 2-6: Base Shear Amplification

Amplification Factor

$\text{ShearAmpFactor} := 4$

See Section 4.2.6

$V_{ELF} := V = 1.8 \times 10^3 \cdot \text{kip}$

ELF base shear

$V_{req} := 4 \cdot V_{ELF} = 7.2 \times 10^3 \cdot \text{kip}$

Amplified base shear

Step 2-7: Overturning Moment

$$OTM_i := \sum_{j=i}^{n_{fl}} \left(Fsum_j \cdot ht_j \right) \quad OTM = \begin{pmatrix} 0 \\ 1.4 \times 10^6 \\ 1 \times 10^6 \\ 7.3 \times 10^5 \\ 4.7 \times 10^5 \\ 2.5 \times 10^5 \\ 8.9 \times 10^4 \end{pmatrix} \cdot \text{kip} \cdot \text{in}$$

Overturning moment

$$OTM_{wall} := \frac{OTM_1}{N_{wall}} = 6.9 \times 10^5 \cdot \text{kip} \cdot \text{in}$$

Overturning moment at base of the wall

142

APPENDIX C – ARCHETYPE DESIGN PROCEDURE

Planar Walls – 6 Story Archetype

Step 3: Preliminary Design

Wall Dimensions

$l_w := 25 \text{ft}$ Length of wall

$t_p := 0.3125 \text{in}$ Plate thickness

$t_w := 16 \text{in}$ Wall thickness

Material Properties

$F_y := 50 \text{ksi}$ Nominal steel strength

$f_c := 6 \text{ksi}$ Nominal concrete strength

$E_s := 29000 \text{ksi}$ Modulus of elasticity of steel (AISC B4.1)

$G_s := 11500 \text{ksi}$ Shear modulus

$E_c := 57 \text{ksi} \cdot \sqrt{\dfrac{f_c}{\text{psi}}} = 4.42 \times 10^3 \cdot \text{ksi}$ Modulus of elasticity of concrete (AISC I2.1b)

Step 4: Structural Analysis
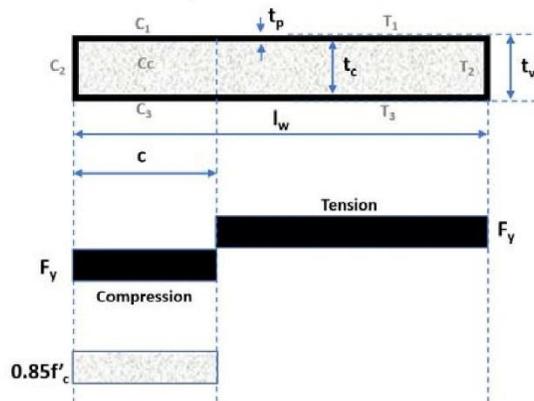
Cross Section

$A_s := 2 t_p \cdot t_w + 2 t_p \cdot (l_w - 2 \cdot t_p) = 197 \cdot \text{in}^2$ Area of steel

$A_{sw} := 2 \cdot t_p \cdot l_w = 187.5 \, \text{in}^2$ Area of web steel

$t_c := t_w - 2 \cdot t_p = 15.4 \cdot \text{in}$ Concrete infill thickness

$$A_c := t_c \cdot \left(l_w - 2t_p\right) = 4603 \cdot in^2$$ Area of concrete

$$A_T := A_c + A_s = 4800 \cdot in^2$$ Total area

Strength Calculation per Section 3-4

$$c_n := \frac{\left(2l_w \cdot F_y \cdot t_p + 0.85f_c \cdot t_c \cdot t_p\right)}{4F_y \cdot t_p + 0.85f_c \cdot t_c} = 67 \cdot in$$ Neutral axis

Compression Block

$$C_1 := \left(c_n - t_p\right) \cdot t_p \cdot F_y = 1037 \cdot kip$$

$$C_2 := t_p \cdot t_w \cdot F_y = 250 \cdot kip$$

$$C_c := \left(c_n - t_p\right) \cdot t_c \cdot 0.85f_c = 5206 \cdot kip$$

$$C_3 := C_1$$

$$C_T := C_1 + C_2 + C_3 + C_c = 7.53 \times 10^3 \cdot kip$$

Tension Block

$$T_1 := \left(l_w - c_n - t_p\right) \cdot t_p \cdot F_y = 3640 \cdot kip$$

$$T_2 := t_p \cdot t_w \cdot F_y$$

$$T_3 := T_1$$

$$T_T := T_1 + T_2 + T_3 = 7.53 \times 10^3 \cdot kip$$

Moment Capacity per Section 3.4.1

$$M_p := \frac{\left(C_1 + C_3 + C_c\right) \cdot \left(c_n - t_p\right)}{2} + C_2 \cdot \left(c_n - \frac{t_p}{2}\right) + \left(T_1 + T_3\right) \cdot \frac{\left(l_w - c_n - t_p\right)}{2} + T_2 \cdot \left(l_w - c_n - \frac{t_p}{2}\right)$$

$$M_p = 1.16 \times 10^6 \cdot kip \cdot in$$ Plastic moment

Factored flexural strength

$$\phi M_p := 0.9 \cdot M_p = 1.05 \times 10^6 \cdot kip \cdot in$$

144

Shear Capacity per Section 3.4.4

$$K_s := G_s \cdot A_{sw} = 2.16 \times 10^6 \, kip$$

$$K_{sc} := \frac{0.7 \cdot \left(E_c \cdot A_c \right) \cdot E_s \cdot A_{sw}}{4 \cdot E_s \cdot A_{sw} + E_c \cdot A_c}$$

$$V_n := \frac{K_s + K_{sc}}{\sqrt{3K_s^{\,2} + K_{sc}^{\,2}}} \cdot A_{sw} \cdot F_y = 9 \times 10^3 \cdot kip$$

$$\phi V_n := 0.9 \cdot V_n = 8.1 \times 10^3 \cdot kip$$ Factored shear strength

Step 5: Design Check

Step 5-3 Shear Check

$$V_{u\_wall} := ShearAmpFactor \cdot \frac{V_{ELF}}{N_{wall}} = 3.59 \times 10^3 \cdot kip$$ Required shear after amplification

$$\frac{\phi V_n}{V_{u\_wall}} = 2.3$$ Shear strength ratio

Step 5-4 Flexure Check

$$M_{u\_wall} := OTM_{wall} = 6.92 \times 10^5 \cdot kip \cdot in$$ Required wall moment

$$\frac{\phi M_p}{M_{u\_wall}} = 1.5$$ Wall strength ratio

Step 5-5 Drift Check

$\text{M\_phi}_{0.6} := 8.2 \cdot 10^{10} \cdot \text{kip} \cdot \text{in}^2$

Tangent of moment curvature at 60% capacity from OpenSees

$\text{EI}_{\text{eff}} := \text{M\_phi}_{0.6}$

$\text{Defl}_{\text{ELF}} := \begin{pmatrix} 0 \\ 0.16 \\ 0.50 \\ 0.96 \\ 1.50 \\ 2.09 \\ 2.70 \end{pmatrix} \cdot \text{in}$

Deflection calculated from elastic analysis

$\text{ElasticDrift}_{\text{max}} := \dfrac{\text{Defl}_{\text{ELF}_6} - \text{Defl}_{\text{ELF}_5}}{14\text{ft}} = 0.36 \cdot \%$

Max elastic drift using above effective stiffness

$\text{InelasticDrift}_{\text{max}} := \text{ElasticDrift}_{\text{max}} \cdot \text{Cd} = 1.997 \cdot \%$

Inelastic drift

$\text{Check}_{\text{Drift}} := \begin{vmatrix} \text{"Ok"} & \text{if} & \text{InelasticDrift}_{\text{max}} < 2\% \\ \text{"NG"} & \text{otherwise} \end{vmatrix} = \text{"Ok"}$

Drift check

Hence design of wall is adequate

146

C-Shaped Walls – 18-Story Archetype

Step 3: Preliminary Design

C-shaped Wall Dimensions

$L_1 := 40\text{ft}$ — Length of wall in uncoupled direction

$t_p := 0.5\text{in}$ — Plate thickness

$t_w := 18\text{in}$ — Wall web thickness

$t_f := 18\text{in}$ — Wall flange thickness

$w := 10\text{ft}$ — Wall flange length
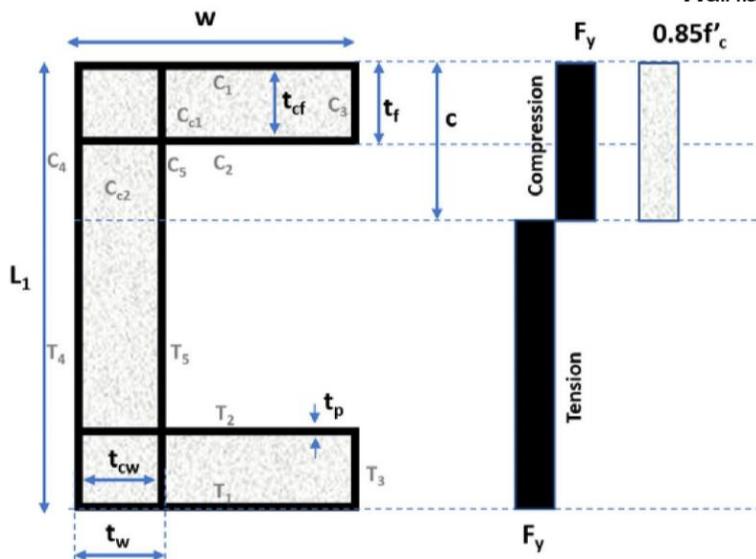
$t_{cw} := t_w - 2 \cdot t_p = 17\,\text{in}$ — Web concrete thickness

$t_{cf} := t_f - 2 \cdot t_p = 17\,\text{in}$ — Flange concrete thickness

$w_c := w - 3t_p = 118.5\,\text{in}$

Material Properties

$F_y := 50\text{ksi}$ — Nominal steel strength

$f_c := 6\text{ksi}$ — Nominal concrete strength

$E_s := 29000\text{ksi}$ — Modulus of elasticity of steel (AISC B4.1)

$G_s := 11500\text{ksi}$ — Shear modulus

$E_c := 57\text{ksi} \cdot \sqrt{\dfrac{f_c}{\text{psi}}} = 4.42 \times 10^3\,\text{ksi}$ — Modulus of elasticity of concrete (AISC I2.1b)

147

Step 4: Structural Analysis

Cross Section

$A_{sw} := 2t_p \cdot L_1 = 480 \, in^2$

Area of steel web

$A_s := 735 in^2$

Total area of steel

$A_c := 2498 in^2$

Total area of concrete

$A_T := t_{cw} \cdot (L_1 - 2t_f) + 2w_c \cdot t_{cf} = 1.158 \times 10^4 \, in^2$

Total area

Strength Calculation per Section 3.4

$c_n := \dfrac{\left[2L_1 \cdot F_y \cdot t_p - 0.85f_c \cdot (t_{cf} \cdot w_c - t_{cw} \cdot t_f) \right]}{4F_y \cdot t_p + 0.85f_c \cdot t_{cw}} = 82 \, in$

Neutral axis

Compression Block

$C_1 := w_c \cdot t_p \cdot F_y = 2.96 \times 10^3 \, kip$

$C_2 := C_1 = 2.96 \times 10^3 \, kip$

$C_3 := t_f \cdot t_p \cdot F_y = 450 \, kip$

$C_4 := c_n \cdot t_p \cdot F_y = 2.05 \times 10^3 \, kip$

$C_5 := C_4 = 2.05 \times 10^3 \, kip$

$C_{c1} := w_c \cdot t_{cf} \cdot 0.85f_c = 1.03 \times 10^4 \, kip$

$C_{c2} := (c_n - t_f) \cdot t_{cw} \cdot 0.85 \cdot f_c = 5.54 \times 10^3 \, kip$

Tension Block

$T_1 := w_c \cdot t_p \cdot F_y = 2.96 \times 10^3 \, kip$

$T_2 := T_1 = 2.96 \times 10^3 \, kip$

$T_3 := t_f \cdot t_p \cdot F_y = 450 \, kip$

$T_4 := (L_1 - c_n) \cdot t_p \cdot F_y = 9.95 \times 10^3 \, kip$

$T_5 := T_4$

148

$$C_T := C_1 + C_2 + C_3 + C_4 + C_5 + C_{c1} + C_{c2} = 2.63 \times 10^4 \, \text{kip}$$

$$T_T := T_1 + T_2 + T_3 + T_4 + T_5 = 2.63 \times 10^4 \, \text{kip}$$

Moment Capacity

$$M_{p1} := C_1 \cdot \left(c_n - \frac{t_p}{2}\right) + C_2 \cdot \left(c_n - t_f + \frac{t_p}{2}\right) + C_3 \cdot \left(c_n - \frac{t_f}{2}\right) + \left(C_4 + C_5\right) \cdot \frac{c_n}{2}$$

$$M_{p2} := C_{c1} \cdot \left(c_n - \frac{t_f}{2}\right) + C_{c2} \cdot \left(\frac{c_n - t_f}{2}\right)$$

$$M_{p3} := T_1 \cdot \left(L_1 - c_n - \frac{t_p}{2}\right) + T_2 \cdot \left(L_1 - c_n - t_f + \frac{t_p}{2}\right) + T_3 \cdot \left(L_1 - c_n - \frac{t_f}{2}\right) + \left(T_4 + T_5\right) \cdot \left(\frac{L_1 - c_n}{2}\right)$$

$$M_p := M_{p1} + M_{p2} + M_{p3} = 8 \times 10^6 \, \text{kip·in} \qquad \text{Plastic Moment}$$

$$\phi M_p := 0.9 \cdot M_p = 7.2 \times 10^6 \, \text{kip·in} \qquad \text{Factored flexural capacity}$$

Shear Capacity per Section 3.4.4

$$K_s := G_s \cdot A_{sw} = 5.52 \times 10^6 \, \text{kip}$$

$$K_{sc} := \frac{0.7 \cdot \left(E_c \cdot A_c\right) \cdot E_s \cdot A_{sw}}{4 \cdot E_s \cdot A_{sw} + E_c \cdot A_c}$$

$$V_n := \frac{K_s + K_{sc}}{\sqrt{3 K_s^2 + K_{sc}^2}} \cdot A_{sw} \cdot F_y = 1.77 \times 10^4 \cdot \text{kip}$$

$$\phi V_n := 0.9 \cdot V_n = 1.59 \times 10^4 \cdot \text{kip} \qquad \text{Factored shear strength}$$

Step 5: Design Check

Step 5.3 Shear Check

$$V_{u\_wall} := \text{ShearAmpFactor} \cdot \frac{V_{ELF}}{N_{wall}} = 5.89 \times 10^3 \cdot \text{kip} \qquad \text{Amplified base shear in each walls}$$

$$\frac{\phi V_n}{V_{u\_wall}} = 2.7 \qquad \text{Shear strength Ratio}$$

Step 5.4 Flexure Check

$$M_{u\_wall} := OTM_{wall} = 3.36 \times 10^6 \cdot kip \cdot in$$

Required wall moment

$$\frac{\phi M_p}{M_{u\_wall}} = 2.1$$

Flexural strength ratio

Step 5.5 Drift Check

Effective Stiffness Calculation

$$I_s := 2 \cdot t_p \cdot w_c \cdot \left(\frac{L_1 - t_p}{2}\right)^2 + 2 \cdot t_p \cdot w_c \cdot \left(\frac{L_1 - 2t_f + t_p}{2}\right)^2 + 2 \cdot t_p \cdot \frac{L_1^3}{12} = 2.2 \times 10^7 \, in^4$$

$$I_c := \frac{2 \cdot w_c \cdot t_{cf}^3}{12} + 2 \cdot w_c \cdot t_{cf} \cdot \left(\frac{L_1 - t_f}{2}\right)^2 + \frac{t_{cw} \cdot (L_1 - 2 \cdot t_f)^3}{12}$$

$$EI_{eff} := E_s \cdot I_s + 0.35 E_c \cdot I_c = 1.159 \times 10^{12} \, kip \cdot in^2$$

Effective stiffness

$$I_{eff} := \frac{EI_{eff}}{E_s} = 4 \times 10^7 \, in^4$$

$$ElasticDrift_{max} := 0.35\%$$

Max elastic drift using above effective stiffness

$$InelasticDrift_{max} := ElasticDrift_{max} \cdot Cd = 1.925\%$$

Inelastic drift

$$Check_{Drift} := \begin{vmatrix} "Ok" & if & InelasticDrift_{max} < 2\% & = "Ok" \\ "NG" & otherwise \end{vmatrix}$$

Drift check

Hence design of wall is adequate